Icing dynamics in the lake-dominated, discontinuous permafrost Taiga Shield, and effects on fluvial biogeochemistry, carbon cycling and microbial communities

by

Nora Alsafi

A thesis submitted in partial fulfillment of the requirements for the degree of

Master of Science

in

Ecology

Department of Biological Sciences

University of Alberta

ABSTRACT

Climate warming is affecting freshwater systems across the western Canadian subarctic, due to widespread shifts in precipitation regimes, permafrost degradation, and multi-decadal increases in winter baseflow. These changes are significant on the Taiga Shield, which comprises ~20% of North America's permafrost-covered area, encompassing an area of over 1.3 million km^2. This region is characterized by "fill and spill" hydrology, where runoff is generated by the exceedance of lake basin storage thresholds across the landscape. In response to increasing winter baseflow, hydrologic connectivity between the lakes which dominate this region is also increasing. In addition, taliks, zones of unfrozen ground within or above the permafrost layer, are expanding in spatial extent and occurrence across the Taiga Shield. These changes are expected to alter the export of novel chemical constituents, including dissolved organic matter (DOM), to fluvial networks, with potential implications for carbon cycling and the structure of microbial communities, which comprise the base of aquatic food webs. Despite this, the impact of warming on wintertime fluvial biogeochemistry on the Taiga Shield is poorly understood.

In this thesis, I use icings, which are sheet-like masses of layered ice which form when subsurface flow is pushed to the ground surface, as a tool to understand wintertime chemistry. Working in the Yellowknife, NT, region, I developed and tested a conceptual model to consider how hydrological processes and source water characteristics affect icing chemistry. I additionally coupled icing samples to surface water samples from winter, spring, and summer to explore seasonal and icing-driven variation in water chemistry, microbial community structure, and carbon processing rates. I found that icing chemistry was driven by physico-chemical processes, notably anoxia, solute exclusion and sediment-water interaction occurring within icing source waters and along flow paths to sites of icing formation. Icing formation and morphology were

driven by temperature and antecedent precipitation levels, which worked together to control wintertime fill and spill hydrology. Icing formation also modified wintertime flow via solute exclusion; icing chemistry was unique, and dominated by DOM that was characteristically aliphatic, protein-like, and was preferentially mineralized to CO_2 during an incubation. Seasonal differences in DOM composition also supported unique microbial communities. Overall, these results suggest that winter flow is dynamic, and icings have the potential to modify the composition of water actively flowing through fluvial networks in the winter, and as they thaw in the spring and summer; thus, changes in icing dynamics due to warming may have significant effects on wintertime chemistry and carbon cycling in this region.

PREFACE

This thesis is an original work of Nora Elizabeth Alsafi and is structured into four chapters. Chapter 1 is an introductory chapter featuring background information on the thesis topic and outlines research rationale and objectives. Chapter 2 and 3 are data chapters written in manuscript format (as cited below). Chapter 4 provides general conclusions and avenues of future research from this work.

This research is part of a collaboration between Nora Alsafi, Drs. Suzanne Tank, and Maya Bhatia (University of Alberta), Maria Cavaco (University of Alberta), Dr. Steven Kokelj and Tim Ensom (Government of the Northwest Territories), Dr. Mike Palmer (Aurora College), Dr. Chris Spence (Environment and Climate Change Canada), Dr. Rob Spencer (Florida State University), and Martin Kurek (Florida State University). Nora Alsafi was responsible for study design, data collection and analysis and manuscript composition. Dr. Tank provided thesis revisions for all data chapters and recommendations for data analysis and storyline ideas. Additionally, Drs. Palmer and Spence, and Tim Ensom provided revisions for Chapter 2; Dr. Bhatia, Martin Kurek and Maria Cavaco provided revisions for Chapter 3.

Chapter 2

Alsafi, N.E., Tank, S.E., Kokelj, S.J., Palmer, M.J., Ensom, T.P., Spence, C. Icings as sentinels and modifiers of water flow through winter landscapes: An exploration of physicochemical processes on the lake-dominated, discontinuous permafrost Taiga Shield. In preparation for submission to *Hydrological Processes.*

Chapter 3

Alsafi, N.E., Tank, S.E., Kokelj, S.J., Palmer, M.J., Bhatia, M.P., Cavaco, M.A., Spencer, R., Kurek, M.R. Icings modify fluvial biogeochemistry, microbial community structure and carbon cycling in the lake-dominated discontinuous permafrost Taiga Shield. In preparation for submission to *Journal of Geophysical Research: Biogeosciences.*

ACKNOWLEDGEMENTS

I would like to express my gratitude to the following individuals who have provided invaluable support and guidance throughout my thesis research:

First and foremost, I would like to thank my supervisor, Dr. Suzanne Tank, for her unwavering encouragement and invaluable expertise. Suzanne's thoughtful guidance has been instrumental in shaping my research and helping me navigate the challenges of graduate school. She has made my MSc an overwhelmingly positive experience.

I am also grateful to my committee members and collaborators, Drs. Maya Bhatia, Mike Palmer, Steve Kokelj, Chris Spence, and Tim Ensom for helping to conceptualize this project and their advice regarding data collection and analysis. A special thanks to Mike, Steve and Tim for your logistical support in the field, without which this project would not have been possible.

I would like to extend my thanks to Jaedyn Smith, who has not only been an amazing friend throughout my MSc, but also helped me immensely in the field and the lab to collect and process my samples. I couldn't have done this without you.

I would also like to thank Dr. Rob Spencer, Megan Moore and Martin Kurek for their help in processing my FTICR-MS samples, and Joanna Li Yung Lung, for her assistance in the lab.

A heartfelt thank you to the members of my lab group, Marina Taskcovic, Jaedyn Smith, Hayley Drapeau, Jeremie Mahaux and Gabrielle Hatten for their support, brainstorming sessions, and good humor throughout my time here. Thanks also to Patrick White for your coding advice.

Finally, I'd like to thank my parents, Corrine and Mike, and my partner, Alec, who have been a source of guidance and love throughout this journey.

TABLE OF CONTENTS

LIST OF TABLES

LIST OF FIGURES

Chapter 1: General Introduction

Climate warming across the western Canadian subarctic

Freshwater systems in the western Canadian subarctic are responding to persistent climate warming. Air temperatures in this region are increasing at approximately twice the rate of the global average, coupled with shifts in precipitation regimes (IPCC, 2021). The effects of this change have been particularly pronounced during the winter season. Increasing autumn precipitation (Spence et al., 2015), has been linked to widespread increases in winter baseflow over the past several decades (Ensom et al., 2020). Warming is also driving less intense active layer freeze back and permafrost degradation, reflected by the increasing extent and occurrence of taliks, which are pockets of perennially unfrozen ground within or above the permafrost layer (Walvoord & Kurylyk, 2016). During winter, water movement is restricted to unfrozen ground, flowing through the active layer and/or taliks, and thus, permafrost degradation is accompanied by increases in surface-groundwater interaction (Walvoord & Kurylyk, 2016), which may alter the export of chemical constituents to streams.

In Yellowknife, which is located in the Taiga Shield ecoregion, annual mean temperatures have increased more than 2° C from the 1950-1970 mean of -5.7° C, with warming occurring mainly in winter (Paul et al., 2021). Despite covering an area of over 1.3 million km^2, (i.e. approximately 20% of North America's permafrost-covered area) (Tarnocai et al., 2009; Wang et al., 2019), the impact of warming on fluvial systems in the Taiga Shield has received little attention to date. The Taiga Shield is underlain by discontinuous permafrost, and features unique hydrology termed "fill and spill"; here, runoff is generated by the exceedance of hillslope and lake basin storage thresholds across the landscape (Mielko & Woo, 2006; Spence & Woo, 2003). Long-term increases in autumn precipitation on the Taiga Shield appear to be increasing hydrologic connectivity between basins during the winter (Spence et al., 2011, 2014), which in tandem with possible talik formation, appears to be driving increased exports of carbon and solutes into rivers and streams (Spence et al., 2015). However, our understanding of how warming is affecting wintertime fluvial biogeochemistry on the Taiga Shield is greatly limited in spatial and temporal extent.

Microbial communities and carbon mineralization

As talik formation expands winter subsurface flow paths, novel biogeochemical constituents including nutrients, metals and dissolved organic matter (DOM) may be exported to fluvial networks; this may have substantial implications for the ecological and biogeochemical functioning of aquatic networks on the Taiga Shield. Dissolved organic carbon (DOC), which is the carbon-specific component of DOM, is an important substrate for microbial metabolism in aquatic systems, and fluvial networks can be significant sources of CO_2 to the atmosphere (Drake et al., 2015); nutrients and select metals are also required for microbial growth and cellular processes (Merchant & Helmann, 2012). Microbial communities constitute the base of aquatic food webs, and their activity and structure are strongly influenced by the composition of dissolved organic matter (DOM) in fluvial networks (Kaiser et al., 2017). If talik expansion enables flowpaths through soil horizons containing larger proportions of DOM which has undergone minimal biological processing, this DOM may be more easily mineralized into CO_2, particularly if it is more aliphatic in nature (Kaiser et al., 2017). While winter is often perceived as a period of limited biological activity, shifts in hydrologic connectivity and surface-groundwater interactions associated with warming may alter the structure of microbial communities and carbon mineralization within fluvial networks; however, research investigating this shift remains relatively unexplored on the subarctic Taiga Shield, but is focused predominantly in Arctic regions (Cavaco et al., 2019; Kaiser et al., 2017; Sipler et al., 2017),

Icings as archives and modifiers of winter subsurface flow

Wintertime chemistry is understudied, in part, due to the logistical challenges associated with sampling in this season. However, a potential tool to study bulk wintertime chemistry are icings, which are a manifestation of winter subsurface flow and archive water actively flowing through northern landscapes in the winter. Icings are sheet-like masses of ice that form throughout the Taiga Shield and are commonly sourced by groundwater or lake outflows as this water is pushed to the ground surface. Icings also have the potential to modify the chemical composition of streamflow as they thaw, as they can last well into the summer depending on their volume. Icing formation in the Taiga Shield is sensitive to winter baseflow, and commonly occurs in valleys where basin storage is exceeded in late autumn and winter (Ensom et al., 2020). Despite their potential use as an archival tool of wintertime chemistry, icing research has mainly focused on physical and meteorological controls of their growth and distribution (Crites et al., 2020; Ensom

et al., 2020; Glass et al., 2021; Hodgkins et al., 2004; Morse & Wolfe, 2015, 2017; Yoshikawa et al., 2007). In particular, the geochemistry of icings derived from lake water sources, which are common throughout the Taiga Shield, is not well known. Because icings can persist on the landscape, their effect on fluvial biogeochemistry, microbial community structure, and biological processing becomes important as temperatures and hydrologic connectivity increases during freshet. Because of their reliance on baseflow and the presence of taliks, icings are also sentinels of hydrologic change; however, the influence of fill and spill dynamics on icing formation is also poorly understood.

Research rationale and objectives

Given the increasing importance of wintertime flow to fluvial networks throughout Arctic regions, it is necessary to understand the nature of wintertime biogeochemistry and its effect on ecological function and microbial community structure, and the role of icings in archiving and modifying wintertime flow. This is particularly true on the Taiga Shield, which despite being dominated by lakes and covering an area of 1.3 million km^2, is overall poorly understood. This work aims to provide insight into how icing dynamics are influenced by lake water sources and fill and spill dynamics, which distinguish the Taiga Shield, and how wintertime biogeochemistry influences microbial communities and carbon mineralization.

This thesis contains two manuscript-style chapters (Chapter 2 and Chapter 3) with appendices. The objective of Chapter 2 was to characterize controls on icing formation and chemistry. The objectives of Chapter 3 were to 1) investigate seasonal variation in water chemistry with a focus on winter flow, 2) explore seasonal differences in, and chemical drivers of, microbial community structure and 3) explore seasonal differences in, and chemical drivers of biological processing.

To do this, I investigate icing and source water chemistry at eight icings in the River Lake and Baker Creek watersheds, located near Yellowknife, NT. In Chapter 2, I develop and test a conceptual model of icing chemistry and formation using icing and wintertime source water chemistry at all eight sites; in Chapter 3, I investigate a subset (three) of these sites, and explore seasonal chemistry from winter to summer, with a focus on how icing presence might alter winter-time flow.

Significance

Understanding the influence of hydrological processes and water sources on icing dynamics is necessary to frame future research investigating icing chemistry, and to understand how icings may archive and modify wintertime flow. Evaluating the chemical composition of icings will also elucidate how the composition of water may change during spring and summer as these icings thaw and contribute to streamflow, which is fundamental to understanding how these features may shift the composition of microbial communities and release of CO_2 in fluvial networks. As microbes constitute the base of aquatic food webs, shifts in community structure may have important implications at higher trophic levels.

I found that fill and spill hydrology was an important control on icing formation and morphology; this provides insight towards how the unique hydrological regime of the Taiga Shield influences icing formation and establishes a framework to understand how increasing winter baseflow may affect icing dynamics. I also found that differences in lake basin characteristics and flow paths resulted in variable icing chemistry via solute exclusion and anoxia, and that icing chemistry displayed notable patchiness over space. Given that the geochemical nature of icings derived from lake water sources is not well known, this work highlights important controls of icing chemistry in the lake-rich Taiga Shield. Furthermore, solute exclusion occurring during icing formation modified the composition of winter surface waters; this resulted in unique icing chemistry, and notably the enrichment of aliphatic, protein-like DOM in ice, which was rapidly mineralized into CO_2 and was correlated with distinct microbial community structure. As icings persist on the landscape, these results suggest that icings provide a labile pulse of DOM as they thaw during the spring and summer, which may affect carbon feedbacks as this water moves downstream. Overall, icings were an important archive and modifier of wintertime fluvial biogeochemistry, and that to accurately characterize winter flow in a warming climate, it is evident that icings must be considered.

Chapter 2: Icings as sentinels and modifiers of water flow through winter landscapes: An exploration of physicochemical processes on the lake-dominated, discontinuous permafrost Taiga Shield

2.1 Introduction

Warming air temperatures and shifting precipitation regimes are changing the dynamics of freshwater systems throughout the western Canadian subarctic. Air temperatures in this region are increasing at twice the rate of the global average (Prowse et al., 2006). Warming has also been associated with a shift towards more pluvial runoff regimes, increasing winter and spring streamflow, and widespread permafrost degradation (Morse et al., 2016; Spence et al., 2015). In winter, water is conveyed to surficial flow paths through the unfrozen portion of the active layer or through taliks; pockets of perennially unfrozen ground within or immediately above permafrost (Walvoord & Kurylyk, 2016). However, permafrost thaw (i.e. talik expansion) and less intense active layer freeze back allow for increased surface-groundwater interactions (Walvoord & Kurylyk, 2016) which may alter the export of chemical constituents to surface water. Despite the widespread evidence for changing winter hydrological pathways, the nature of winter chemistry remains understudied in northern regions, partly due to its perception as a period of limited chemical and biological activity. As climate warming drives changes in winter surface water supply and surface-groundwater interactions, understanding the resulting impacts on winter streamflow chemistry becomes increasingly important to predict changes at a watershed level and across larger geographic scales.

On the Taiga Shield, annual mean temperatures in Yellowknife have increased more than 2° C from the 1950-1970 mean of -5.7° C, with warming occurring mainly in winter (Paul et al., 2021). This warming is occurring in a region that is underlain by widespread discontinuous permafrost, which is particularly vulnerable to thaw due to the possibility of both vertical and lateral heat transfer (Wright et al., 2022). In addition, the Taiga Shield features unique hydrology, whereby runoff is generated by the exceedance of hillslope and lake basin storage thresholds across the landscape (termed “fill and spill” hydrology) (Mielko & Woo, 2006; Spence & Woo, 2003). This hydrological regime causes fluvial networks on the Taiga Shield to experience orders of magnitude variation in surface water flow between years (Spence & Rouse, 2002), however, long-term increases in autumn precipitation appear to be increasing hydrologic connectivity between basins (Spence et al., 2011, 2014), enabling a regional increase in winter

baseflow (Crites et al., 2020). Emerging evidence suggests that this enhanced winter baseflow and hydrologic connectivity may be increasing exports of carbon and solutes into rivers and streams (Spence et al., 2015). However, despite covering an area of over 1.3 million km^2 (i.e., approximately 20% of North America's permafrost-covered area) (Tarnocai et al., 2009; Wang et al., 2019), fluvial biogeochemistry, and its change, has received little attention on the Taiga Shield.

Across the Taiga Shield, a manifestation of winter subsurface flow are icings, which are sheet-like masses of layered ice that form through freezing of successive flows of water onto the ground surface, and can be sourced via groundwater seepage, from springs, or from water below river or lake ice as it flows through ice fractures (Ballantyne, 2017). Icings in the Taiga Shield are often sourced by lake outflow and are intermittent across the landscape on an annual basis, commonly forming in valleys where basin storage is exceeded in late autumn and winter (Ensom et al., 2020; Morse & Wolfe, 2017; Spence et al., 2014). Icings may create geohazards, as they can accumulate on road surfaces, block drainage structures, erode stream channels, cause ground uplift and subsidence, and divert water, causing infrastructure embankments (Carey, 1973; Ensom et al., 2020). However, these features also archive water actively flowing through northern landscapes in the winter, and thus, may be useful tools to investigate wintertime fluvial biogeochemistry. Icings features can benefit communities by maintaining river or stream baseflow, as they can persist well into the summer and contribute to streamflow as they thaw (Ensom et al., 2020). From an environmental and socio-economic perspective, understanding the nature of icing dynamics and chemistry under a warming climate has become increasingly relevant.

Research of icings has mainly focused on physical and meteorological controls of growth and icing distribution (Crites et al., 2020; Ensom et al., 2020; Glass et al., 2021; Hodgkins et al., 2004; Morse & Wolfe, 2015, 2017; Yoshikawa et al., 2007). However, the geochemistry of icings derived from lake water sources, which are common throughout the Taiga Shield, is not well known. Furthermore, little is understood of how the variable water sources across the Taiga Shield influence icing chemistry, and how hydrological processes such as fill and spill dynamics, which distinguish the Taiga Shield and other lowland lake-rich environments, affect icing formation. Here, we aim to characterize controls on icing formation and chemistry within the fill-

and-spill Taiga Shield landscape. To do this, we developed a conceptual model which considers how hydrological processes and source water characteristics affect icing chemistry and formation and tested this model with a series of icing and coupled winter source water samples from the Yellowknife, NT, region. Our work explores the ability of icings to both archive and modify the composition of water actively flowing through wintertime landscapes, and thus change the biogeochemical dynamics of wintertime flow.

2.2 Conceptual Model of Icing Formation and Chemistry

The mechanics of icing formation have been explored since the 1970s, with literature primarily focused on processes driving icing growth (Carey, 1973; Hu & Pollard, 1997a, 1997b; Kane, 1981). Early research, which was associated with groundwater-sourced icing growth in streambed settings, outlined three stages of icing growth: freeze-up, obstruction, and overflow, (Hu & Pollard, 1997b). Freeze-up begins with a primary ice layer forming over a stream or river channel, restricting flow beneath the ice. As ice thickens on the riverbed and channel banks, the subsurface conduit of flowing water shrinks, until a critical point is reached where discharge overwhelms channel capacity (Hu & Pollard, 1997b). This is termed the "obstruction" stage, where mounting water pressure facilitates the formation of fractures in the overlying ice (Hu & Pollard, 1997b). This is followed by the "overflow" stage when water moves upwards through ice fractures and overflows onto overlying ice. Eventually, a secondary ice layer again restricts the underlying channel flow and the three-stage process repeats, leading to successive freezing of ice in sheets over time (Hu & Pollard, 1997b).

Recent research exploring the physical and meteorological controls on icing development and distribution has further refined this conceptualization, including by demonstrating the importance of winter baseflow, warming air temperature intervals, snow cover, and talik presence. This research suggests that icings will only form in locations where winter baseflow is sufficient to sustain their growth, which can be supplied through rainfall and basin storage, or deep-sourced groundwater (Ensom et al., 2020). Autumn rainfall is critical to icing growth in regions where hydrology is dominated by fill and spill dynamics, such as lake rich lowlands in the zone of continuous permafrost or on the Canadian Shield (Ensom et al., 2020; Morse & Wolfe, 2017). Winter warming periods have also been correlated with increased icing spatial density, however the mechanism behind this has not been characterized (Morse & Wolfe, 2015, 2017). Finally, the

insulating properties of snow have been shown to regulate icing formation, whereby a thin early winter snow cover tends to promote icing formation, and the saturation of riparian zone snow and its incorporation into icings can promote streambed freezing which facilitates flow obstruction and overflow events (Wankiewicz, 1984). A conceptual model of icing formation from the continuous permafrost region of Nunavik, Canada indicated that talik configuration may also be important to icing formation, and detailed how a downstream constriction of a water-bearing talik beneath a river channel promoted a buildup of water pressure and drove overflow events leading to icing growth (Liu et al., 2021).

Icing dynamics are highly complex on the Taiga Shield, given the pronounced variation in water sources, hydrologic connectivity, and topography across this landscape. While our understanding of physical formation processes driving icing growth continues to improve, the influence of various physico-chemical and hydrological processes on icing formation and chemistry in lake-rich, fill and spill environments is poorly understood.

Here, we consider three main landscape components that drive icing growth, morphology, and chemical composition, with specific consideration of fill and spill environments: hydrological processes within source waters; physico-chemical processes within source waters; and the physical properties of flow paths (Figure 2-1).

2.2.1 Hydrological processes of source waters

Several hydrological processes influence icing source waters and may affect icing growth and morphology. The Taiga Shield is characterized by low precipitation, modest surface water runoff generation, and high basin storage in lakes. In these settings, lakes can become hydrologically disconnected from their surrounding landscape during dry periods, thus inhibiting further water movement downstream (Phillips et al., 2011). Whether a lake is a closed system, (i.e., hydrologically disconnected), or an open system (i.e., actively receiving and discharging water) drives the capacity of upstream lakes to contribute to downstream icing formation. Furthermore, variations in lake outflow volume affect discharge, and resultant water pressure, which may alter downstream icing morphology. Therefore, although a lake-rich environment such as the Taiga Shield can host high icing densities, annual variation in the water balance of these lakes can control year-to-year variation in icing presence. In addition to fill and spill dynamics, the

formation of lake-outflow ice dams (Marsh & Hey, 1989), might be expected to alternatively inhibit icing formation, or promote icing growth if water seeps through ice fractures.

2.2.2 Physico-chemistry of source waters

The nature of water sources to icings will also affect icing chemistry: icings may be sourced by river baseflow, upstream lakes, groundwater, or a combination thereof. Thus, we propose that the chemistry of lake-fed icings is driven by lake-specific physico-chemical processes (described below) in addition to flow path routing from the lake outlet to the location of icing formation, while groundwater-fed icing chemistry is mainly driven by flow path variation including the length of soil-water interaction.

Within lakes, catchment characteristics and within-lake biological processing establish a baseline for the physico-chemical characteristics of surface waters (Kalff, 2002). Seasonally, variation in winter-time surface water chemistry is driven by redox gradients within the ice-covered water column, and solute exclusion during the development of ice cover. Under-ice depletion of dissolved oxygen in shallow lakes and ponds enables the production of reduced chemical species via redox processes. These processes are driven by the duration of ice cover, water volume under ice, and the chemical and biological characteristics of surface waters and lake sediments (Barrett et al., 2019; Hamilton-Taylor et al., 2005; Hamilton-Taylor & Davison, 1995; Palmer et al., 2021).

Lakes may remain ice covered for over half the year in the subarctic Taiga Shield (Palmer et al., 2019). As a result of this loss of connection to the overlying atmosphere, source waters may have a lower redox state later in the winter than shortly after ice cover forms. The progression of oxygen depletion is also dependent on lakebed sediment composition, as higher organic matter content in lake bottom sediments drive increased microbial respiration and wintertime oxygen depletion (Jansen et al., 2021). Biologically and chemically mediated redox reactions occur at the sediment-water interface, and larger ratios of sediment surface area to water volume in shallow lakes drive greater winter oxygen depletion rates (Jansen et al., 2021; Mathias & Barica, 1980). Thus, lake depth (as often inferred from lake size; (Oliver et al., 2016) may have a critical influence on temporal and spatial variations in the chemistry of icings sourced from lake waters. Important redox processes under anoxic conditions include the reductive dissolution of iron and manganese oxides in near-surface lake sediments (Hamilton-Taylor & Davison, 1995) and the

coupled release of elements such as phosphorus and arsenic into overlying surface waters (Giles et al., 2016; Palmer et al., 2021). Alteration of redox conditions can also occur along surface and subsurface flow paths. For example, the redox state of source water may change during transit to icings through the oxidation or reduction of waters within the downstream flow path, or upon atmospheric exposure at the icing surface. Because oxygen exposure and depletion may be patchy over space (i.e. varying in concentration along flow paths to icings) and time, this may drive spatial variation in icing chemistry.

In addition to chemical variation caused by anoxia, the chemical signature of water sourcing icings may reflect the effects of solute exclusion associated with lake ice formation. As lake ice forms, solutes are excluded to underlying waters, and therefore effective concentration of solutes in the unfrozen water column increases with increasing lake ice: lake water ratios (Belzile et al., 2002; Jansen et al., 2021; Santibáñez et al., 2019). Given that ice depth is a function of air temperature and thus relatively similar between geographically proximate lakes, the importance of solute exclusion is likely to be most significant in small, shallow waterbodies within a given region. Solute exclusion of inorganic ions, metals, dissolved organic carbon (DOC) and phosphorus have all been observed during lake ice formation (Imbeau et al., 2021; Santibáñez et al., 2019). Similarly, aliphatic, protein-like dissolved organic matter (DOM), which is typically a preferred substrate for microbial metabolism (Spencer et al., 2015) is preferentially included into the ice phase, while aromatic DOM is preferentially excluded (Santibáñez et al., 2019; Zhou et al., 2023).

2.2.3 Physical properties of flow paths

While the hydrological and physico-chemical processes described above apply to lake-fed icings, groundwater-fed icings are also common across the subarctic. These features are controlled hydrologically by the presence of springs (forming spring icings) or suprapermafrost taliks (forming groundwater-fed icings) and are controlled chemically by sediment composition within flow paths (Yoshikawa et al., 2007). Spring icings are fed by large reserves of sub-permafrost water, are common in mountainous or hilly areas, and often recur from year to year (Glass et al., 2021). More common across the Canadian Shield, groundwater-fed icings are sourced by temporary seepage of shallow groundwater, resulting from water in the active layer becoming trapped between the top of the permafrost layer and a freezing front, which occurs

during suprapermafrost talik formation. Given the ephemeral nature of these processes, the reoccurrence of groundwater-fed icings is more intermittent than their spring-fed counterparts (Glass et al., 2021).

In lake-fed icings, transit from the upstream (lacustrine) water source to downstream sites of icing formation is associated with processes that may modify icing chemistry and influence icing growth. For example, longer flow paths from water sources to icing formation may result in flow contributions from additional (non-lacustrine) water sources, and potentially increase soil-water interactions when water flow is through sediments, rather than a flowing channel. In both lake and groundwater-fed icings, several factors influence the nature of flow paths that feed icings. Variation in the depth to confining layers and the occurrence of taliks, and the nature of substrate (texture, mineralogy, hydraulic conductivity) will affect the transit time of water. For example, the presence of permafrost or fine-grained sediments such as glaciolacustrine clays restricts subsurface flow (Walvoord & Kurylyk, 2016), which may encourage increased interaction with surficial organic-rich soil layers and thus potentially increase the export of more recently fixed, aromatic DOM (Barnes et al., 2018). In contrast, the presence of coarse-grained sediments or taliks may facilitate deeper flow paths, interaction with mineral rich soils, and thus greater export of major ions, metals, and more aged, aliphatic DOM (Barnes et al., 2018; Lyon et al., 2010; Parazoo et al., 2018). Thus, in discontinuous permafrost regions such as the Taiga Shield, the heterogeneous nature of permafrost and talik occurrence (Morse & Wolfe, 2014, 2017) may enable spatial and temporal variation in the flow paths that source icings, and therefore their composition.

Variation in flow within the icing channel itself may also contribute to variation in icing growth and morphology, and thus chemistry. For example, downslope channel constrictions may increase water pressure, facilitating overflow events leading to icing formation and growth (Liu et al., 2021). Constrictions can occur in nearby water-bearing taliks but can also occur as a result of icing growth, whereby the channel in which an icing grows becomes narrower and can be blocked by ice over time, decreasing flow velocity and promoting incorporation of frazil crystals along the upstream edge of the ice cover (Hu & Pollard, 1997b). This damming effect allows icings to grow at their upstream end simultaneous to ongoing downstream growth, which is driven by overflow events (Hu & Pollard, 1997b). Blockages that allow lateral expansion of

icings beyond channel banks may result in increased interaction with soil and bankside vegetation. Lateral seepage of water along vegetation can be significant, as water can move quickly along ice-encased stems due to differences in thermal conductivity between water and woody stems (Hu & Pollard, 1997b). Additionally, natural obstructions in a channel, such as beaver dams, can facilitate icing development through obstructions to flow.

Finally, icing morphology and changes in hydraulic pressure control within-icing flow paths. Water flow within and through icings may be surficial, during an overflow event; occur between icing layers as intra-icing flow; or occur at the interface between the ground or channel surface and the overlying icing, as basal flow. While intra-icing flow necessarily exists near the freezing point, surficial flow paths can be rapidly exposed to sub-freezing temperatures. Rapid freezing at the icing surface may result in lesser exclusion of solutes in surficial icing layers, as opposed to slower freezing resulting in greater solute exclusion along intra-icing flow paths (DeGrandpre et al., 2021). Additionally, surficial overflow water may incorporate snow, if present, into icing layers, resulting in layers that may be chemically dilute relative to the underlying ice (Hodgkins et al., 2004). Finally, basal flow may increase soil-water interaction, potentially enabling water to pick up novel substrates.

To investigate icing dynamics, it is important to understand how the hydrological and physico-chemical processes described above affect icing chemistry and formation. Here, we use the framework provided by this conceptual model to specifically explore how the hydrology of source waters, physico-chemistry of source waters, and physical properties of flow paths affect icing formation and chemistry within the lake dominated Taiga Shield. We do this via a detailed study of icing formation across two hydrologically distinct years, and icing chemistry across gradients of differing source water types and lake basin characteristics, distance from water source to icing formation, and soil characteristics along flow paths from source water to icing. Our findings show the overall importance of source water type and lake size on icing chemical dynamics and reveal icings as a critical control on the composition of wintertime flow within the Taiga Shield region.

2.3 Methods

2.3.1 Study area

Yellowknife, NT is located in the Taiga Shield ecozone. The area was glaciated until approximately 13, 000 yBP and was subsequently inundated by glacial Lake McConnell until around 9, 500 yBP, leaving behind discontinuous till and reworked lacustrine veneers interspersed in lowlands between bedrock outcrops that dominate the environment (Ecosystem Classification Group, 2008; Morse et al., 2016). Glacial scouring and fault systems have influenced the configuration of lakes and drainage networks that occupy this region. The presence of near-surface bedrock, hundreds of thousands of small to medium sized lakes, and a continental subarctic climate result in the "fill-and-spill" hydrological regime (Spence & Woo, 2003) characteristic of first to third order lakes in this region, where runoff generation occurs only when the storage capacity of lakes is exceeded (Mielko & Woo, 2006). This hydrological regime differs from regions of the North American Arctic outside of the Canadian Shield, in that lakes represent a series of storage reservoirs, and downstream flow does not occur until upstream storage thresholds are reached (Spence & Woo, 2003). As a result, lakes switch between being hydrologically connected or disconnected from the surrounding landscape depending on antecedent precipitation over the past several years, and discharge can vary by orders of magnitude on an annual basis (Morse & Wolfe, 2017; Spence, 2006).

Local climate is characterized by short, cool summers (17 °C July mean) and long, cold winters (-26 °C January mean) with below freezing temperatures between November and March (1981 – 2010 climate normal) (ECCC, 2022a). Mean annual air temperature is increasing, but remains below freezing (-1 °C to -7 °C from 1942-2016) (Sivarajah et al., 2021). The Taiga Shield is situated within the southern portion of discontinuous permafrost (~50-65% of land underlain by permafrost) (Morse et al., 2016; Zhang et al., 2014). Vegetation is characterized by open forests of black spruce (*Picea mariana),* jack pine (*Pinus banksiana)* and paper birch (*Betula papyrifera),* and bare outcrops dominated by lichens and shrubs (Ecosystem Classification Group, 2008).

2.3.2 Sampling scheme and site characteristics

To investigate spatial variation in chemistry between icings, a series of ice cores were collected in March 2021 at six icings in the River Lake watershed (S1, S3, S6, S5a, S5b, S8), and one icing in the Baker Creek watershed (BC) (Figure 2-2). To explore the effect of water source

on icing chemistry, we compared icings fed by groundwater (S1, S3), small lakes (S5a, S6, BC) and large lakes (S5b, S8).

To investigate spatial variation in chemistry within icings, we explored how flow path distance, catchment characteristics, and source waters affected icing chemistry. To do this, we selected sites that varied in surrounding soil characteristics and distances between source waters to sites of icing formation. Soil characteristics varied across a gradient of fine-grained (S5a, S5b, S6, S8, BC) to coarse-grained (S1, S3) materials and transit distances ranged from 26 to 486 m from source waters to icings (Table 2-1). We sampled lakes upstream of each site of icing formation and stream water flowing below icings during winter from 2020-2021 (Figure 2-2). To investigate within-icing chemical variation in greater spatial resolution, we extensively sampled the surficial layer of an additional icing near Jackfish Lake (JL) in March 2022. More frequent source water sampling was conducted at S1, S5a, and S5b, which were chosen as focal sites due to ease of access. These sites were sampled approximately biweekly from March 2021 to early May 2021 (Table A1-1). The remaining icings on River Lake, the BC icing, and the JL icing were sampled once for source water during March 2021 or February 2022 (Table A1-1).

Study sites are all located within the watershed of Great Slave Lake. The study sites represented a range of surficial geology. S5a, S5b, S6, S8, BC and JL were underlain by fine-grained glaciolacustrine sediments consisting of fine sand to silty clay, whereas S1 and S3 are underlain by discontinuous till veneer and isolated patches of coarse-grained glaciofluvial sediments consisting of sand and clay (Stevens et al., 2017; Wolfe & Kerr, 2014). River Lake is part of the Cameron River system, but the lake is also fed by several ephemeral streams draining networks of smaller lakes and ponds. Their intermittent, low flows drive semi-annual icing formation in their downstream channels. The Baker Creek basin is 165 km^2 and is characterized by a chain of 349 lakes connected by short channels with highly variable stream connectivity (Phillips et al., 2011; Spence & Hedstrom, 2018). Streamflow has been monitored in Baker Creek at the outflow of Lower Martin Lake since 1983 by the Water Survey of Canada (Station ID: 07SB013) (Spence & Hedstrom, 2018). The icing sampled at Baker Creek is located along a channel downstream of a small unnamed lake which flows into Vital Lake to the south and continues to Lower Martin Lake. Jackfish Lake is located within Yellowknife city limits, and supplies water to an icing directly to its east, on the other side of a highway embankment.

Jackfish Lake has been impacted by a legacy of anthropogenic impacts from mining emissions and municipal activities. A diesel-power generating station which discharges warm water is located on the lake (Sivarajah et al., 2021). Nutrient enrichment from runoff from the solid waste disposal site north of Jackfish Lake in combination with climate warming in the region has led to eutrophication of the lake (Sivarajah et al., 2021). A summary of site-specific physical characteristics for icings within the River Lake and Baker Creek catchments is provided in Tables 2-1 and A1-2.

2.3.3 Sample collection methods

2.3.3.1 Ice

Ice cores were collected along a transect from the upstream to the downstream end of each icing. Cores were extracted using a Dewalt SDS Max hammer drill with an AMS 2-3/8" diameter core auger with carbide teeth. Three to seven locations were sampled from each icing on River Lake and Baker Creek (Figure 2-2). Individual ice cores were separated into three to four 30 cm sections and each section was processed separately for water chemistry; the 30 cm core section intervals of each icing sample were classified as top (T), middle (M), and bottom (B). At S1 and S5a, a composite ice sample consisting of 10 to 15 full depth cores from the same area was collected to provide a more integrated assessment of bulk water chemistry. In addition, the icing near Jackfish Lake was sampled for 25 surficial cores (~ 10 cm depth) (Figure 2-9). At several icings, water was encountered at the bottom of drill holes or flowing partway through the icing. These samples were collected and labelled as "basal water" and "intra-icing water" respectively. Several core sections from S6 were lost in transport and are not included in this study.

2.3.3.2 Water

Lake and stream water samples were collected directly below the ice surface through a hole drilled with an ice auger. Water was filtered on-site using a peristaltic pump fitted with Teflon lines and attached to a 0.45 μm high-capacity Polyethersulfone (PES) in-line capsule filter. Raw water was run through the pump lines for three minutes before filling sample vials with filtered water. To avoid oxidation of reduced chemical species, vials were filled using an anoxic sampling technique in which the pump line was placed in the bottom of the vial and water was allowed to overflow approximately three full sample volumes before the vial was capped. At focal lakes (lakes upstream of S1, S5a, S5b), dissolved oxygen concentration and oxidation-reduction potential (ORP) measurements were taken at 1 m intervals using a YSI (EXO2) water

quality meter to assess redox conditions in the water column. To further explore the influence of anoxia on source water chemistry, dissolved sulfide (S^{2-}) and ferrous iron (Fe^{2+}) concentrations were quantified in water samples from the upstream lake at S1 on April 17th and 21st, 2021 using a Hach DR1900 spectrophotometer at the field site. This site was chosen due to ease of access to transport the spectrophotometer safely, and because this small lake typically becomes anoxic during the winter.

At Jackfish Lake, regular water quality monitoring is conducted by the Aurora Research Institute including one wintertime sampling date during our study period (winter 2021/2022). Data from this sample was used to compare Jackfish Lake icing chemistry to upstream source water.

2.3.4 Ice core processing

To minimize contamination from the core barrel, the outer layer of each core (~1-2 mm) was removed using a combusted straight-razor blade, which was rinsed with 30% v/v ethanol between cores. Processing was performed on a sterile surface covered with combusted aluminum foil. Processed cores were placed into sterile Whirl-Pak bags and kept frozen until filtration for chemical analyses. Prior to filtration, ice cores were thawed in the dark at 4 °C. Thawed ice samples were filtered with a 0.45-µm Sterlitech PES filter in the laboratory, except samples for DOC concentration and DOM composition which were filtered using muffled (450ºC for 4 h) glass fibre (Whatman GF/F 0.7-µm nominal pore size) filters.

2.3.5 Sample processing for chemical analyses

We analyzed thawed icing water and winter source water for major cations (Ca^{2+}, K^{+}, Mg^{2+}, Na^{+}), major anions (Cl^{-}, SO_4^{2-}), trace metals (Al^{3+}, dAs, Ba^{2+}, dCo, dCr, dCu, dFe, dMn, Ni^{2+}, dV, Zn^{2+}), nutrients (total dissolved nitrogen (TDN), ammonium (NH_4^{+}), nitrite + nitrate (NO_2^{-} +NO_3^{-}), water isotopes ($\delta^{18}O$-H_2O and $\delta^{2}H$-H_2O), and DOC concentration and DOM composition (via fluorescence spectroscopy) to investigate variation in flow paths and water sources to icings and to explore seasonal variation in winter water chemistry.

Samples collected for $\delta^{18}O$-H_2O and $\delta^{2}H$-H_2O were filtered into 2 mL glass vials without headspace. Samples for DOC concentration were filtered into 40 mL pre-combusted glass EPA vials and acidified to pH 2 using trace-metal grade hydrochloric acid, and samples for DOM composition were filtered into 40 mL pre-combusted amber glass EPA vials. Samples for NH_4^{+}

were filtered into 50 mL plastic bottles pre-filled with trace-metal grade hydrochloric acid and frozen until analysis. Samples for major cations and trace metals were filtered into 15 mL trace-metal free centrifuge tubes and acidified to pH 2 using trace metal grade nitric acid. Samples for TDN were filtered in a 40 mL glass EPA vial. Samples for NO_2^-+NO_3^-, major anions and major cations were filtered into 2 mL ion-chromatography (IC) vials and samples were frozen until analysis.

2.3.6 Sampling coverage

All ice cores were analyzed for the full suite of organic and inorganic constituents described above. At non-focal sites (S3, S6, S8, BC), lake and stream samples were not analyzed for water isotopes, NO_2^-+NO_3^-, NH_4^+, or DOM composition. At Jackfish Lake, analyses for NO_2^-+NO_3^- and NH_4^+ were not run on one icing sample due to lack of sample volume.

2.3.7 Chemical analyses

Analyses for TDN, NO_2^-+NO_3^-, NH_4^+, major cations and anions, and trace metals were conducted at the ISO-certified Taiga Environmental Laboratory in Yellowknife, NT where NO_2^-+NO_3^-, major cations and major anions were analysed via ion chromatography, trace metals via inductively coupled plasma mass spectrometry (ICP-MS), TDN via chemiluminescence-pyrolysis, and NH_4^+ via colorimetry (APHA et al., 2017a, 2017b; ISO, 2019; U.S. Environmental Protection Agency, 1996).

Analyses for DOC concentration and DOM composition, $\delta^{18}O$-H_2O and $\delta^{2}H$-H_2O were conducted at the University of Alberta, where $\delta^{18}O$-H_2O and $\delta^{2}H$-H_2O were measured using a L2130i Isotope + Gas Concentration Analyzer (Picarro), DOC concentration was measured using a Shimadzu TOC-L analyzer, and DOM composition was measured using a Horiba Aqualog spectrofluorometer. DOC concentration was determined as non-purgeable organic carbon (NPOC) and measured via high-temperature catalytic oxidation (HTC). MilliQ blanks and reference waters were analyzed routinely to measure instrument drift and remained within 5% of accepted values. References were made using caffeine and KHP standards (AccuSPEC, SCP Science). A ten-point standard curve was constructed for each run, with concentrations ranging to a maximum of 60 ppm. Evaluation of DOC concentration was determined as the mean of the best three of five sample injections that had a coefficient of variation < 2%. DOM composition was assessed via fluorescence spectroscopy. Fluorescence excitation emission matrices (EEM)

were constructed across excitation wavelengths spanning 230–500 nm at 5-nm increments, and emission wavelengths spanning 300-600 nm at 2.33-nm increments. Raw EEMs were corrected for inner-filter effects, normalized to Raman units, and blank corrected (Hansen et al., 2018).

2.3.8 Physical data

To better link chemical variation of icings to drivers of icing formation, physical data was collected at several sites. A trail camera was installed at the S5b icing on October 11th, 2020 (Figure 2-2) and collected photographs at 11:00 and 13:00 each day until the data was retrieved on October 7th, 2021. From this data, overflow events were documented and classified into "overflow" and "partial overflow" categories. Partial overflow events were identified as overflow that filled less than half of the image, whereas full overflow events filled most of the image (Figure A1-1). Snow accumulation was also documented and classified into either "light" which was identified as a small change in snow accumulation or "heavy" which was characterized by larger increases (Figure A1-1). We did not distinguish snowfall from snow drift in this study.

A pressure transducer (Hobo U20) was installed on the bottom of the lake upstream of S5a in Fall 2020 to provide water depth hourly from September 16th, 2020, to October 7th, 2021. At BC, Environment and Climate Change Canada maintains a permanent pressure transducer (Campbell Scientific CS451) in the lake immediately upstream of the icing, which records water depth data on a half-hourly basis. Pressure records from the submerged transducers were first corrected using concurrent records of nearby atmospheric pressure, and then converted to water depth. To present water levels relative to a consistent datum, benchmarks were established at S5a and BC and were used to connect water level surveys immediately after transducer installation and subsequent retrieval, and twice more at BC during the logging period. Hourly (S5a) and half-hourly (BC) water level values were averaged to produce daily values.

To determine the approximate dates of ice on versus ice off for source water lakes, Sentinel-2 L2A satellite imagery was obtained from modified Copernicus Sentinel data [2021]/Sentinel Hub (Sinergise Ltd, 2021). Lake surface areas were measured by tracing each feature in Google Earth. Daily maximum temperatures recorded from 2020-2022 were obtained from the Yellowknife A meteorological station (ECCC, 2022b).

2.3.9 Statistical analyses

All statistical analyses were performed in R 4.1.1 (R Core Team, 2022). Sampling ceased at the onset of spring conditions, which was demarcated by daily maximum temperatures consistently above 0 °C. These conditions occurred on May 5, 2021 (Figure A1-2) (ECCC, 2022b).

To explore variation in water sources to icings, $\delta^{18}O\text{-}H_2O$ and $\delta^{2}H\text{-}H_2O$ were used to calculate deuterium excess (d-excess), as $d = \delta^{2}H\text{-}H_2O - (8 * \delta^{18}O\text{-}H_2O)$ (Pfahl & Sodemann, 2014). Deuterium excess values reflect deviation from the Global Meteoritic Water Line (GMWL), and are driven by evaporative conditions (Gibson et al., 2020). Values reflect the influence of evaporation compared with equilibrium fractionation on water isotopic ratios (Brooks et al., 2014; Gibson et al., 2020; Smith et al., 2015). The average d-excess of precipitation is 10, and d-excess values below this value indicate increasing evaporation in surface waters (Brooks et al., 2014). Boxplots were used to visualize d-excess across different sites, and across ice versus source water.

A correlation analysis using Pearson's r using the packages *stats* and *corrplot* was implemented to explore relationships between chemical parameters and select variables of interest (Wei & Simko, 2021) (Figure A1-3). Chemical concentrations below the detection limit were set to half the detection limit (U.S. Environmental Protection Agency, 2000). Major cations were analyzed as their molar sum to avoid collinearity.

A parallel factor (PARAFAC) analysis was run to analyze EEMs using MATLAB and the drEEM toolbox, following Murphy et al. (2013). PARAFAC analysis decomposes EEMs into underlying components and quantifies the relative contribution of each component to the total fluorescence signal (Murphy et al., 2013). To increase model robustness and allow for validation (Murphy et al., 2013), the global PARAFAC included study site-specific samples from winter, spring and summer (n=98); however, only winter samples (n=65) are included in this chapter. The final model, identifying three components, explained 99.8% of sample variance, and was validated using a split-half analysis. Fluorescence components were matched to published components in the OpenFluor database, and all components matched with similarity scores > 0.95 for both excitation and emission spectra (Murphy et al., 2013).

A principal component analysis (PCA) was conducted using the *stats* package to explore chemical variation of icing water and open winter flow across and within-sites (Wickham, 2016).

To visualize differences in raw chemistry between ice and open winter flow, and to compare variation in carbon source and reactivity between icings and open winter flow, chemistry data and PARAFAC components were visualized using point plots (Wickham, 2016).

To explore within-icing chemistry at greater spatial resolution, icing and source water chemistry from the JL icing were visualized using a grid plot showing chemical concentrations at each sampling point, with latitude and longitude coordinates displayed as Universal Transverse Mercator (UTM) coordinates (Wickham, 2016).

2.4 Results

2.4.1 Physical observations of icing formation processes

Satellite imagery indicated that the ice-covered period at all upstream lakes began on Oct 24th, 2020, and ended by May 27th, 2021 (Figure A1-4; Figure A1-5). Trail camera photos at S5b show the beginning of icing formation on November 3rd, 2020, and a total of 12 large overflow events and five partial overflow events during the winter (Figure 2-3). Overflow events were most frequent from November to December, during which time five full overflow events and four partial overflow events occurred. This period was characterized by an onset of cold conditions and notable temperature fluctuations; temperatures peaked at 1.4 °C on December 3rd and fell to -37.9 °C by December 16th, and several warming intervals near or above 0 °C occurred in November (Figure 2-3). Most of the partial overflow events (four of five) during this period spanned less than 24 hours, whereas full overflow events usually lasted several days. Overflow events become more sporadic after December 25th (with one event on Jan 7th and another on Mar 3rd), and temperatures were consistently cold (mean -20° C) during this period (Figure 2-3). The frequency of overflow events then increased substantially with a series (five) of large events beginning on March 24th, consistent with several warming intervals and temperature fluctuations from a minimum of -14.1 °C on March 24th to 9 °C on April 20th (Figure 2-3). Precipitation in the open water season preceding icing formation (May-October 2020) totalled 233 mm (ECCC, 2022b).

In 2020-2021, water levels in lakes sourcing the BC and S5a icings show similar patterns reflecting the overflow and temperature patterns described for S5b (Figure 2-4). Lake levels declined modestly (~6-10 cm) from October-December 2020 and remained low until mid-March at BC and early-March at S5a; temperatures during this period (December-early March) were generally cold (average -19.5 °C), with a warming interval, described above, in early December (Figure 2-4). In early March, water levels rose quickly (~40-80 cm) until they peaked in mid-April and late-March at BC and 5a, respectively. Temperatures during the period of rising lake levels (March to mid-April) were moderate, with daily maximum temperatures averaging -10 °C and ranging from -19 °C to 6.5 °C. Thereafter, water levels declined substantially (~40-60 cm) and rapidly (over 16-22 days) in the two systems. During the period of rapid water level decline, conditions were warm at S5a (mean -9.6 °C, maximum -1.6 °C) and warm and sunny at BC (mean -4.1 °C, maximum 9 °C) with temperatures near or above zero (Figure 2-4).

In winter 2021-2022, a similar pattern of rising and then rapid decline in lake levels is observed at Site BC, with the rapid decline similarly associated with temperatures above 0 °C (increasing by ~26 °C over the course of three months to reach 7.5 °C at lake level peak (Figure 2-5). In contrast, water levels were relatively constant and lower than in 2021 at S5a during winter 2021-22 (Figure 2-5). Field observations showed icing formation at BC in 2022, but not at S5a. Precipitation in the months preceding icing formation (May-October) in 2021 totalled 162 mm (ECCC, 2022b).

2.4.2 Water chemistry of icings and source waters: an overview

Icings at S1 and S3 displayed distinct isotope signatures, with elevated d-excess (-2.6 to 10.8) compared to other icing features (-24.1 to -6.7), indicative of less evaporative loss (i.e., lower surface exposure and/or lower exposure to evaporative losses) for this water (Figure 2-5). Sampling of upstream lake water at S1 showed that lake water had markedly lower d-excess (-13.8) than its downstream icing (Figure 2-5). In addition to the distinct isotopic signatures of S1 and S3 icings, no visible channel connecting S1 to the upstream lakes was observed in the winter of 2021, while at S3, outflow from the upstream pond is diffuse drainage through a wetland and sandy soils. Taken together, this suggests that S1 and S3 are groundwater- rather than lake-fed, with water movement through bedrock fractures and suprapermafrost flow through coarse-grained soils.

Icing meltwater across all sites was generally more dilute in concentrations of major cations, trace metals, TDN, and DOC compared to paired stream and upstream lake water, except for some sites (S5b, S5a, S8) which had several core sub-sections that showed isolated patches of higher concentrations (Figure 2-6). Some sites displayed icing chemistry distinct from upstream lake water (e.g., S1, S8), while others displayed similar chemistry across all sample types (e.g., BC) (Figure 2-6). Similarly, some sites showed higher within-icing chemical variation (S5a, S5b, S8) than others (S1, S3, S6, BC), although this varied depending on chemical constituents (Figure 2-6, Figure 2-7). Intra-icing and basal water were consistent with icing water chemistry, except for several basal water samples (S5b, BC) which tended to be more concentrated (Figure 2-7). Based on patterns of isotopic composition and variation in within-icing and source water chemistry, we grouped icings into three key system types: groundwater-fed icings (S1, S3), large-lake fed icings (S5b, S6), and small lake-fed icings (S5a, S8, BC), and move forward with this demarcation using subscripts GW (groundwater), LL (large lake) and SL (small lake) to distinguish between system types.

Analyses of DOM composition via PARAFAC analyses resulted in a validated model with three different components: two humic-like components which are associated with aromatic, high molecular weight compounds typically of terrestrial origin (C1 and C2), and one protein (tryptophan)-like component, which is characteristic of DOM of microbial origin (C3), (Figure A1-6, Table A1-3) (Gonçalves-Araujo et al., 2016; Guéguen et al., 2014; Imbeau et al., 2021, 2021). Overall, icing samples across all sites had considerable variation in percentage of protein-like (1-71%) vs. humic-like (29-99%) DOM (Figure 2-8). In contrast, source water DOM was relatively similar between sites and dominated by humic-like components (Figure 2-8).

2.4.3 Groundwater-fed icings

Meltwater from groundwater-fed icings at $S1_{GW}$ and $S3_{GW}$ displayed little variation in DOC, major cation, trace metal, and TDN concentrations (Figure 2-6). However, concentrations of NO_2^-+NO_3^- at $S1_{GW}$ were more variable than other chemical constituents at this site (Figure 2-7). Furthermore, icing meltwater at $S1_{GW}$ was chemically distinct from its upstream lake, which was more concentrated in DOC, major cations, and trace metals (Figure 2-6). DOM sourced from $S1_{GW}$ icing meltwater was primarily composed of humic-like material (77-92% C1+C2), whereas

$S3_{GW}$ had a lower proportion of humic-like DOM (38-66% C1+C2) (Figure 2-8). Basal water and intra-icing water were not encountered at these sites.

2.4.4 Lake-fed icings: overview

Compared to groundwater-fed icings, most lake-fed icings displayed somewhat greater within-icing chemical variation of DOC, major cations, inorganic nitrogen, TDN, and trace metals (Figure 2-6, Figure 2-7), and had DOM largely composed of humic-like material (34-99% C1+C2) (Figure 2-8). Differing patterns of within-icing chemical variation were observed between icings fed by large lakes ($S5b_{LL}$, $S6_{LL}$) and those fed by small lakes/ponds ($S5a_{SL}$, $S8_{SL}$, BC_{SL}), with further variation that appeared driven by lake-to-icing transit distance.

2.4.4.1 Icings fed by large lakes

$S5b_{LL}$ and $S6_{LL}$ are sourced by relatively large lakes and have similar transit distances from source waters to icings (200-300 m) (Table 2-1). At $S5b_{LL}$, isotopic composition of icing meltwater and source waters were consistent with each other, ranging from -23.5 to -13.6‰, with the exception of one icing meltwater outlier (-7.9‰) (Figure 2-5). At $S6_{LL}$, icing d-excess similarly varied between -24.1 and -15.6‰; source water isotope data was not available at this site. Icing samples at $S5b_{LL}$ and $S6_{LL}$ were chemically consistent within each icing, with the exception of three out of eight icing cores at $S5b_{LL}$, which were more concentrated in Zn^{2+}, dCr and dCu (Figure 2-6). Icing meltwater at these sites were consistent with paired source water samples, except for one out of three late-winter lake samples at $S6_{LL}$ which was more concentrated in major cations, trace metals and TDN (Figure 2-6). One basal water sample at $S5b_{LL}$ was enriched in major cations, trace metals and TDN (Figure 2-6).

2.4.4.2 Icings fed by small lakes

$S5a_{SL}$, $S8_{SL}$ and BC_{SL} are sourced by small lakes and vary in transit distance between source waters and the onset of icing formation (128, 376 and 352 m, respectively) (Table 2-1). Within-icing chemical variation at $S5a_{SL}$ and $S8_{SL}$ was pronounced when compared to larger lake-fed icings (Figure 2-6, Figure 2-7). Additionally, icing meltwater was more distinct from paired source waters at these sites (Figure 2-6).

Despite similar d-excess between icing meltwater and source water at $S5a_{SL}$, this site showed the greatest within-icing chemical variation of all sampled icings (Figure 2-5, Figure 2-6, Figure 2-7). Icing meltwater at this site was highly variable in DOC, NO_2^-+NO_3^-, NH_4^+, and had

elevated Al^{3+} (up to 141 µg L^{-1}), and dFe (up to 268 µg L^{-1}) concentrations (Figure 2-7, Figure A1-7). Several lake samples at $S5a_{SL}$ showed concentrations of DOC, major cations, TDN and trace metals that were similar to the higher concentration icing samples (Figure 2-6); the above constituents peaked in lake samples on March 18th and dropped by 1-2 orders of magnitude by March 22nd, corresponding to the lake outflow event (Figure 2-6, Figure A1-7). Several stream samples at $S5a_{SL}$ were similarly enriched in the above constituents, with concentrations peaking on March 22nd; streamwater dFe was particularly elevated, ranging from 467-765 µg L^{-1} (Figure 2-6, Figure A1-7).

At $S8_{SL}$, core sampling locations ranged from 40-376 m downstream of the lake, with most samples located 120-376 m downstream. Overall, icing meltwater was less concentrated than source water at this site (Figure 2-6), and within-icing chemistry was less variable at $S8_{SL}$ compared to $S5a_{SL}$ with respect to DOC, NO_2^-+NO_3^-, NH_4^+, Al^{3+}, and dFe (Figure 2-7). Compared to groundwater- and large lake-fed icings, metal concentrations were also elevated at this site in icing (92 µg L^{-1} Al^{3+}, 873 µg g L^{-1} dFe) and lake (226 µg L^{-1} Al^{3+}, 5580 µg L^{-1} dFe) waters (Figure 2-7).

In contrast to the other two shallow lake-fed icings, the BC_{SL} icing showed little variability in within-icing chemistry However, several basal and intra-icing samples were more concentrated in DOC, and NO_2^-+NO_3^- compared to icing meltwater at this site (Figure 2-6, Figure 2-7). Metal concentrations in icing meltwater at BC_{SL} were not as high as S5a and S8, reaching concentrations of 62 µg L^{-1} and 20 µg L^{-1} for Al^{3+} and dFe, respectively (Figure 2-7). Notably, soil characteristics at the Baker Creek site feature an organic soil layer underlain by glaciolacustrine clay, which acts as an aquitard (Table 2-1).

2.4.5 Spatial variation in icing chemistry: Jackfish Lake

To explore within-icing chemical variation at greater spatial resolution, the Jackfish Lake icing was extensively sampled for surficial ice and intra-icing water, for comparison with upstream lake water (Figure 2-9). Ice samples were all below detection (<20 µg L^{-1}) for dFe, which was removed from subsequent analyses at this site. Although constituents showed clear correlation to one another (i.e., indicating coherent patchiness in concentration across space) (Figure A1-8), this patchiness did not follow a clear spatial pattern (Figure 2-9). Constituent concentrations in intra-icing water also showed no clear relationship to icing meltwater collected

in the same locations, but were generally concentrated in major cations and Al^{3+}, and dilute in DOC, NO_2^-+NO_3^- and NH_4^+ compared to icing samples (Figure 2-9). At one site where two ice core sections were available across the full depth of the icing (~60 cm), DOC concentrations showed stark variation over depth (4 and 47 mg L^{-1}) (Figure 2-9). Upstream lake water collected in February 2021 at Jackfish Lake was similar to icing meltwater in DOC, major cation, and NO_2^-+NO_3^- concentrations, but was more concentrated in NH_4^+ and less concentrated in Al^{3+} compared to most icing samples (Figure 2-9).

2.5 Discussion

2.5.1 Fill-and spill hydrology and winter air temperatures drive icing dynamics

Our observations show that water movement through small lake systems during the winter is an important driver of icing formation and overflow events. Lake level records highlight the movement of water in these small systems occurring well before freshet, which align with observations of increasing winter baseflow occurring over the past several decades in the region (Spence et al., 2015). The importance of winter streamflow (influenced by antecedent precipitation) via processes analogous to fill-and-spill runoff generation to icing formation and inter-annual variability in icing density on the Canadian Shield has been previously characterized, and is consistent with our results (Ensom et al., 2020; Morse & Wolfe, 2015). The influence of fill-and-spill dynamics on icing formation is evident through lake level records and antecedent precipitation. In 2020-2021, high levels of antecedent precipitation, and the exceedance of lake storage thresholds resulted in relatively abundant icing presence in the River Lake catchment. Conversely, the following year (2021-2022), antecedent precipitation was markedly lower, and hydrological disconnectivity prevented icing formation at all study sites on River Lake; lake levels remained consistently low at $S5a_{SL}$ during this year. However, the Baker Creek catchment, which is fed by a chain of larger lakes, and where residence time of the BC icing source lake is likely low (Phillips et al., 2011), low antecedent precipitation during summer-fall 2021 may have been less of a constraint on icing formation during winter 2021-22.

Air temperature appeared as an additional control on icing formation (see also (Morse & Wolfe, 2015, 2017, Crites et al., 2020)). Our results are indicative of three key stages of icing growth as they relate to winter air temperatures and lake hydrology. First, a period of cold air temperatures was associated with initial icing growth at $S5a_{SL}$, $S5b_{SL}$, and BC_{SL}. Previous work

has outlined the importance of cold temperatures in enabling initial freezing and obstructions to flow, which drive the onset of icing formation (Crites et al., 2020). However, this period was interspersed with warming intervals, which were associated with an overflow event $S5b_{SL}$; this warming and associated overflow appeared to enable stable lake levels during this period, and have previously been established as a driver of icing formation (Morse & Wolfe, 2015). Following this period, a period of sustained cold air temperatures occurred. This period was associated with minimal overflow and icing growth at $S5b_{SL}$, and a rapid rise in lake levels at $S5a_{SL}$ and BC_{SL}. These rising lake levels point towards the formation of an ice dam at each lake's outlet, which was reinforced by visual observations of lake ice doming at $S5a_{SL}$. Finally, a rapid temperature increase with movement toward spring caused ice dams to break, permitting a series of large outflows of water at $S5b_{SL}$. These outflows may have eroded existing ice masses, which was observed at $S5a_{SL}$ where ice was hollowed out beneath the icing surface. During this warm period, overflow events returned and increased in frequency.

2.5.2 Lake basin characteristics as a first order control on icing chemistry

Across icings, chemistry was largely driven by water source, where icings fed by small lakes ($S5a_{SL}$, $S8_{SL}$, BC_{SL}) displayed distinct chemistry compared those fed by deeper lakes ($S5b_{LL}$, $S6_{LL}$). Wintertime chemistry within shallow lakes is driven by the development of anoxia through the water column and solute exclusion from the formation of ice cover. Additionally, processes occurring within lakes also influenced the nature of icing chemistry, including diffusive efflux across the sediment-water boundary, and possible inflows of oxygenated water.

In small lakes, variation in wintertime lake chemistry is enhanced through the development of anoxia within the water column, and lakes with greater sediment surface area: lake volume tend to experience greater winter oxygen depletion rates (Mathias & Barica, 1980). Past work on the Canadian Shield and in northern Alaska demonstrated reduced wintertime variation in water chemistry in large lakes, and minimal oxygen depletion in lakes with maximum depths exceeding 4 m (Leppi et al., 2016; Palmer et al., 2019). These patterns are consistent with our results, where elevated redox-sensitive element (dAs, dFe) concentrations were observed in small lakes and were reflected in downstream icing samples. Solute exclusion is also more pronounced in shallow lakes and may cause enrichment of chemical concentrations in surface waters as the ice front advances throughout the winter (Santibáñez et al., 2019); given the

ephemeral nature of the overflow events that form icings, this may be an additional factor driving chemical variation within small lake-fed icings. At some sites, enrichment of major cations and trace metals may additionally occur as a result of enhanced sediment-water interaction occurring in source waters. For example, at $S5a_{SL}$, several ice and source water samples were highly concentrated in trace metals and cations, compared to the bulk of remaining samples; concentrations peaked in source waters before the ice dam breakup at this site and fell dramatically afterwards. This suggest that progressive anoxia and prevention of outflow may have allowed major cations and metal (As, Fe, Mn) concentrations to build up over time through diffusive efflux across the sediment-water interface (Hamilton-Taylor & Davison, 1995), which likely facilitated the observed shift in icing and source water chemistry. Alternatively, at deeper lakes unlikely to have anoxic outflows ($S5b_{LL}$,$S6_{LL}$) (Palmer et al., 2019), high concentrations of metals (Al^{3+}, dFe, dCr, dCu, Zn^{2+}) may be associated with substantial interaction with sediment along constrained flowpaths that feed icings. This may be attributed to the very shallow outflow bays at $S5b_{LL}$ and $S6_{LL}$, where water interacts with substrate for some time before transiting through the landscape.

While anoxia and cryoconcentration influenced lake chemistry, and thus icing chemistry, fill-and-spill hydrology in this region may have a significant influence on whether lakes, regardless of size, become anoxic during the winter. A study of shallow lakes in the Baker Creek basin documenting the winter cycling of dAs, dFe and dS showed that water column redox potential differed greatly depending on watershed hydrology during the year of study (Palmer et al., 2021). In particular, years of hydrologic isolation (i.e. lack of inflow) can cause lakes to become anoxic during the winter, while inflows of oxygenated water from upstream sources can maintain oxic conditions throughout the water column (Palmer et al., 2021). Similarly, our results showed the BC_{SL} icing to have lower concentrations of redox-sensitive metals compared to similarly small lake-fed icings. Notably, the Baker Creek basin above BC contains 33 lakes – three larger than 1 km^2 in size – connected by short channels with highly variable stream connectivity (Phillips et al., 2011), suggesting that the lake feeding this icing may have been well connected to the upstream landscape.

2.5.3 Physical properties of flow paths as a second order control of icing chemistry

Water chemistry varies along the source water to icing continuum due to processing occurring along flow pathways. We observed distinct patterns of chemical variation within and across small versus large lake-fed icings, and groundwater-fed icings. These patterns reflect additional drivers of icing chemistry, including the physical properties of, and transformation along, flow paths to sites of icing formation. Flow path distance and apparent flow path depth were important drivers of icing chemistry for both lake-fed and groundwater-fed icings. Longer flow path distances encompass more variability in depth to confining layers and oxygen exposure, facilitating a chemical shift between source waters and icings. At $S5a_{SL}$, where flow path distance was short, icing water reflected source water chemistry from both before and after the ice dam breakup, consistent with minimal transformations along flow paths to icings. At $S8_{SL}$, where flow path distance was long, source waters were notably concentrated in DOC, cations and trace metals compared to icing meltwater, and within-icing chemical variation was pronounced. However, this pattern was not observed at BC_{SL}, which has a long flow path distance but was characterized by icing chemistry that was overall similar to source waters. This may be attributed to a combination of hydrologic connectivity maintaining within-lake oxic conditions and thus a lack of redox transformations along the flow path to the BC_{SL} icing, and the presence of a clay aquitard that may have limited sediment-water interaction and enabled rapid conveyance along the icing channel.

Substrate characteristics also appeared to drive groundwater-fed icing ($S1_{GW}$, $S3_{GW}$) chemistry, where isotopic signatures were consistent with sources not exposed to high evaporative losses (Brooks et al., 2014; Cui et al., 2017). This finding is consistent with substrate characteristics at these sites, which are situated within outcrops of coarse-grained glaciofluvial sands that convey water quickly through the landscape. The lack of chemical variation within these icings reflects a lack of wintertime variation in their water sources. Additionally, the prevalence of protein-like DOM at these icing sites is indicative of water contributions from flow through deeper mineral soils, where humic-like OM tends to preferentially sorb and become protected (Oren & Chefetz, 2012).

2.5.4 Within-icing dynamics: effects of surficial, basal, and intra-icing flow

Within icings, solute exclusion, snow inclusion into icing layers, and sediment-water interaction, may have additionally controlled icing chemistry. These factors were likely

controlled by the nature of within-icing flow paths. Intra-icing and basal flow samples were generally more concentrated in chemical constituents compared to icing meltwater samples. In the case of intra-icing flow, solute exclusion with progressive transit through the icing may have enabled cryo-concentration. In fact, because slower freezing has been shown to exclude solutes more effectively, the buffered temperatures within icing layers relative to the icing (air-exposed) surface may lead to higher concentrations of solutes in intra-icing flow (Belzile et al., 2002). This is reinforced through icing chemistry available in higher spatial resolution at the JL icing, which displayed pronounced dilution of most chemical constituents in icing meltwater relative to that observed in intra-icing samples. Notably, inorganic nitrogen was not similarly concentrated in intra-icing flow at JL, which may be due to differences in exclusion factors between different ions; NO_3^- has been observed to be 2-10 times less prone to solute exclusion than Ca^{2+} and Mg^{2+} in Arctic lakes (Welch & Legault, 1986). Stark chemical variation across the surficial layer of the JL icing highlights the potential patchiness of icing chemistry over short distances. While this patchiness may be driven by seasonal chemical variation in source waters, as described above, temporal variation in air temperatures, which would drive varying degrees of solute exclusion at the icing surface may also be important. Surficial flowpaths may also contribute to chemical variation through incorporation of snow into icing layers. Snow inclusion may have occurred at $S5b_{LL}$, where one d-excess signature was substantially elevated relative to its counterparts, indicative of a precipitation signal. Isotopic characterization of icings in southwestern Yukon show similar inclusions of isotopically enriched snow into surficial icing layers (Michel, 2011).

Although basal flow may additionally subject water to interaction with sediment, our basal flow samples were not notably more concentrated than intra-icing flow samples. Thus, it is difficult to discern whether chemical differences between basal flow and ice cores are solely driven by solute exclusion, sediment-water interaction, or a combination of the two. While isotopic signatures of intra-icing and basal flow were not characterized in this study, isotopic analysis may be a useful tool to tease apart the effects of solute exclusion and sediment-water interaction across intra-icing and basal flow paths. Isotopic fractionation has been shown to occur during freezing, and slower freezing results in the preferential inclusion of heavier isotopes into ice, which may be used to discern variable freezing conditions between basal and intra-icing layers (Michel, 2011).

2.5.5 The dynamics of winter flow and implications at a watershed scale

The stark variability in icing chemistry observed in this study show the importance of lakes in creating dynamic wintertime hydrochemistry. Fill and spill hydrology, coupled with ice dam formation, strongly regulated overflow event timing and subsequent icing formation. Redox processes occurring within lakes were key drivers of distinct chemistry observed across icings, and variability across space was caused by differences in lake size and water sources (i.e., groundwater versus lake flow). The Taiga Shield features an incredibly high density of lakes, and it is likely that variation in lake basin characteristics, and thus, physico-chemical processes, lead to high temporal and spatial diversity in wintertime chemistry across small spatial scales. Given that the Taiga Shield comprises ~20% of North America's permafrost-covered area (Wang et al., 2019), the distinct wintertime hydrochemistry highlighted here shows the significant role this region may play in modifying wintertime chemical exports to larger aquatic networks. As climate warming shifts precipitation regimes to increase hydrologic connectivity and winter baseflow in this region (Spence et al., 2011) changes to winter stream chemistry may be significant, through the enrichment of redox-sensitive metals and other solutes in winter flow.

We show that lake ice accumulation, and icing formation have the potential to shift the composition of what is actively flowing through fluvial networks during the winter, and during the spring and summer as icings thaw and contribute to streamflow. Along wintertime flowpaths, solute exclusion selectively reduces chemical species in icing samples, and enables solute enrichment in flowing water. These results contrast with the common expectation that winter flow is necessarily dilute in organics and enriched in ions due to groundwater-dominated water sources to flow. Enrichment of ions and DOC in winter flow has been observed on the Taiga Shield (Spence et al., 2015); enrichment was attributed to early winter runoff generation events, which facilitate hydrologic connectivity and flow paths through shallow, organic soil layers. Solute enrichment in winter flow may have implications for biogeochemical cycling as this water combines to flow through the landscape during the winter, and as icings thaw in the spring and summer. Studies investigating solute enrichment under lake ice show significant DOC increases in the water column as lake ice forms, and particularly, the enrichment of high molecular weight, aromatic DOM into the liquid phase coupled with enrichment of labile, amino acid-like material in lake ice (Belzile et al., 2002; Imbeau et al., 2021; Santibáñez et al., 2019; Zhou et al., 2023);

however, the ability of organisms to use increased solute concentrations during the winter is not well studied (Jansen et al., 2021).

With levels of winter baseflow increasing in the subarctic over the past several decades (Crites et al., 2020; Spence et al., 2015), sufficient baseflow may become less of a constraint on icing formation, with winter air temperatures possibly becoming a more important factor driving icing formation in a warming climate. Climate warming is responsible for shorter, warmer winters across the subarctic, which may inhibit initial icing growth, or may augment icing growth over a shorter period due to more frequent incursions above zero (Crites et al., 2020; Morse & Wolfe, 2015). If climate warming increases the extent and magnitude of icings, then surface waters may become enriched in solutes during the winter, coupled with the delivery of dilute water to surficial flowpaths as icings thaw. If a similar partitioning of DOM, as described above, occurs during icing formation, icing thaw may have significant implications for carbon cycling as icing meltwater contributes to streamflow during the spring and summer. As solute enrichment of winter flow and chemical changes associated with icing thaw may persist through time and space across the subarctic, more work is needed to delineate their effects on carbon cycling. Lastly, as warming expands the spatial extent and occurrence of taliks in the region, continued subsurface flow through deeper flow paths enables the export of novel constituents to flow. While talik presence was not explicitly studied here, icings prove to be useful sentinels of hydrological change and can be used to explore the effects of warming on wintertime chemistry.

2.6 Conclusions

We investigated the influence of fill-and-spill hydrological processes on icing dynamics, and explored how icing chemistry was affected by varying water sources. Icing formation was dynamic, strongly mediated by fill and spill hydrology across years, and additionally controlled by winter air temperatures within years. Chemical variation within icings was controlled by physico-chemical processes occurring in lake basins, including anoxia, solute exclusion, and sediment-water interaction. Lake size governed these relationships, with greater within-icing chemical variation observed within icings fed by small lakes. While winter is commonly perceived as a hydrologically inactive period, the results of this study reveal the dynamic nature of winter flow. Trail camera records highlight the sporadic timing and apparent magnitude of overflow events, which may subsequently drive variation in icing chemistry and morphology.

Fill and spill dynamics also facilitated within-icing chemical variation through the formation of ice dams and subsequent sediment-water interactions; large outflows of water following ice dam breakup also led to the erosion of the icing feature at $S5a_{SL.}$ Chemically distinct from lake-fed icings, groundwater-fed icings displayed minimal within-icing variation, likely reflecting a lack of source water variation throughout the winter. Finally, longer flow path distances from upstream lakes to sites of icing formation drove distinct icing versus source water chemistry through reaeration of redox-sensitive metals and sediment-water interaction during transit. Flow paths within icing channels further modified icing chemistry through solute exclusion and sediment-water interaction.

This research provides a conceptual framework to understand how icing growth and chemistry may be influenced by hydrology, winter air temperatures, and lake basin characteristics; this may be used to frame future work investigating icing chemistry in the Taiga Shield and in other lake-rich lowland environments. Future work may consider icing sampling to characterize wintertime chemistry, however, the phenomenon of icing erosion observed at $S5a_{SL}$ presents a challenge in using icings to evaluate cumulative winter flow, as icing features can be transient depending on winter hydrology on the Canadian Shield. Furthermore, while our study highlights the dynamics of overflow event timing and magnitude, this data was limited in spatial and temporal scale. Therefore, future work should further characterize relationships between fill and spill dynamics, overflow events and icing chemistry across longer time periods and larger spatial scales.

2.7 Tables

Table 2-1. Description of physical features and discharge characteristics of lakes upstream from each sampled icing, and soil characteristics along transit distance to icings.

Site	Transit Distance [b] (m)	Soil Characteristics	Lake Surface Area (ha)	Lake Depth[a] (m)	Lake Bottom Characteristics[a]	Discharge Characteristics[a]
S1	390 / 486	Glaciofluvial, sandy	6.45	1	Thick layer organic matter	Ephemeral creek that forms during freshet and flows until mid-summer
S3	N/A	Glaciofluvial, sandy	N/A	N/A	N/A	Groundwater-fed icing, diffuse drainage from upstream pond through wetland
S5a	47 / 128	Glaciolacustrine, silty clay	3.03	~ 2-3	Thick layer organic matter	Ephemeral creek that forms during freshet and flows intermittently throughout summer
BC	211 / 352	Glaciolacustrine clay, overlain by 30 cm organic soil	8.11	Unknown, likely shallow	Unknown	Perennial stream
S6	236 / 299	Glaciolacustrine, silty clay	49.40	6	Unknown	Perennial stream
S5b	333 / 366	Bedrock at north end, glaciolacustrine at south	34.3	~ 4-5	Thin layer organic matter	Perennial stream
S8	26 / 376	Glaciolacustrine, silty clay and permafrost	4.61	Unknown, likely very shallow	Unknown	Perennial creek

[a] Field observations of lake depth, lake bottom and discharge characteristics. [b]Transit distance measured from lake outlet to nearest and furthest core sample, respectively

2.8 Figures

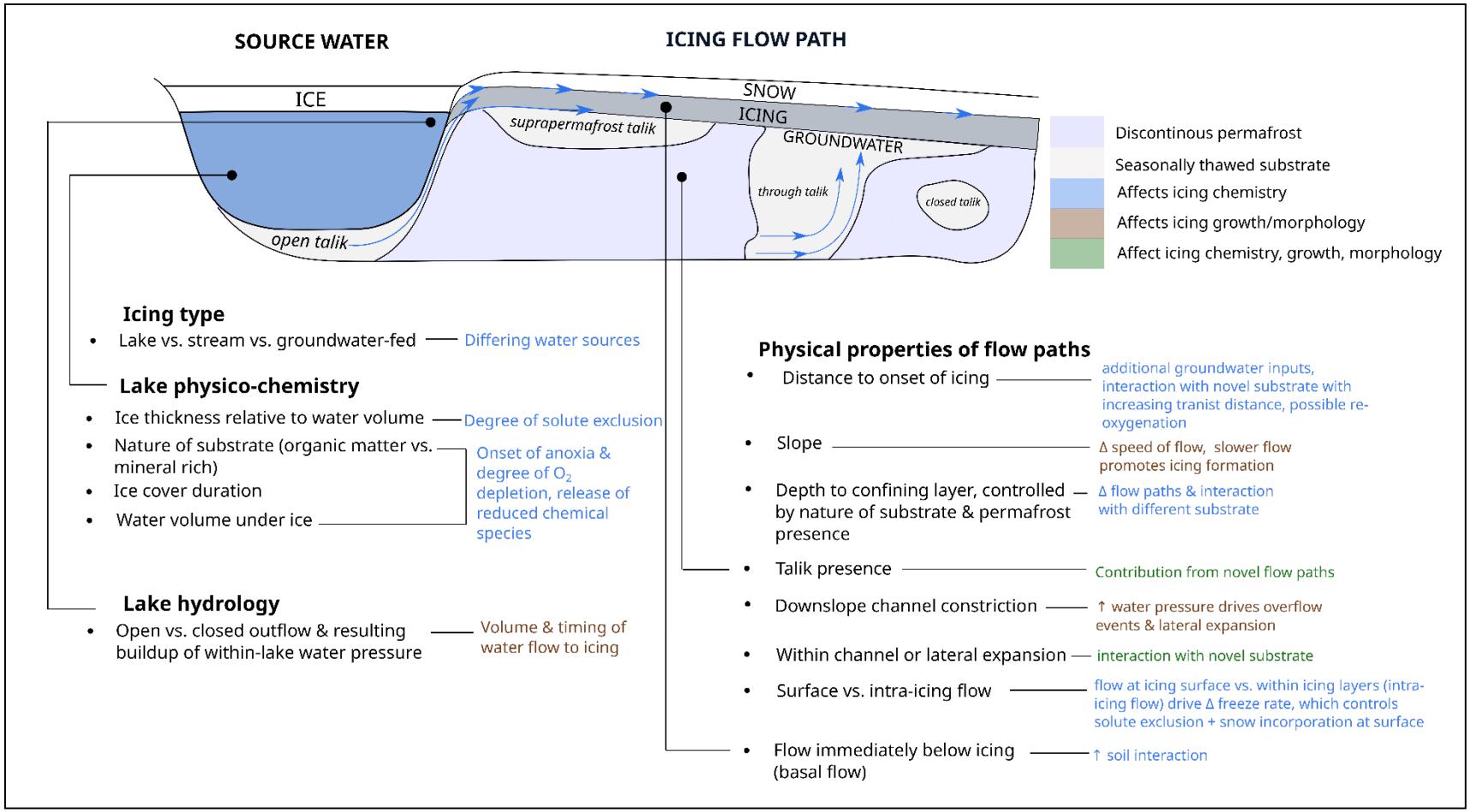

Figure 2-1. Conceptual model of icing formation outlining the effects of icing type, lake physico-chemistry, lake hydrology, and physical properties of flow paths on icing growth, morphology and chemistry.

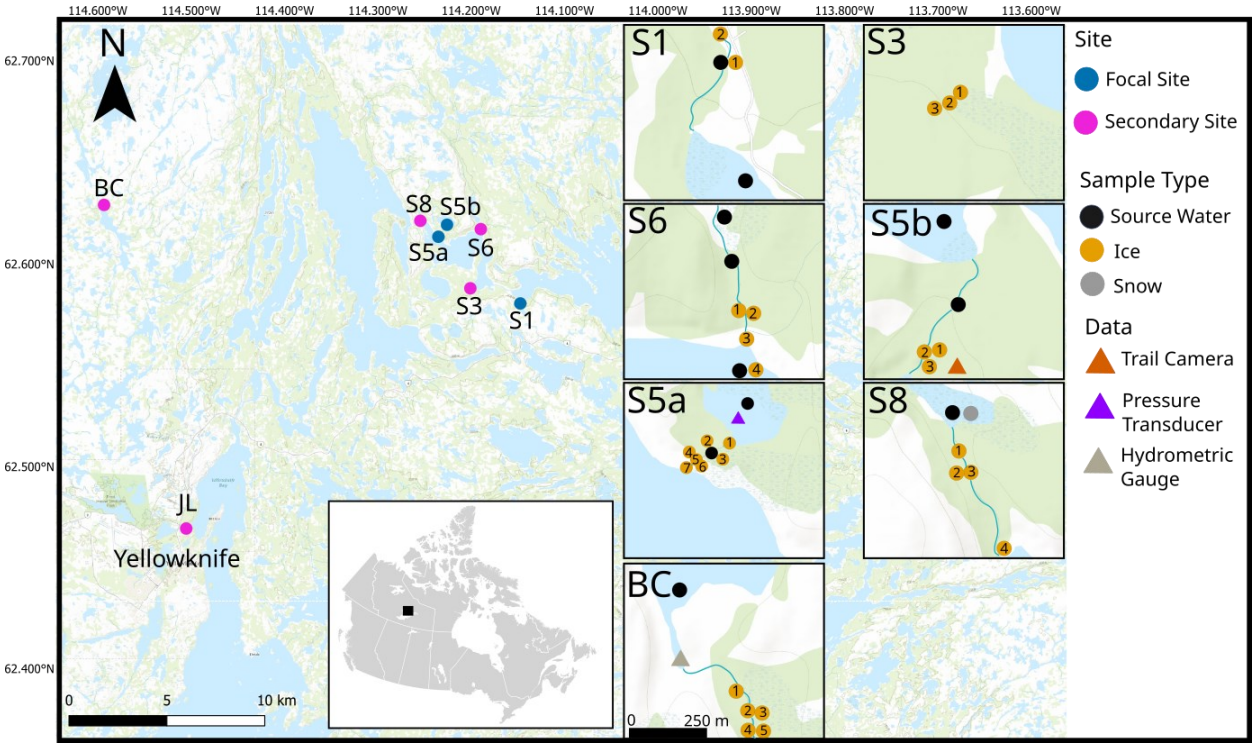

Figure 2-2. Sampled icing locations within the River Lake and Baker Creek watersheds. Focal sites with more frequent source water sampling (in blue), and secondary sites with limited source water sampling (in pink) are shown. Channels where ephemeral (S5a, S1) or perennial (S6, S5b, S8, BC) streams are located are shown as blue lines; no channel was observed at S3. Ice core locations are shown in yellow, with numbers corresponding to labels in Figure 2-6. Source water sampling locations are shown in black and snow sampling locations are shown in grey. A trail camera was installed at S5b, a pressure transducer at S5a and a hydrometric gauge is located at BC. Sampling locations within the Jackfish Lake icing are further detailed in Figure 2-9.

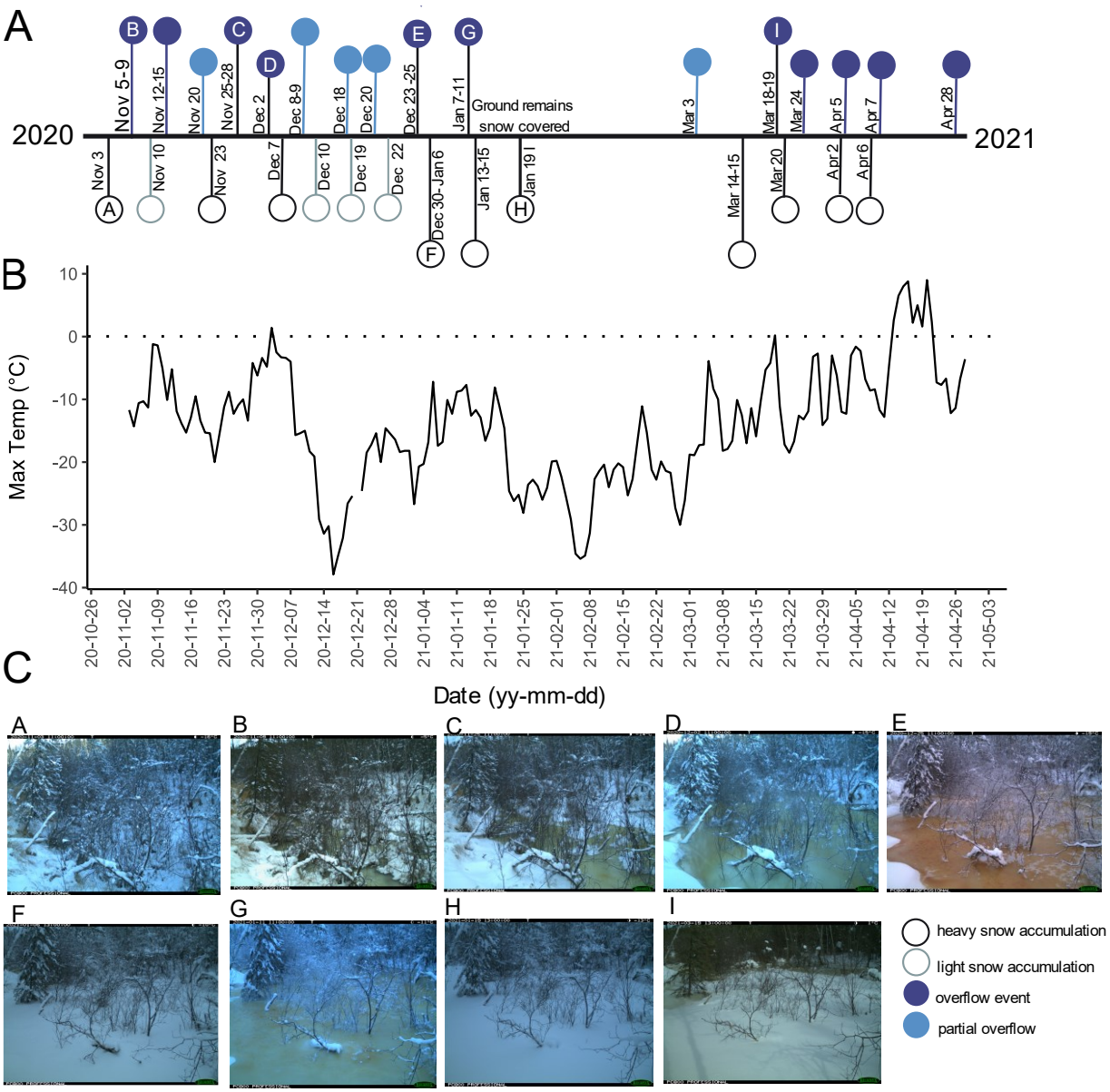

Figure 2-3. Panel A: record of overflow, partial overflow, snow accumulation, and light snow accumulation events at Site 5b from trail camera images (shown in Panel C) captured twice daily from October 10th, 2020, to October 7th, 2021. Images show the beginning of icing formation on November 3rd, 2020 and the last overflow event on April 28th, 2021. Panel B: Daily maximum temperature data during the study period, obtained from Yellowknife Station A from Environment and Climate Change Canada.

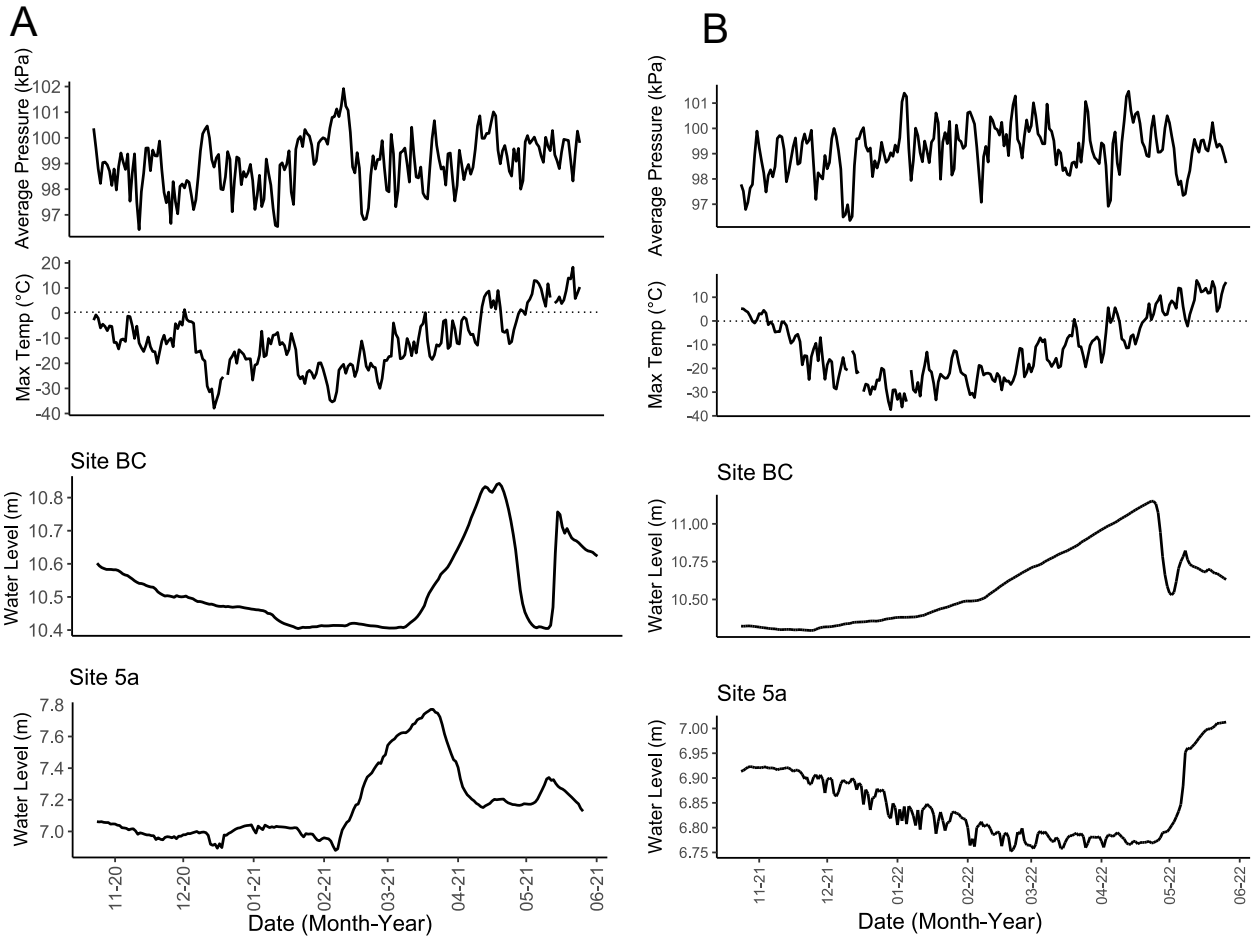

Figure 2-4. Daily atmospheric pressure, maximum temperature and water levels at lakes sourcing the BC and Site 5a icings . Panel A shows the period from Oct 24, 2020 to May 26, 2021. Panel B shows the period from Oct 24th, 2021 to May 26, 2022. In both panels, daily atmospheric pressure is an average value of 11 measurements taken at Yellowknife Station A, and maximum temperature data was obtained from the same station from Enviornment and Climate Change Canada (ECCC, 2022b).

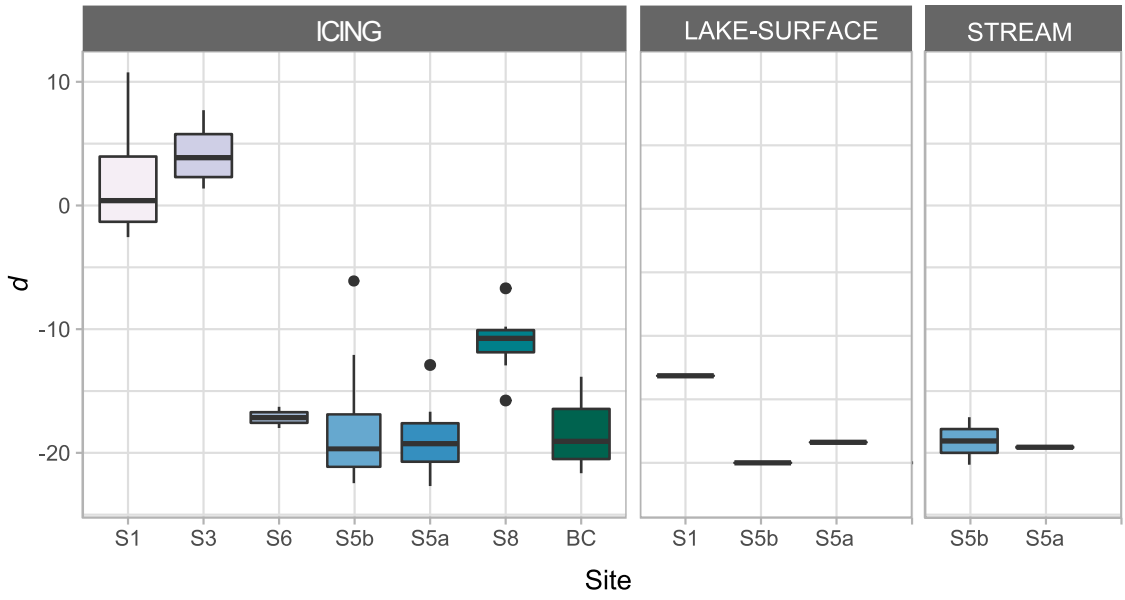

Figure 2-5. Boxplots of d-excess (d) of icing meltwater at seven sites and of paired lake surface and stream samples at focal sites (S1, S5b, S5a). Box plots show d-excess range, median, first and third quartiles, and outliers.

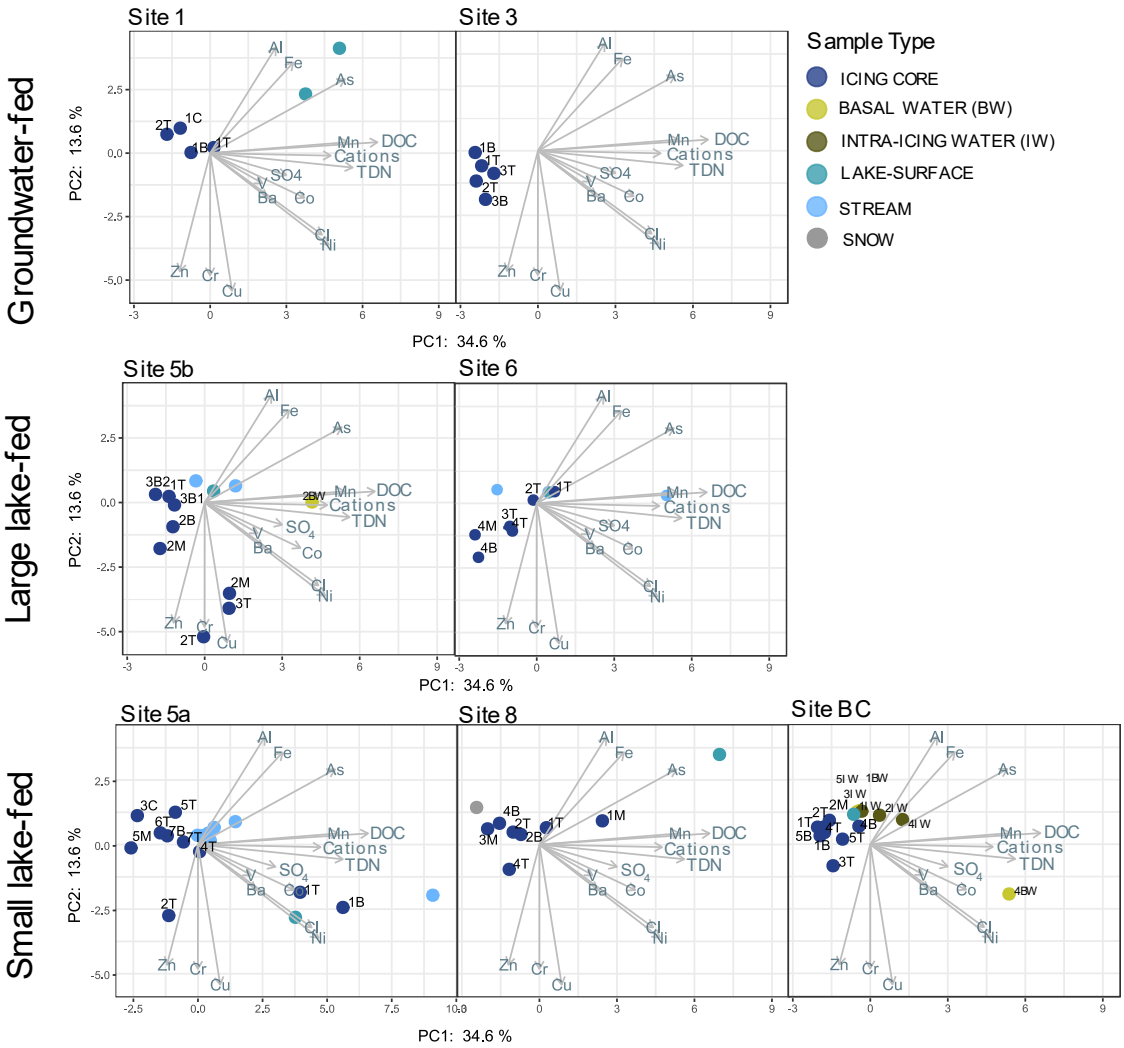

Figure 2-6. Principal component analysis (PCA) of water quality data for icing cores, basal water, intra-icing water, upstream lake, and stream samples collected during March 2021-May 2021 at seven icings. Individual PCA panels illustrate a common global PCA. Axis 1 and 2 explain 34.6% and 13.6% of variance, respectively. Icing cores, basal and intra-icing water are labelled by their sampling position respective to the upstream lake at each site and correspond to labels in Figure 2. The depth interval of each sample is also labelled as top (T), middle (M), bottom (B) for icing cores or intra-water (IW) and basal-water (BW) for basal and intra-icing samples. Basal water represents water samples collected at the bottom of drill holes during ice core drilling, and intra-icing water represent water flowing in between icing layers.

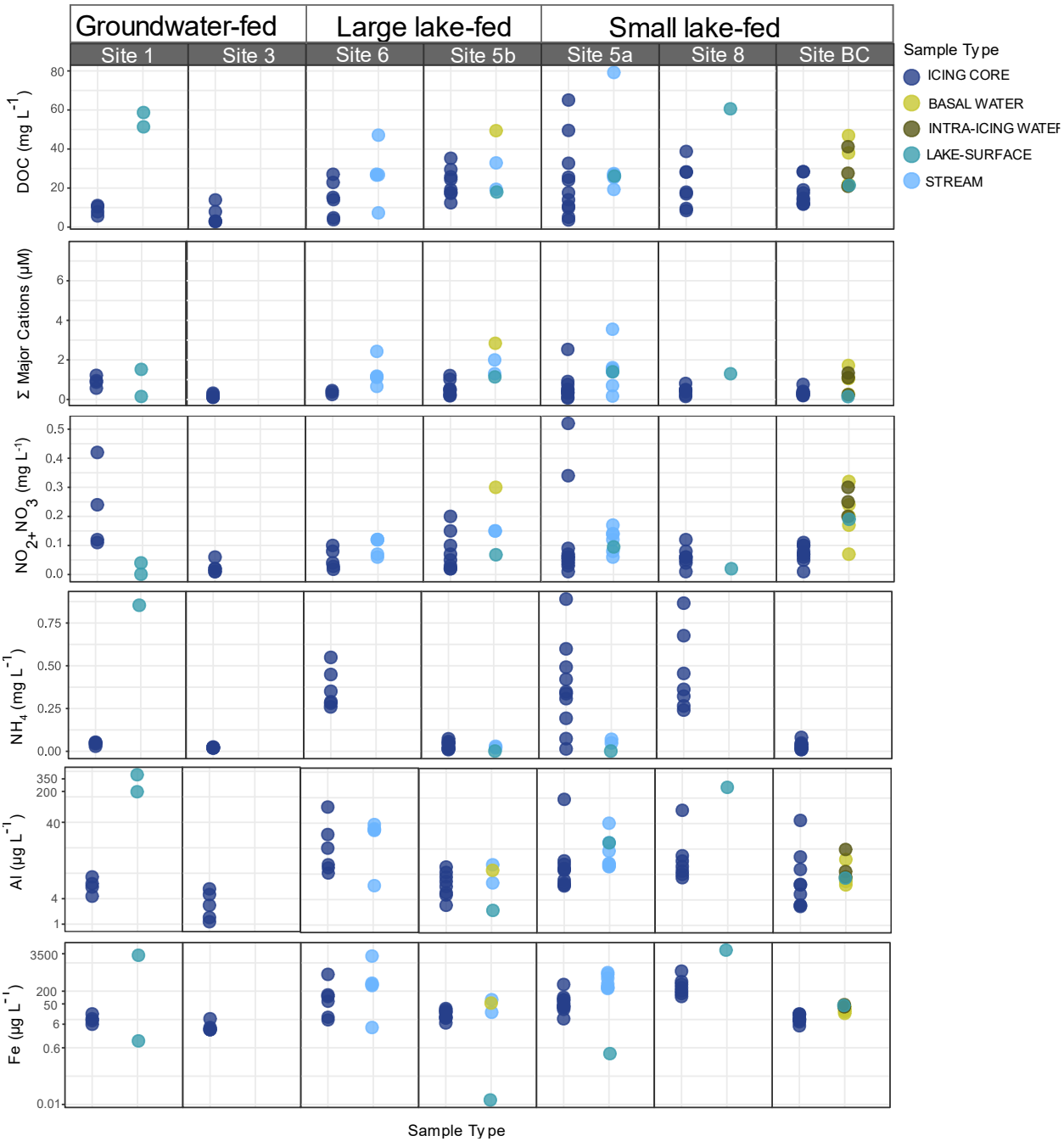

Figure 2-7. Concentrations of DOC, the molar sum of major cations (Ca^{2+}, Mg^{2+}, K^{+}, Na^{+}), NO_2^- +NO_3^-, NH_4^+, Al^{3+}, and dFe of icing, core, lake, and stream water. Basal water represents open flow samples collected at the bottom of drill holes during ice core drilling, and intra-icing water represent water sampled flowing in between icing layers. Note the log scale for the Al and Fe panels.

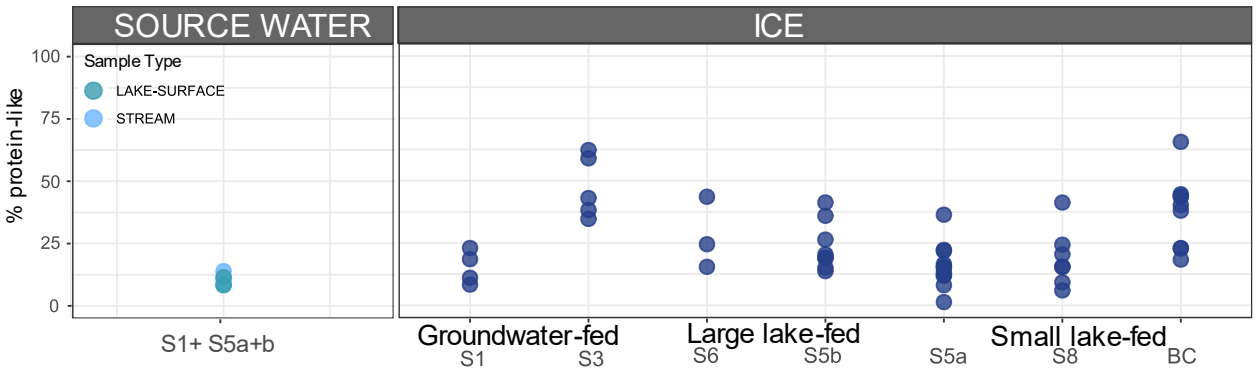

Figure 2-8. Percentage of protein-like (C3) dissolved organic matter (DOM) across seven icings, and of paired source water (upstream lake and stream) samples.

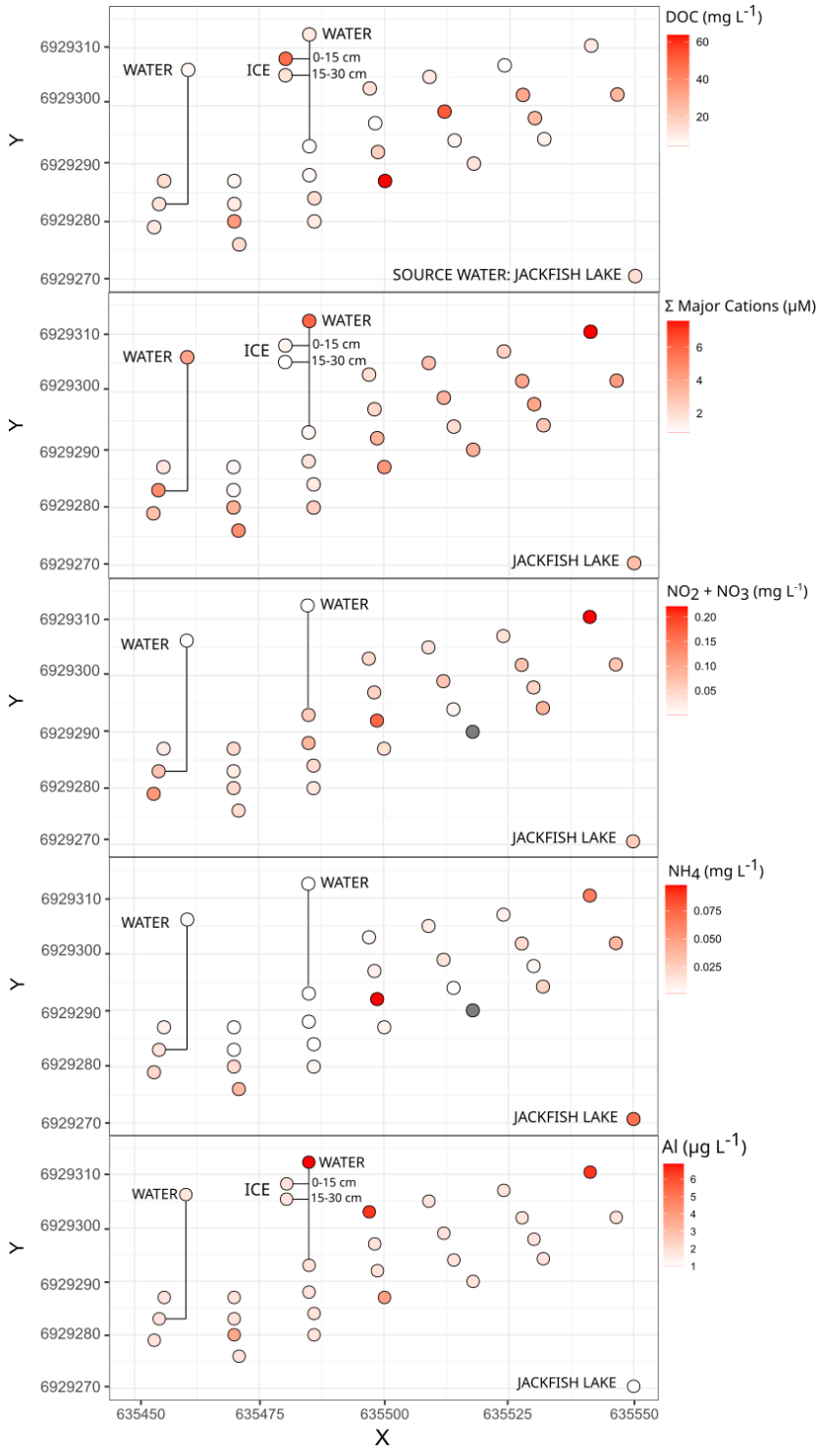

Figure 2-9. Jackfish surficial ice (~10 cm depth) , ice core sections (labelled ice), intra-icing water (labelled water) and upstream source water (labelled Jackfish Lake) chemistry. X and Y axes represent UTM coordinates. The icing was sampled in March 2022 and Jackfish Lake was sampled in February 2021. Dark grey points indicate that no sample was collected.

Chapter 3: Icings modify fluvial biogeochemistry, microbial community structure and carbon cycling in the lake-dominated discontinuous permafrost Taiga Shield

3.1 Introduction

The dynamics of freshwater systems across the western Canadian subarctic are in transition. Winter baseflow has been increasing over the past several decades, which has been driven by a shift towards more pluvial runoff regimes in autumn (Ensom et al., 2020), and widespread permafrost degradation that enables continued subsurface flow during the winter (Morse et al., 2016). Permafrost degradation has led to the increased occurrence and expansion of taliks in regions including the Canadian Taiga Plains (Connon et al., 2018; Crites et al., 2020; Devoie et al., 2019), and around Yellowknife – the Taiga Shield (Spence et al., 2020). Taliks are pockets of perennially unfrozen ground within or immediately above permafrost (Walvoord & Kurylyk, 2016)**.** In winter, flow is conveyed through these unfrozen layers and thus, talik expansion allows for increased surface-groundwater interaction (Lamontagne-Hallé et al., 2018), potentially altering the export of chemical constituents to streams draining these landscapes; additionally, when this flow is conveyed to the ground surface, an icing may form, growing in sheetlike masses over time and archiving talik flow. Although emerging research has documented chemistry offsets between winter and open water flow indicative of talik presence (Spence et al., 2020), the specific influence of taliks on subarctic rivers is almost entirely focused on hydrologic effects (Bense et al., 2012; Lamontagne-Hallé et al., 2018; St. Jacques & Sauchyn, 2009). Furthermore, the nature of wintertime chemistry remains poorly understood in northern regions, partly due to its historic perception as a period of limited chemical and biological activity. However, as climate warming increases winter baseflow and surface-groundwater interactions, understanding the resulting impacts on winter streamflow chemistry is increasingly important to predict changes at a watershed level and across larger geographic regions.

Understanding the dynamics of wintertime chemistry is especially important on the Taiga Shield, which is a vast area over 1.3 million km^2, that comprises approximately 20% of North America's permafrost-covered landmass (Tarnocai et al., 2009; Wang et al., 2019). This region is underlain by widespread discontinuous permafrost, which is particularly vulnerable to thaw due to the possibility of both vertical and lateral heat transfer (Wright et al., 2022). Over the past

several decades, warming has been pronounced in winter, and annual mean air temperatures having increased more than 2° C from the 1950-1970 mean (Paul et al., 2021).

The Taiga Shield landscape is dominated by lakes, which number in the hundreds of thousands, and can be expected to substantially affect the biogeochemical signature of water moving through this region (Palmer et al., 2019). The granitic, undulated topography which cause lakes to be abundant on the Taiga Shield also gives rise to a unique "fill and spill" hydrology, whereby runoff is only generated by the exceedance of lake basin storage thresholds within landscape components (Spence & Woo, 2003). Effectively, the lakes on the Taiga Shield represent a series of storage reservoirs, with outflow mediated by antecedent precipitation levels; the occurrence of outflows vary temporally and spatially depending on the storage volume of individual lakes and degrees of hydrologic connectivity (Spence & Woo, 2003). With higher winter baseflow, hydrologic "spill" between basins is more likely (Spence & Woo, 2003), which increases surface-groundwater interactions and overall water flux through this landscape with potential implications for wintertime chemistry.

Increasing baseflow contributions to streams, and the expansion of subsurface flow paths is likely to alter the export of chemical constituents to flow and shift the quality of dissolved organic matter (DOM) in fluvial networks. Aged, aliphatic DOM and metals may be exported to surface waters if flow paths access deeper soil horizons where these constituents tend to be enriched (Barnes et al., 2018). These changes may in turn have important effects on microbial communities and carbon mineralization, the study of which is minimal or entirely missing in this region (Aukes, 2019; Kurek et al., 2023). Recent work on lakes in the region show that hydrologic connectivity to surface flow paths is correlated with decreasing dissolved organic carbon (DOC) and increasing aromaticity (Kurek et al., 2023).

One physical manifestation of wintertime flow through taliks are icings, which are sheet-like masses of layered ice that form through freezing of successive flows of water onto the ground surface. As taliks can continuously convey water along subsurface flow paths, they are able to facilitate icing growth throughout the winter (Ensom et al., 2020; Liu et al., 2021). On the Taiga Shield, icings are most commonly sourced from groundwater or from water below river or lake ice as it flows through ice fractures (Ballantyne, 2017). The maximum extent of individual icings on the Taiga Shield varies widely on an annual basis, but has been observed to range from 0.02

to 0.36 km^2 (Morse & Wolfe, 2015). Icing formation in this region is dependent on winter baseflow levels, and is commonly restricted to valleys where water storage thresholds are exceeded in late autumn and winter (Ensom et al., 2020). Icings may serve as a valuable tool to study wintertime chemistry, as they both archive and modify (via selective freezing processes; (Santibáñez et al., 2019; Zhou et al., 2023) the composition of water actively flowing through northern landscapes in the winter. Furthermore, as icings can persist well into spring and summer, contributing to streamflow as they thaw, icing chemistry may have an important effect on seasonal biogeochemistry and carbon feedbacks in this region. Research of icing chemistry is limited, and has focused on mineral precipitation within icings forming in the high Arctic (Hall, 1980; Pollard, 2005); the geochemistry of lake-fed icings common across the Taiga Shield is poorly understood.

Here, we aim to characterize seasonal variation in water chemistry on the Taiga Shield, with a focus on wintertime flow. We do this via a detailed exploration of icing and seasonal surface water chemistry at several locations near Yellowknife, NT, including an examination of DOM composition via ultra-high resolution mass spectrometry (FT-ICR-MS). We also investigate microbial community composition and carbon mineralization to assess wintertime chemical drivers. Our results suggest that icings actively modify the composition of water flowing in subarctic fluvial networks, and icings contain larger proportions of aliphatic DOM; this DOM is biolabile, rapidly mineralized and appears to significantly impact microbial community structure.

3.2 Methods

3.2.1 Study area

Yellowknife, NT is located in the Taiga Shield High Boreal ecoregion, which features a multitude of lakes and streams that are largely remnants of glacial scouring. The exposed bedrock uplands and soil-filled valleys that comprise much of the Taiga Shield are responsible for the surface-water dominated hydrological regime characteristic of the region (Spence & Woo, 2003). This hydrological regime follows a “fill and spill” process, whereby runoff is only generated when the storage capacity of lakes are exceeded; thus, lakes represent a series of storage reservoirs, and downstream flow is restricted until upstream storage thresholds are reached (Spence & Woo, 2003). These lakes switch between being hydrologically connected or disconnected from the surrounding landscape depending on antecedent precipitation over the

past several years, causing annual discharge to vary by orders of magnitude within a given system; in winter, runoff has been observed to vary over one order of magnitude interannually (Morse & Wolfe, 2017). A common manifestation of winter flow in the subarctic Canadian Shield are icings, which can persist throughout much of the summer season, but thaw before the following year. Icings form when flow is confined beneath a surficial ice layer, and continual subsurface flow is then routed through ice fractures onto the ground surface, resulting in the freezing of water in sheetlike masses over time (Ballantyne, 2017). Icings can be sourced by groundwater seepage, from springs, or more commonly across the Taiga Shield, from water below river or lake ice as it flows through ice fractures (Ballantyne, 2017). Fill and spill dynamics control the formation of these lake-fed icings, leading to intermittent icing presence on a year-to-year basis, depending on hydrologic connectivity and basin storage (Ensom et al., 2020; Morse & Wolfe, 2017; Spence et al., 2014).

The climate of Yellowknife is characterized by short, cool summers (17 °C July mean) and long, cold winters (-26 °C January mean) with below freezing temperatures between November and March (1981 – 2010 climate normal) (ECCC, 2022a). Mean annual air temperature is increasing (+4.9 °C in winter, +2.7 °C in summer over the past 70 years), but remains below freezing overall (-1 °C to -7 °C from 1942-2016) (Sivarajah et al., 2021). Permafrost underlies approximately 50-65% of the Taiga Shield High Boreal ecoregion, is found on fine-grained sediments, and is associated with all forested ecotypes (Morse et al., 2016; Zhang et al., 2014). Surficial geology of the Taiga Shield broadly features discontinuous till and lacustrine veneers between outcrops of bedrock (Ecosystem Classification Group, 2008; Morse et al., 2016). Within the Taiga Shield High Boreal, vegetation is characterized by open forests of black spruce (*Picea mariana),* jack pine (*Pinus banksiana)* and paper birch (*Betula papyrifera),* which commonly occur on thin soils over bedrock, and on well-drained coarse-grained outwash deposits (Ecosystem Classification Group, 2008). Moss forest can be found on deeper, moister soils, and bare outcrops are dominated by lichens and shrubs (Ecosystem Classification Group, 2008).

3.2.2 Sampling scheme and site characteristics

To investigate seasonal variation in water chemistry, we analyzed ice, lake, and stream samples from three sites (S5a, S5b and S1; Figure 3-1). These sites were chosen due to icing formation occurring during the study year, and because sites were associated with channels with

active flow, featuring upstream lakes with the potential to source icing formation. Study sites are located in the River Lake watershed, which is a sub-watershed of the Great Slave Lake and broader Mackenzie watersheds. As is common across the Taiga Shield, River Lake is fed by numerous smaller lakes, and outflow from these lakes drives icing formation in their downstream channels (Viscek, 2020). Icings can persist on the landscape well into spring and summer; at our sites, icings were still present by the end of June. At its outflow, River Lake drains an area of ~ 7,745 km^2 and thus represents a large regional water reservoir, with water residence times likely much longer than the smaller lakes which feed it (Viscek, 2020). Lake depth varies across our specific study sites, with S1 and S5a fed by lakes approximately 1 and 2-4 meters deep, respectively, and S5b fed by a deeper lake of ~4-5 m. Surficial geology surrounding S1 features coarse-grained glaciofluvial sediments consisting of sand and clay, whereas S5a and S5b are located within an area of fine-grained glaciolacustrine sediments consisting of fine sand to silty clay.

To investigate seasonal differences in flow, a series of ice cores representing winter subsurface flow were collected in March 2021 at each icing site (Figure 3-1). Upstream lakes and stream water within channels where icings formed were also sampled at each site (Figure 3-1). Site 1 was chosen as a focal site for more frequent sampling due to ease of access; S5a and S5b were sampled approximately biweekly, and S1 weekly from March 2021 to August 2021 (Table A2-1). An additional sampling trip was conducted in March 2022 to obtain more wintertime lake and stream samples at each focal site, however, no icings formation occurred at these sites in winter 2021-22 (Table A1-1) (Alsafi, Ch. 2).

Icing, lake, and stream samples were analyzed for a suite of organic (dissolved organic carbon (DOC) and dissolved organic matter (DOM) composition) and inorganic (nutrients, ions, water isotopes) parameters. To explore how variation in water chemistry influenced the base of aquatic food webs, we analyzed microbial community structure across sites and seasons. Lastly, to directly investigate how seasonal differences in water chemistry drove carbon cycling, we performed an incubation experiment.

3.2.3 Sample collection methods

3.2.3.1 Ice

Ice cores were collected along a transect from the upstream to the downstream end of each icing, following methods described in Alsafi (Ch. 2). At S1 and S5a, a composite ice sample consisting of 10 to 15 full depth (~90 cm) cores from the same area was collected to provide enough pooled sample volume for an incubation experiment, Δ^{14}C-DOC analyses, and 16S rRNA gene sequencing (see below).

3.2.3.2 Surface water

From late March-early May, lake and stream water samples were collected directly below the ice surface using an auger. During all seasons, water was filtered on-site site using a peristaltic pump attached to a 0.45 µm high-capacity Polyethersulfone (PES) in-line capsule filter. Raw water was run through the pump lines for three minutes before filling sample vials with filtered water. Before sampling, collection bottles were pre-rinsed three times with 10% v/v hydrochloric acid followed by a triple-rinse of Milli-Q water. Bottles were then triple rinsed with filtered water on site before being filled; samples were chilled in the summer using ice packs prior to sample processing. In the winter, an anoxic sampling technique was used to prevent oxidation of reduced chemical species (Alsafi, Ch. 2; Garcia-Robledo et al., 2021).

3.2.3.3 Groundwater

Groundwater was sampled by digging pits ~0.5 m deep and allowing water to infill into the pit for several minutes before collection in clean PCA bottles (Ackley et al., 2021). Groundwater was pre-filtered using 2-3 stacked coarse (20-µm pore size) filters which were pre-rinsed with Milli-Q water, before being filtered with 0.45-µm PES filters (Sterlitech).

3.2.4 Ice core processing

Ice cores for chemical analyses were processed using methods described in Alsafi (Ch. 2) with additional precautions to avoid contamination of ice cores collected for 16S rRNA gene sequencing. First, in the laboratory in Yellowknife, ~1-2 mm of ice was removed mechanically from each core using combusted razor blades on a sterile surface covered with combusted aluminum foil. Then, the outer layer of each core was allowed to melt until at least 5-7 mm of the original ice core diameter (6 cm) had melted away. This was accomplished by placing cores in sterile Whirl-Pak bags which had small drainage holes cut into the bottom. The diameter of each ice core was measured from outside the bag using a caliper, and the bag was suspended to

allow it to fully drain. The melted ice was monitored using a caliper over the course of ~20 minutes**.** The remaining "sterile" cores were then placed into new sterile Whirlpaks and allowed to thaw in the dark at 4 °C prior to processing.

3.2.5 Sample processing for chemical analyses

We analyzed thawed icing cores and surface water (lake and stream) samples for major cations (Ca^{2+}, K^{+}, Mg^{2+}, Na^{+}), major anions (Cl^{-}, SO_4^{2-}), trace metals (Al^{3+}, dissolved (d)As, Ba^{2+}, dCo, dCr, dCu, dFe, dMn, Ni^{2+}, Sr^{2+}, dV, Zn^{2+}), nutrients (total dissolved nitrogen (TDN), ammonium (NH_4^{+}), nitrite + nitrate (NO_2^{-}+NO_3^{-}), soluble reactive phosphorus (SRP)), water isotopes (δ^{18}O-H_2O and δ^{2}H-H_2O), DOC source and age (via δ^{13}C-DOC and Δ^{14}C-DOC), and DOC concentration and DOM composition (via absorbance and fluorescence spectroscopy and FT-ICR-MS to investigate seasonal variation in water chemistry. Sample collection, processing and preservation for major cations, trace metals, inorganic and organic nitrogen constituents, water isotopes, and fluorescence spectroscopy are described in (Alsafi, Ch. 2) and Appendix 2.

3.2.6 Sample processing for microbial analyses

Samples for 16S rRNA gene sequencing were collected in duplicate via filtration of 2L of raw sample water onto 0.22-µm Sterivex (Millipore-Sigma) filters within 8h of collection. Water was filtered at a low speed (<25 rpm), to avoid cell breakage, using a peristaltic pump. After filtration, the Sterivex units were excavated of any remaining air using a sterile syringe, prior to flash freezing. In between samples, pump tubing was rinsed with 200 mL of hydrochloric acid and 400 mL of 18.2 MΩ (MilliQ) water. Sample water was also run through tubing prior to attaching Sterivex filters. Filters were stored in a liquid nitrogen dry shipper until transport to a -80 °C freezer where they were stored until analysis.

3.2.7 Chemical Analyses

3.2.7.1 Nutrients, cations, trace metals

Analyses for TDN, NO_2^{-}+NO_3^{-}, NH_4^{+}, SRP, major cations and anions, and trace metals were conducted at the ISO-certified Taiga Environmental Laboratory in Yellowknife, NT where NO_2^{-}+NO_3^{-}, major cations and major anions were analysed via ion chromatography, trace metals via inductively coupled plasma mass spectrometry (ICP-MS), TDN via chemiluminescence-pyrolysis, and SRP and NH_4^{+} via colorimetry (APHA et al., 2017a, 2017b; ISO, 2019; U.S. Environmental Protection Agency, 1996).

3.2.7.2 Carbon concentration and composition

Analyses for DOC concentration, DOM absorbance and fluorescence, and water isotopes were conducted at the University of Alberta, where $\delta^{18}O\text{-}H_2O$ and $\delta^{2}H\text{-}H_2O$ were measured using a L2130-I Picarro analyzer, DOC concentration was measured using a Shimadzu TOC-L analyzer, and DOM absorbance and fluorescence were measured using a Horiba Aqualog spectrofluorometer. DOC concentration was determined as non-purgeable organic carbon (NPOC) and measured via high-temperature catalytic oxidation (HTC). MilliQ blanks and reference waters were analyzed routinely to measure instrument drift and remained within 5% of accepted values. References were made using caffeine and KHP standards (AccuSPEC, SCP Science). A ten-point standard curve was constructed for each run, with concentrations ranging to a maximum of 60 ppm. DOC concentration was determined as the mean of the best three of five sample injections that had a coefficient of variation < 2%. DOC composition was first assessed via absorbance and fluorescence spectroscopy. Absorbance measurements were collected across wavelengths spanning 240 – 800 nm at 1-nm increments and were blank corrected (Hansen et al., 2018). Absorbance data was used to calculate several compositional metrics: absorbance at 254 nm (A_{254}), specific UV absorbance at 254 nm ($SUVA_{254}$), absorbance slopes ($S_{275\text{-}295}$, $S_{350\text{-}400}$), and slope ratio (S_R). S_R is calculated as $S_{275\text{-}295}$ divided by $S_{350\text{-}400}$ (Helms et al., 2008). A_{254} is associated with DOC concentration, S_R with molecular weight, and $SUVA_{254}$ with aromatic content (Weishaar et al., 2003).

Fluorescence excitation emission matrices (EEMs) were constructed across excitation wavelengths spanning 230–500 nm at 5-nm increments, and emission wavelengths spanning 300-600 nm at 2.33-nm increments. Raw EEMs were corrected for inner-filter effects, normalized to Raman units, and blank corrected (Hansen et al., 2018).

A global parallel factor (PARAFAC) analysis was performed (Alsafi, Ch. 2) to analyze EEMs (n=98) using the drEEM toolbox in MATLAB, following Murphy et al. (2013). The final model, identifying three components, explained 99.8% of sample variance, and was validated using a split-half analysis. A subset of samples (n=75) from the global PARAFAC is shown in this chapter. Fluorescence components were matched to published components in the OpenFluor database, and all components matched with similarity scores > 0.95 (Murphy et al., 2013). The model consisted of two humic-like components, associated with aromatic, high molecular weight

compounds (C1 and C2), and one protein (tryptophan)-like component, which is characteristic of DOM of microbial origin (C3), (Ch. 2, Figure A1-6, Table A1-3) (Gonçalves-Araujo et al., 2016; Guéguen et al., 2014; Imbeau et al., 2021, 2021).

Additionally, several fluorescence metrics were calculated in the drEEM toolbox to broadly characterize DOM composition, including: fluorescence peaks B, T, A, C, fluorescence peak ratios (A:T, C:T), humification index (hix) and fluorescence index (FI). Peaks A and C characterize humic-like fluorescence components, peak T protein (tryptophan)-like components, and peak b protein (tyrosine)-like components (Coble, 1996). Fluorescence ratios A:T and C:T describe the ratio of humic-like to fresh fluorescent DOM in a sample (Coble, 1996; Hansen et al., 2018). The fluorescence index provides insight into the relative contributions of terrestrial and microbial sources to the DOM pool, while the humification index provides insight into the degree of humification within a sample (Hansen et al., 2018).

In addition to assessing absorbance and fluorescence characteristics, we also used FT-ICR-MS on a subset of samples to gain a more comprehensive understanding of DOM complexity. Acidified samples (pH 2) were solid-phase extracted onto BondElut PPL columns to a final target mass of 50 μg carbon (C), assuming 65% extraction efficiency (Dittmar et al., 2008). Samples were stored at -20 °C until analysis on a 21T FT-ICR-MS at the National High Magnetic Field Laboratory in Tallahassee, Florida (Hendrickson et al., 2015; Smith et al., 2018) with negative electrospray ionization. Each mass spectrum consisted of 100 time-domain acquisitions averaged for all experiments (Blakney et al., 2011).

Molecular formulae were assigned to peaks with signal-to-noise ratios >6σ root-mean-square baseline noise (O'Donnell et al., 2016; Spencer et al., 2019) using PetroOrg ©™ software (Corilo, 2015). Formulae were used to calculate a corresponding oxygen to carbon ratio (O/C), hydrogen to carbon ratio (H/C), nitrogen to carbon ratio (N/C), and modified aromaticity index (AI_{mod}) (Koch & Dittmar, 2006). The O/C, H/C and AI_{mod} were used to delineate formulae into five compound classes: aliphatic ($1.5 \leq H/C \leq 2.0$, $O/C \leq 0.9$), condensed aromatic ($AI_{mod} \geq 0.66$), polyphenolic ($0.5 < AI_{mod} < 0.67$), highly unsaturated and phenolic high O/C ($HUP_{High\ O/C}$) ($AI_{mod} < 0.5$, $H/C < 1.5$, $O/C \geq 0.5$), and highly unsaturated and phenolic low O/C ($HUP_{Low\ O/C}$) ($AI_{mod} < 0.5$, $H/C < 1.5$, $O/C < 0.5$) (Rogers et al., 2021). Relative abundance of each formula was calculated by normalizing peak magnitudes to the sum of all peaks in each sample. The

contribution of every compound class in each sample was calculated as the sum of relative abundances of each peak per compound class, divided by the summed abundances of all assigned formulae per sample (expressed as percentages) (Behnke et al., 2021).

3.2.7.3 Carbon source and age

δ^{13}C-DOC analyses were conducted at the University of Ottawa in the Jan Veizer Stable Isotope Laboratory using an IRMS (Thermo Finnigan DeltaPlus XP) following established methods (Lalonde et al., 2014; St-Jean, 2003). Δ^{14}C-DOC analyses were conducted at the University of Ottawa at the Andre E. Lalonde AMS Laboratory using an Ionplus AG MICADAS (Mini Carbon Dating System) AMS analyzer following chemical combustion using established methods (Crann et al., 2017; St-Jean et al., 2017). Radiocarbon data are reported as Δ^{14}C.

3.2.8 Microbial analyses

DNA was extracted from Sterivex filters at the University of Alberta using the DNeasy PowerWater Sterivex kit (Qiagen), as per the manufacturer's protocol, except for the use of extended chemical lysis with rotation at 70 °C, rather than 95 °C, for one hour. This modification was implemented to maximize DNA yield. Eluted genomic DNA concentrations were quantified on a QubitTM 4 Fluorometer (Invitrogen), with results ranging between 0.03 – 14.1 ng μL^{-1}. To target and analyze microbial community composition, we used universal prokaryotic primers 515F (Parada et al., 2016) and 926R (Quince et al., 2011) for library construction. Each primer also contained a six-base index sequence for sample multiplexing (Bartram et al., 2011). The PCR mix (25µL total volume) contained 1x Q5 reaction buffer, 0.5 µM forward primer, 0.5 µM reverse primer, 200 µM dNTPs, 0.500 U high fidelity Q5 polymerase (New England Biolabs, Ipswich, M.A) and 2.5 µL of genomic template. Genomic extracts with DNA concentrations greater than 10 ng μL^{-1} were diluted 1:10 in nuclease free water. The PCR was performed as follows: 95 ºC for 3 min, 35 cycles of 95 ºC for 30 s, 60 ºC for 30 s, 70 ºC for 1 min and a final extension at 70 ºC for 10 min. All amplicon and barcoded products were verified on a 1.5% agarose gel and those that could be successfully visualized were then pooled (total pool concentration:13.5 ng μL^{-1}). The final quality of the pool was checked on an Agilent 2100 Bioanalyzer at the Molecular Biology Service Unit (University of Alberta) using a high sensitivity dsDNA assay kit (Agilent High Sensitivity DNA Kit), prior to submitting the library for 16S rRNA gene sequencing at the Applied Genomics Core (TAGC, University of Alberta).

The final prepared 2 nM library, containing 50% PhiX Control v3 (Illumina, Canada Inc., NB, Canada) was sequenced on an Illumina MiSeq (Illumina Inc., CA, USA) using a 2 × 300 cycle MiSeq Reagent Kit v3 (Illumina Canada Inc). The MiSeq reads were demultiplexed using the Miseq Local Run Manager GenerateFastQ Analysis Module 3.0. Assembled reads were analyzed using the Quantitative Insights Into Microbial Ecology pipeline (QIIME2; version 2021.11) (Bolyen et al., 2019). Sequences were assembled into amplicon sequence variants (ASVs) with chimeric sequences, singletons and low abundance ASVs removed using DADA2 (Callahan et al., 2021). All representative sequences were classified with the SILVA taxonomic database, using the most recent release (version 138; Quast et al., 2012). Ten out of a total of 45 collected samples were ultimately excluded from sequencing due to unsuccessful PCR amplification.

3.2.9 Incubation experiment

To investigate how seasonal variation in water chemistry influenced DOC mineralization we utilized an incubation experiment. Samples were collected three times from S1 for the experiment: in winter (April 21st), spring (May 12th), and summer (June 14th). Winter was demarcated by daily maximum temperatures consistently below 0 °C (Alsafi Ch. 2), spring by consistent above 0 °C daily maximum temperatures and freshet conditions, and summer as the period following the cessation of spring freshet. The lake at S1, and downstream icing or stream (depending on season) water were sampled, filtered (0.2-µm Sterlitech PES) and immediately frozen. Inocula was collected from downstream River Lake on Oct 7th and immediately shipped to Edmonton. Samples were incubated in tandem for 28 days at 10 °C, which reflects measured in-situ temperatures in the eventual outlet of River Lake and the downstream Great Slave Lake (Rouse et al., 2008).

We assessed carbon mineralization using changes in DOC and total carbon dioxide (CO_2) (i.e., measured as dissolved inorganic carbon (DIC) concentrations at the beginning and end of the experiment, as well as daily measurements of oxygen (O_2; PreSens). Oxygen concentration was also recorded in four bottles containing Milli-Q water to provide a blank control and verify sensor function. To explore drivers of carbon mineralization, incubation samples were analyzed for nutrients (TDN, NO_2^-+NO_3^-, NH_4^+, TDP, SRP), DOC concentration, DOM composition (via absorbance and fluorescence metrics) and pH before the incubation period. Methods describing

sample collection, sample processing, incubation setup and chemical analyses (see above) are provided in Appendix 2.

3.2.10 Statistical analyses

All statistical analyses were performed in R 4.1.1 (R Core Team, 2022).

Isotopes were used to explore seasonal variation in water sources. $\delta^{18}O\text{-}H_2O$ and $\delta^{2}H\text{-}H_2O$ were used to calculate deuterium excess (d-excess), as $d = \delta^{2}H\text{-}H_2O - (8 * \delta^{18}O\text{-}H_2O)$ (Pfahl & Sodemann, 2014).

Water chemistry data was explored using a correlation analysis using Pearson's r (packages *stats, corrplot)* to observe relationships between chemical parameters and select variables of interest (Wei & Simko, 2021) (Figure A2-1). Chemical concentrations below the detection limit were set to half the detection limit (U.S. Environmental Protection Agency, 2000). Major cations were analyzed as their molar sum due to their correlation with each other (Figure A2-1). Nitrogen parameters were represented as dissolved inorganic nitrogen (DIN; sum of NO_2^-+NO_3^- and NH_4^+) and dissolved organic nitrogen (DON; as TDN-DIN). We used scatter plots to examine seasonal variation in PARAFAC components, general water chemistry (DOC, major cations), water isotopes, fluorescence/absorbance metrics (hix, $SUVA_{254}$), $\Delta^{14}C$-DOC ‰ and $\delta^{13}C$-DOC ‰ (package *ggplot;* Wickham, 2016).

A principal component analysis (PCA) was conducted (package *stats)* to explore chemical variation between icings and surface water across sites and seasons (Wickham, 2016).

To investigate seasonal differences in carbon composition in more depth, we visualized FT-ICR-MS compound classes using boxplots (Wickham, 2016). Molecular formulae identified in all samples and formulae unique to each season were visualized with van-Krevelen diagrams (Wickham, 2016). A PCA was conducted (package *stats*) to explore compositional variation across icings and surface water, using FT-ICR-MS parameters. Vectors for select (sum of major cations, DOC, S_R, A_{254}, $SUVA_{254}$, hix, DIN, DON, SRP, $\delta^{13}C$-DOC) parameters were calculated post-hoc and overlain on the PCA to visualize chemical variation across FT-ICR-MS samples.

Based on overall ASV richness, assessed via rarefaction curve (package *vegan;* Oksanen et al., 2022; Figure A2-2), microbial data were rarified (Hughes & Hellmann, 2005; McKnight et al., 2019; Weiss et al., 2017) to the minimum number of identified ASVs across all samples

(46,492), and this dataset was used in all subsequent microbial analyses except the indicator species analysis.

To explore the distribution of taxa across samples and sites, the top 18 orders represented across all samples by ASV count were identified. Relative abundance of orders in each sample were calculated as the ASV count of each order divided by the sum of ASVs across all orders. Relative abundances of top orders across sites and season were visualized using bubble plots (Wickham, 2016).

A non-metric multidimensional scaling (NMDS) analysis was performed on rarefied microbial data using a Bray-Curtis dissimilarity matrix to visualize differences in microbial community structure across sites and samples (Oksanen et al., 2022; Wickham, 2016); winter included pooled surface waters and icing samples. A permutational multivariate analysis of variance (perMANOVA) (package *vegan)* was also conducted to evaluate the significance of site and season in determining microbial community structure, followed by pairwise perMANOVA tests to evaluate significant differences between each season and site; p-values from pairwise perMANOVA tests were Bonferroni corrected (Oksanen et al., 2022).

To identify characteristic ASVs across space and time, an indicator species analysis (ISA) was performed (package *indicspecies*), using test "r.g.", which corrects for differences in sample size between groups (Cáceres et al., 2022; Caceres & Legendre, 2009; Dufrêne & Legendre, 1997; Tichý & Chytrý, 2006). perMANOVA results of the NMDS analysis revealed significant differences in microbial community structure between sites, thus, we separated S1 and S5 (S5a+S5b) into different groups for the ISA; the ISA evaluated differences across winter (pooled winter and icing), spring and summer at S1 or S5. Indicator values (IV) ranged from 0-1, with higher values for stronger indicators. We selected ASVs with $IV > 0.77$ and $p < 0.05$ as key indicators across winter, spring and summer at each site (Dufrêne & Legendre, 1997). We calculated the relative abundance of each indicator ASV in each sample and visualized this at the genus level using a stacked barplot; genera with relative abundances < 0.2% were not distinguished in this plot (Wickham, 2016).

To explore how water chemistry drove differences in microbial community structure, a distance-based redundancy analysis (dbRDA) was performed on rarified microbial data. First, a

forward and reverse selection of all chemical parameters was run (package *vegan)* to build a model containing only significant (p=0.05) explanatory variables of microbial community structure (Oksanen et al., 2022), followed by an analysis of variance (ANOVA) to determine levels of significance (R Core Team, 2022). A dbRDA was then created using Bray-Curtis distance (package *vegan)* and visualized in a biplot (Oksanen et al., 2022; Wickham, 2016). To explore the influence of DOM composition on microbial community structure in more depth, a dbRDA was performed using a subset of microbial samples with matching FT-ICR-MS data using the methods described above.

To explore carbon mineralization across sites and seasons, initial and final O_2 and CO_2 measurements from the incubation experiment were normalized and visualized using biplots and point plots (Wickham, 2016); detailed methods are provided in Appendix 2.

To assess the influence of initial (T_0) chemistry parameters on carbon mineralization, incubation data was analyzed using a mixed effects model. Three models were built with unique dependent variables: percent O_2 loss, percent CO_2 gain, and rate of O_2 loss. First, a forward and reverse selection was run to determine significant T_0 chemistry parameters. After explanatory variables were identified and models were created, an ANOVA was run to determine the significance of explanatory variables in each model. The variance inflation factor (VIF) of each model was calculated to exclude collinear explanatory variables.

3.3 Results

3.3.1 Seasonal variation in carbon source and age

δ^{13}C-DOC varied more across ice samples (-17‰ to -28‰) than lake and stream samples (-27‰ to -28‰) (Figure 3-2). In particular, two ice cores from S5a were enriched in δ^{13}C-DOC (-17‰ to -18‰) compared to other ice samples (-24% to -28%) (Figure 3-2). Analyses of Δ^{14}C-DOC showed all analysed samples to be characterized by a bulk modern carbon signature (Figure 3-2). Δ^{14}C-DOC was most depleted (~13-16 ‰) in icing meltwater samples (i.e., ice cores in Figures 2-9) and most enriched (98 ‰) in winter stream samples; surface water Δ^{14}C-DOC declined slightly over time from winter to summer (Figure 3-2).

3.3.2 Seasonal variation in water chemistry and carbon composition

Analysis of d-excess showed icing meltwater at S1 to be isotopically distinct, with an elevated (-2.6 to 10.8) d-excess signature relative to winter, spring, and summer surface water (i.e., lake

and stream waters) (-21.6 to 1.9). S5a and S5b icing meltwaters were consistent with surface water d-excess, except for one S5b icing meltwater outlier, which showed elevated d-excess indicative of a precipitation signal (7.4) (Figure 3-3, Figure 3-4). In general, d-excess declined as the summer progressed (Figure 3-4).

Across all sites, icing meltwater was chemically distinct from winter, spring and summer surface water, and was generally more dilute in DOC, DIN, major cations and trace metals, with the exception of SRP which was enriched in icing meltwater (Figure 3-3, Figure 3-4). DOC, major cation, and trace metal concentrations were overall low, and similar within icing meltwaters, with the exception of several ice cores at the head of the S5a icing, which had elevated DOC (29-35 mg L^{-1}) and cation (2.5 µM) concentrations (Figure 3-4). In contrast, surface water (lake and stream) DOC concentrations within sites were higher in winter and moderately elevated in spring, relative to summer, while major cation concentrations were greatest in winter surface water (Figure 3-4). Groundwater samples had similar DOC and major cation concentrations to surface waters, but one showed elevated concentrations of select trace metals (dCu, dCr) (2.5 and 7.6 µg/L, respectively (Figure 3-3, Figure 3-4).

Icing meltwater DOM was compositionally unique from winter, spring, and summer surface waters (Figure 3-3, Figure 3-4). Relative to surface waters, icing meltwater was elevated in protein-like (range 1-41%, mean 18.5%) DOM (Figure 3-5), and characterized by low A_{254}, $SUVA_{254}$, hix, FI, and peak ratios A:T and C:T, but high S_R (Figure 3-3). Surface waters showed little variability in DOM composition and percentage of protein-like DOM (3-14%) (Figure 3-4, Figure 3-5). DOM composition of spring surface water was the most distinct from icing meltwater, exhibiting high $SUVA_{254}$, high hix, high fluorescence peak ratios, and low S_R (Figure 3-3).

FT-ICR-MS analyses identified 17,078 total molecular formulae across all samples (Figure A2-3). FT-ICR-MS analyses confirmed the observed composition differences using UV-Vis spectroscopy across icing meltwater (n=9), and winter (n=3), spring (n=4), and summer (n=8) surface waters. Winter samples and more notably, icing meltwater were enriched in aliphatics and depleted in aromatics relative to spring and summer surface waters (Figure 3-6). Icing meltwater also displayed stark variation in aliphatic formulae (6.2-12.4%RA) (Figure 3-6). Icing meltwater and winter surface waters had a lower nominal oxidation state of carbon (NOSC) and

tended to be elevated in N-rich formulae (N/C), and H/C ratios and AI_{mod} reflected the overall less aromatic nature of wintertime chemistry (Figure 3-6, Figure A2-4). Relative to icing meltwater, winter surface waters were elevated in O/C, $HUP_{High\ O/C}$ and CHO, and CHONS-containing formulae (Figure 3-6, Figure A2-4); conversely, CHON and CHOS-containing formulae were elevated in icing meltwater (Figure A2-4). Mean formulae mass, in terms of molecular weight (Da), was similar between icing meltwater and winter surface waters, but was more variable in winter surface water (Figure A2-4). Finally, across all compound classes except for aliphatics (condensed aromatics, polyphenolics, $HUP_{Low\ O/C}$, and $HUP_{High\ O/C}$), spring surface waters displayed the greatest variation in average %RA (Figure 3-6); H/C was also quite variable in spring surface waters.

A PCA of FT-ICR-MS parameters further highlighted unique DOM composition in icing meltwater. Icing meltwater had higher scores for aliphatic formulae, and lower scores for total formulae mass and AI_{mod} compared to other samples, which negatively correlated with low $SUVA_{254}$ and A_{254} (Figure A2-5).

Formulae unique to icing meltwater, winter, spring, or summer surface waters totalled 3,800. (Figure 3-7, Table A2-2). Within icing meltwater samples, the percentage of unique formulae in each compound class was highest for aliphatics (14.4%) compared to formulae in remaining compound classes (0.6-1.4%), with minimal (0.4%) unique condensed aromatics (Figure 3-7, Table A2-2). Unique formulae in winter surface water followed similar patterns to icing meltwater (Figure 3-7, Table A2-2). Spring surface water contained the highest (8.1%) percentage of unique condensed aromatic formulae, compared to winter and spring surface waters (2.4 and 1.34 %, respectively) (Figure 3-7, Table A2-2). The percentage of unique polyphenolic formulae was also highest in spring surface water (3.7%) compared to icing meltwater, and surface water from winter and summer (0.9, 1.2 and 1%, respectively) (Figure 3-7, Table A2-2).

3.2.3 Seasonal variation in microbial community structure and chemical drivers

The relative abundance of the top 18 orders represented across all samples show spatial and temporal variation in microbial community structure (Figure A2-6). Order Burkholderiales showed the highest relative abundance across sites and seasons but did not notably vary seasonally (Figure A2-6).

Unique ASVs identified across seasons were most numerous in summer, followed by spring and winter (Figure A2-7). Shared ASVs across all seasons were comparatively lower (1,346) than unique ASVs identified in each season (5,505-12,789) (Figure A2-7). S1 had the highest number of unique ASVs identified across sites (9,468), followed by S5b and S5a (6,858 and 4,238, respectively) (Figure A2-7).

A NMDS analysis of microbial community structure revealed significant (p=0.001) differences between both sites and seasons (Figure A2-8, Table A2-3). Microbial community structure within (pooled) winter surface water and icing meltwater was significantly different from summer (p=0.024) and spring (p=0.042) surface waters (Table A2-3). Community structure differences between sites varied, with S1 and S5a being the most distinct (p=0.006) from each other (Table A2-3). Indicator species analysis revealed 96 significant (IV>0.77, $p < 0.05$) indicator ASVs. Indicator ASVs were represented by the genera *Flavobacterium*, *Pedobacter*, *Polaromonas, Polynucleobacter,* and *Sediminibacterium*, which were key indicators at S1 during winter and summer, and at S5a and S5b in spring (Figure A2-9). Several (33) indicator ASVs were unclassified at the genus level but were low in relative abundance across all samples (0-0.3%) (Figure A2-9).

Next, dbRDA analyses revealed several significant ($p < 0.05$) chemical drivers of microbial community structure (Figure 3-8, Table A2-4, Table A2-5). In a global RDA (R^2 29%) that included all microbial samples, community structure was significantly driven ($0.005 \leq p \leq 0.01$) by DOM composition (S_R, Component 1 %, Component 2 %, $S_{275\text{-}295}$, FI) and major cation concentration and significantly ($0.01 < p < 0.04$) driven by nutrients (DIN, DON) and select trace metals (Ba^{2+}, dCu) (Table A2-4). In an RDA (R^2 36%) that only included microbial samples with matched FT-ICR-MS data, community structure was driven by the relative abundance of aliphatic and condensed aromatic formulae (p=0.001) and the relative abundance of polyphenolic formulae (p=0.04) (Table A2-5). In general, ice core microbial communities were associated with moderate scores for S_R, FI, Component 2 %, aliphatics, and major cations, and DIN (Figure 3-7).

3.2.4 Seasonal variation in biological processing and chemical drivers

Measured change in O_2 and CO_2 following incubation of icing, winter, spring, and summer waters from S1 with a common microbial inocula, were generally consistent with each other

(Figure A2-10). When normalized for TOC, carbon mineralization rates were markedly higher in icing meltwater samples (7-15% CO_2:TOC) and spring lake samples (18-20% CO_2:TOC) than all other sampling dates and locations (1-4% CO_2:TOC) (Figure 3-9). Carbon mineralization in winter lake samples was considerably lower (1-3% CO_2) than in icing meltwater (Figure 3-9). Some carbon mineralization was observed in non-inoculated samples and was highest in spring stream samples (~80 µM absolute CO_2 gain) and lowest in icing meltwater (18-26 µM absolute CO_2 gain) and spring lake water (~15 µM absolute CO_2 gain) (Figure A2-10). Mixed effect models indicated that DOM composition (bix, fluorescence peak C) and nutrients (TDP, SRP) were significant ($p<0.05$) drivers of carbon mineralization (Table A2-6) with mineralization rates positively correlated to metrics of autochthonous carbon (bix) and nutrient content (TDP), and negatively correlated to metrics of aromaticity (peak C).

3.4 Discussion

3.4.1 Seasonal variation in water chemistry and carbon age

Similar to other studies in northern regions, we observed clear seasonal differences in the chemical composition of streamflow on the Taiga Shield (Holmes et al., 2012). Spring and winter flow were the most chemically distinct from each other, however icing meltwater had novel chemistry compared to winter surface waters. DOM composition also showed clear differences between winter and spring flow. Here, spring had the highest relative abundance of condensed aromatic and polyphenolic formulae, and the lowest relative abundance of aliphatic formulae. This is consistent with other observations of bulk DOM signatures in spring, which are typically dominated by aromatics and consist of increased terrestrial DOM contributions (Behnke et al., 2021). Spring surface water also had the highest number of unique formulae in all compound classes except aliphatics, which reflects the chemically diverse range of DOM exported in runoff (Lawson et al., 2014), which is likely driven by runoff contribution from larger areas associated with freshet.

Headwater catchments in northern regions have been shown to release old permafrost-origin DOC, which is rapidly mineralized as water transits downstream (Abbott et al., 2014; Littlefair & Tank, 2018; Spencer et al., 2015; Jorien E. Vonk et al., 2013). However, we show that this may differ regionally, as the headwaters within this study exhibited relatively modern $\Delta^{14}C$ signatures. This is consistent with other work on the Canadian Shield, which show similarly

young DOC export in rivers and attribute this to lower inputs of aged DOC, caused by thin surface soil deposits on the Shield which result in shallower flow paths (Campeau et al., 2020). However, the bulk $\Delta^{14}C$ pool in icing meltwater was notably depleted compared to winter surface waters, though still modern. This depletion in $\Delta^{14}C$ may be the result of moderate inputs of aged carbon through subsurface inputs to flow during icing formation. Here, we also show a young (i.e., enriched) $\Delta^{14}C$-DOC signature in surface waters during winter and spring, which progressively declined over the season as baseflow contributions proportionally increased.

3.4.2 Icing-specific modification of water flowing through fluvial networks

Icings modify the composition of water actively moving through fluvial networks in the winter. Icing formation appears to partition DOM and solutes, resulting in distinct chemistry from surface waters; these patterns can be attributed to solute exclusion occurring during icing formation. Solute exclusion appeared to enrich $\delta^{13}C$ –DOC in icing meltwater, likely via fractionation of carbon isotopes during freezing; similar fractionation, leading to preferential incorporation of lighter isotopes into the solid phase, has also been shown to occur with water isotopes during freezing in several studies (Guo et al., 2012; Michel, 2011). Solute exclusion also appeared to dilute cations and DOC in icings compared to surface waters (DeGrandpre et al., 2021); however, some icing samples exhibited high concentrations of these solutes, which is likely attributed to sediment-water interaction occurring in lake sources and along flow paths to sites of icing formation (Alsafi, Ch. 2). DOM composition across icing meltwater and surface waters was also unique, and selective exclusion of DOM has been previously observed during lake ice formation, where allochthonous, aromatic DOM is preferentially excluded from ice due to its hydrophobic nature; whereas smaller, hydrophilic compounds are preferentially included into the solid phase (Zhou et al., 2023). Similarly, in this study, FT-ICR-MS analyses further revealed that winter flow is partitioned into unique DOM pools. Icing meltwater had the highest proportion of aliphatic formulae, many of which were unique, coupled with enriched N/C and CHON-containing formula compared to winter surface waters. In contrast, winter surface waters were relatively depleted in aliphatics and exhibited a higher aromaticity index (AI_{mod}), which indicates the degree of aromaticity of a molecule based on the density of C-C double bonds (Koch & Dittmar, 2006). These results are overall consistent with recent work by Zhou et al. (2023), who show selective exclusion of condensed aromatics and polyphenolics, and higher

N/C, aliphatics and CHON-containing formulae in ice. Here, we also observed elevated NOSC and O/C in winter surface water compared to icing meltwater. This is in contrast to other studies examining Arctic riverine DOM, which show O/C to be lowest in winter surface waters (Behnke et al., 2021) This may be attributed to solute exclusion during icing formation, which enriches oxygen-rich DOM in the liquid phase (Zhou et al., 2023). Thermodynamic analyses show higher NOSC values to provide the most energy yield during respiration; other studies show preferential degradation of higher NOSC DOM resulting in an overall negative NOSC signature (LaRowe & Van Cappellen, 2011; Mostovaya et al., 2017). As DOM in winter surface waters had relatively lower NOSC compared to spring and summer, it is possible that preferential degradation of higher NOSC DOM resulted in this signature (Mostovaya et al., 2017). The lowest NOSC in icing meltwater may be driven by solute exclusion, where oxygen-rich DOM is excluded from the solid phase as described above. Some studies have shown high biolability with NOSC values < -1, reflecting contributions from protein and lipid-like fractions in DOM (Zhou et al., 2019); the dominance of aliphatic compounds in icing meltwater suggests that a portion of this DOM may be more bioavailable compared to winter surface waters.

Variation in icing meltwater chemistry may also reflect variable freezing conditions, which cause differing degrees of solute exclusion. Solute exclusion is in part, controlled by rates of freezing, and rapid freezing results in greater solute inclusion into the solid phase over time (DeGrandpre et al., 2021). Once source waters reach a site of icing formation, they may travel along basal, intra or surficial flow paths within the existing icing and are subsequently exposed to varying temperatures (Alsafi, Ch. 2). For example, temperatures within icing layers may be insulated relative to the icing (air-exposed) surface, and flow within icing layers may thus experience lesser solute inclusion into the ice phase. However, if freezing conditions are similar along basal and intra-icing flow paths, solute exclusion in flowing water will dilute solutes in icings with minimal variation over space. Thus, when flowpaths are routed to the surface and exposed to colder temperatures, degrees of solute exclusion will be similar, however variation in surficial flow path routing will drive patchiness in chemistry over space. Here, patchiness in freezing conditions may result in chemical variation of icing meltwater, as we observed in several samples exhibiting enriched DOC, cation, and trace metal concentrations.

Beyond modifying the composition of winter surface waters, icings may also provide an energy rich DOM subsidy upon icing thaw during the spring and summer. Condensed aromatics and polyphenolic formulae, which consist of polycyclic aromatics (PCAs), soil derived-polyphenols and PCAs with aliphatic chains, are characteristically less biolabile (Šantl-Temkiv et al., 2013). All these compound classes are markedly lower in our icing meltwaters, in addition to the aromaticity index. Icing meltwater contained higher H/C molar ratios than winter surface water, which in addition to a high proportion of aliphatic and low molecular weight formulae, and a high number of unique aliphatic formulae, suggest that icing meltwater may be dominated by energy rich compounds when compared to winter flow (Behnke et al., 2021; Lawson et al., 2014). Taken together, these results suggest that icing meltwater contains a biolabile DOM pool, which has the potential to modify the composition of in-stream headwater DOM during spring and summer as icings thaw, providing an energy rich subsidy beyond the traditional spring pulse. This labile DOM pool present in icing meltwater may have important implications for microbial processing and carbon feedbacks as icings thaw and contribute to streamflow.

3.4.3 Microbial community structure varies across time and space on the Taiga Shield

We found that microbial community structure was significantly different across sites and seasons. However, we found a core community present in all samples; in particular, Burkholderiales was the most abundant order across all sites, and did not notably vary seasonally in relative abundance. Burkholderiales made up 50% (relative abundance) of the core community, and it represents metabolically and ecologically diverse microbial lineages with notable versatility in aromatic compound metabolism (Pérez-Pantoja et al., 2012). Nonetheless, despite the prevalence of Burkholderiales, several indicator genera were identified for S1 in winter (pooled icing meltwater and winter surface waters) and S5 (S5a+S5b) in spring. *Flavobacterium*, which was a key indicator at both sites, is commonly isolated from polar lakes, streams, rivers and sea ice, and is widely distributed across aquatic ecosystems (Bernardet & Bowman, 2006). Winter at S1 was distinguished by *Sediminibacterium*, which has previously been found in freshwater sediments (Ogata et al., 2022; Sethuraman et al., 2022) and *Polynucleobacter,* which is widespread in freshwater environments (Watanabe et al., 2009). Spring at S5 was distinguished by *Polaromonas,* which is commonly isolated from glacial ice, sea ice, and sub-glacial sediments (Darcy et al., 2011; Gawor et al., 2016), and thus may be indicative of contributions of ice-associated taxa in spring as the large icing at this site thaws.

Additionally, *Pedobacter* was an indicator at S5 in spring, and is predominantly found in soils; psychrophilic and psychrotolerant species of this genus have also been isolated in northern regions (Dahal et al., 2020).

Microbial community structure was also unique across small spatial scales. S5a and S5b are located along the same stream network, with ~800 m separating the S5b lake and the S5a stream outlet (Figure 3-1). Despite being connected by a relatively short transit distance, soil characteristics and flow paths vary along this route, providing unique microbial sources to flow. Water transiting from S5b's lake outflow bay, which is very shallow, interacts with bottom sediment prior to outflow, and flow paths are routed over bedrock initially, and then over glaciolacustrine clays closer to S5a. S5a also contains a beaver dam at its outlet, which further modifies flow paths. The distribution of unique ASVs across sites and seasons may also highlight the varying nature of flow paths through this landscape. At S1 and S5b, the unique ASV counts at each site (across all sample types) were markedly higher than at S5a, which features a comparatively shorter transit distance from lake to stream.

3.4.4 DOM and nutrients drive microbial community structure across seasons

We found that differences in DOM composition drive microbial community structure, and that the partitioning of the DOM pool between winter surface water and icings may modify in-stream community composition as icings thaw and contribute to flow. Specifically, the degree of aromaticity and relative abundance of aliphatic, protein-like DOM were important determinants of microbial community structure. Our results are consistent with other studies in freshwater (Kaiser et al., 2017; Müller et al., 2018), and marine (Bruhn et al., 2021) environments as well as microcosm experiments (Wu et al., 2018), which show community composition to be driven by DOM composition. Nutrients (DIN, DON) and major cations also appeared as important drivers of community structure; these constituents are required for microbial growth and cellular processes (Larouche et al., 2012; Merchant & Helmann, 2012). DON also appears to be an important constituent of bioavailable DOM in Arctic rivers (Wickland et al., 2012). Several trace metals (Cu, Ba) were also important for community structure. Cu has an important biological role in many microbial cells (Merchant & Helmann, 2012), and Ba is involved in metabolic activities for some bacteria and archaea (Barbara, 2014). While icing meltwater and winter surface waters were pooled in our microbial analyses, the unique DOM pool in icing meltwater

suggests that icings may support unique microbial communities upon thaw during spring. Seasonal differences in DOM composition, nutrients and metals drove microbial community structure, but may also have implications for carbon cycling in this region.

3.4.5 Icing DOM is rapidly mineralized upon melt

Our incubation experiments confirmed that DOM from icing meltwater was rapidly mineralized compared to surface water from winter and summer. Mineralization was driven most strongly by DOM composition and was positively related to the relative abundance of DOM of autochthonous origin (bix), but negatively related to humic-like DOM (peak C). These positive drivers of decomposition were all prevalent in icing meltwater relative to surface water from winter and summer, suggesting that with icing formation, the biolabile fraction of winter flow is preferentially incorporated into ice (via solute exclusion), and enables rapid mineralization upon thaw. Our results were consistent with several recent incubation studies from Arctic and subarctic regions, which show preferential degradation of aliphatic, protein-like carbon (Balcarczyk et al., 2009; Drake et al., 2015; Littlefair & Tank, 2018; Spencer et al., 2015). Nutrients (TDP, SRP) were also significant drivers of biological processing in our incubation experiment.

While DOM biolability was also high in spring surface waters, this was only true for lake (versus stream) water, as stream water at S1 was comprised of less biolabile DOM pools. At the time of springtime sampling, the lake at S1, progressed from anoxic to oxic conditions during the spring (Alsafi, Ch. 2), which may have facilitated co-precipitation of aromatic DOM to iron oxides and oxyhydroxides, reducing the relative aromatic DOM pool (Du et al., 2018). This was evidenced by the much lower DOC concentrations in spring lake water (~2 mg L^{-1}) versus stream water (~30 mg L^{-1}), and a protein-like autochthonous DOM signature in lake water, which drove increased biolability. Similarly, icing meltwater had low DOC concentrations, but exhibited rapid mineralization due to its protein-like signature (Balcarczyk et al., 2009; Berggren et al., 2020).

3.5 Conclusions

Icings are important wintertime hydrological features on the Taiga Shield, and form through continued subsurface flow. We found that icings modify the composition of water actively moving through fluvial networks in the winter, enriching surface water in DOC and cations.

Furthermore, it appears that the highly bioavailable, aliphatic and protein-like DOM typical of winter flow on the Taiga Shield is selectively trapped in icings, which provides an energy-rich subsidy that becomes available for processing upon icing thaw during spring and summer. The biolabile nature of icing DOM may have significant effects on carbon cycling in the region, given the high density of lakes on the Taiga Shield which support icing formation. In the absence of icing formation, this labile DOM pool is actively transported through fluvial networks in the winter, and while in situ mineralization is limited by cold temperatures, the increasing prevalence of warmer winters on the Taiga Shield (Morse & Wolfe, 2015), may drive increased mineralization during this season. These results challenge the perception of winter as a chemically and hydrologically inactive period and highlight the dynamic nature of wintertime chemistry on the Taiga Shield, which is modified through icing formation and lake presence within this landscape. While we did not observe export of permafrost-origin DOM in the headwaters of this study, the presence of an aliphatic, protein-like DOM pool in icing meltwater suggests that this region may, nonetheless, be an important source of biolabile carbon in the winter. The distinct chemistry between icing meltwater and winter surface waters suggests that to characterize winter flow accurately in a warming climate, it is necessary to consider icings, and studies which only sample surface water may be missing an important aspect of wintertime chemistry. Finally, variations in biolability were tied to microbial community structure, which was similarly controlled by DOM composition and nutrients, with variation across seasons that included characteristic indicator taxa that may suggest unique microbiota contributions from icings to downstream environments during the spring thaw.

Our work highlights the need to understand how water is moving through the landscape during the winter on the Taiga Shield, as climate warming alters winter baseflow and levels of hydrologic connectivity between basins. Future work should consider the influence of interannual variation in icing formation on winter surface water chemistry and basal food web processes, to understand the effects of shifting icing dynamics under a warming climate. Given the water rich nature of the Taiga Shield, and overall lack of research focusing on microbial communities in this region, we highlight the need for further work delineating community structure in these highly dynamic systems. Lastly, changes in carbon cycling may have

implications over larger spatial scales as this water transits downstream, with shifting microbial community structure initiating cascading effects at higher trophic levels.

3.6 Figures

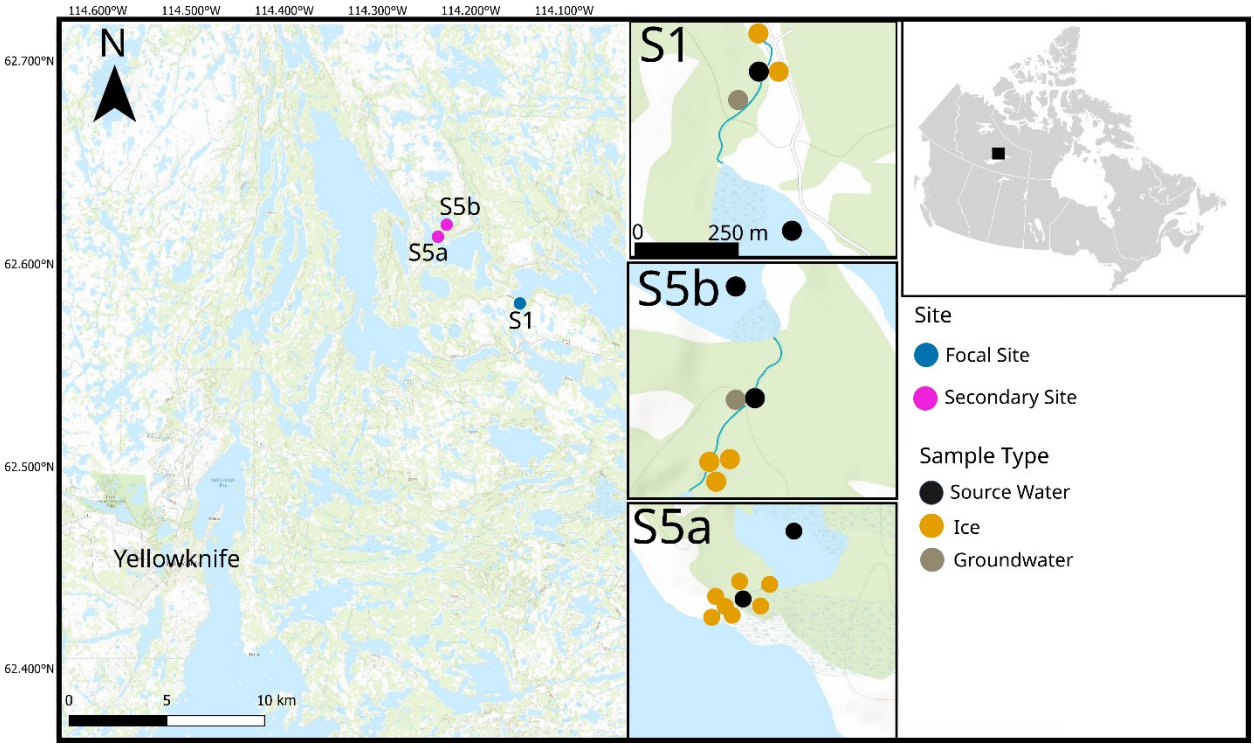

Figure 3-1. The River Lake watershed with sample sites. Focal sites with more frequent water sampling (in blue), and secondary sites with limited water sampling (in pink). Channels where ephemeral (S5a, S1) or perennial streams (S5b) are located are shown as blue lines. Ice core locations are shown in yellow, open water (lake and stream) sampling locations are shown in black and groundwater sampling locations are shown in brown.

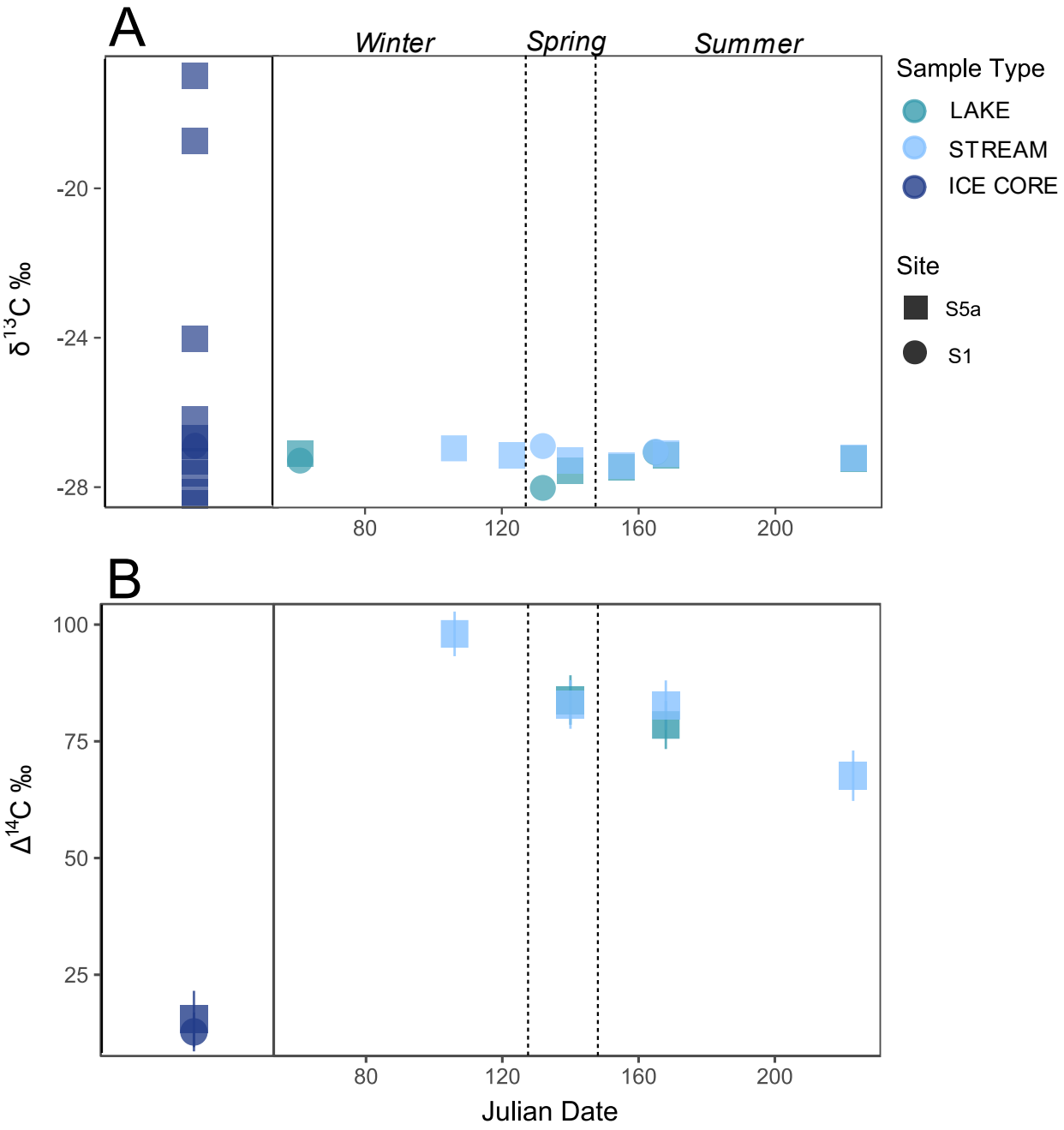

Figure 3-2. Panel A: Percentage of $\delta^{13}C$ ‰ across ice core, lake, and stream samples at S5a and S1 over time. Panel B: Percentage of $\Delta^{14}C$ ‰ ± error (1σ) of ice core, lake, and stream samples over time at S5a, and $\Delta^{14}C$ ‰ of an ice core from S1. Dotted lines demarcate winter, spring, and summer.

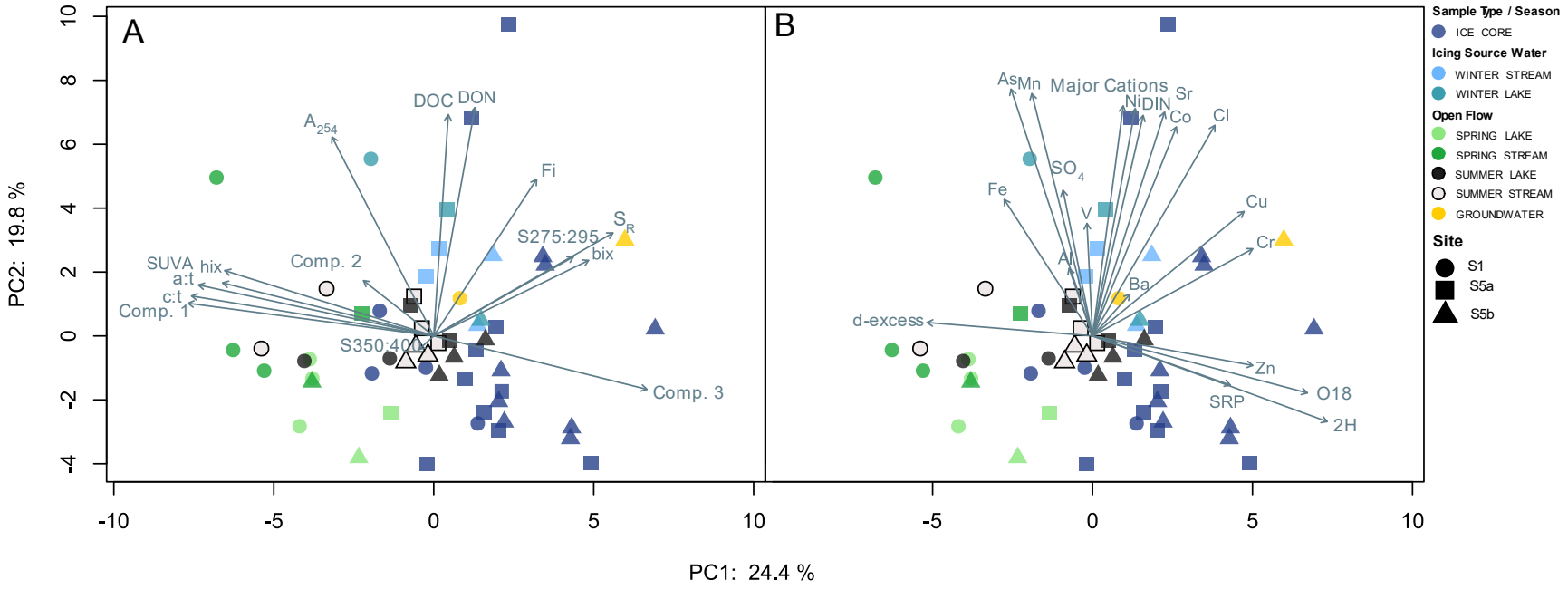

Figure 3-3. Principal component analysis (PCA) of water chemistry data for icing cores, stream, lake and groundwater over time (winter, spring and summer) across S1, S5a and S5b. Panels A and B represent the same global PCA, with panel A showing organic parameters and panel B showing inorganic parameters.

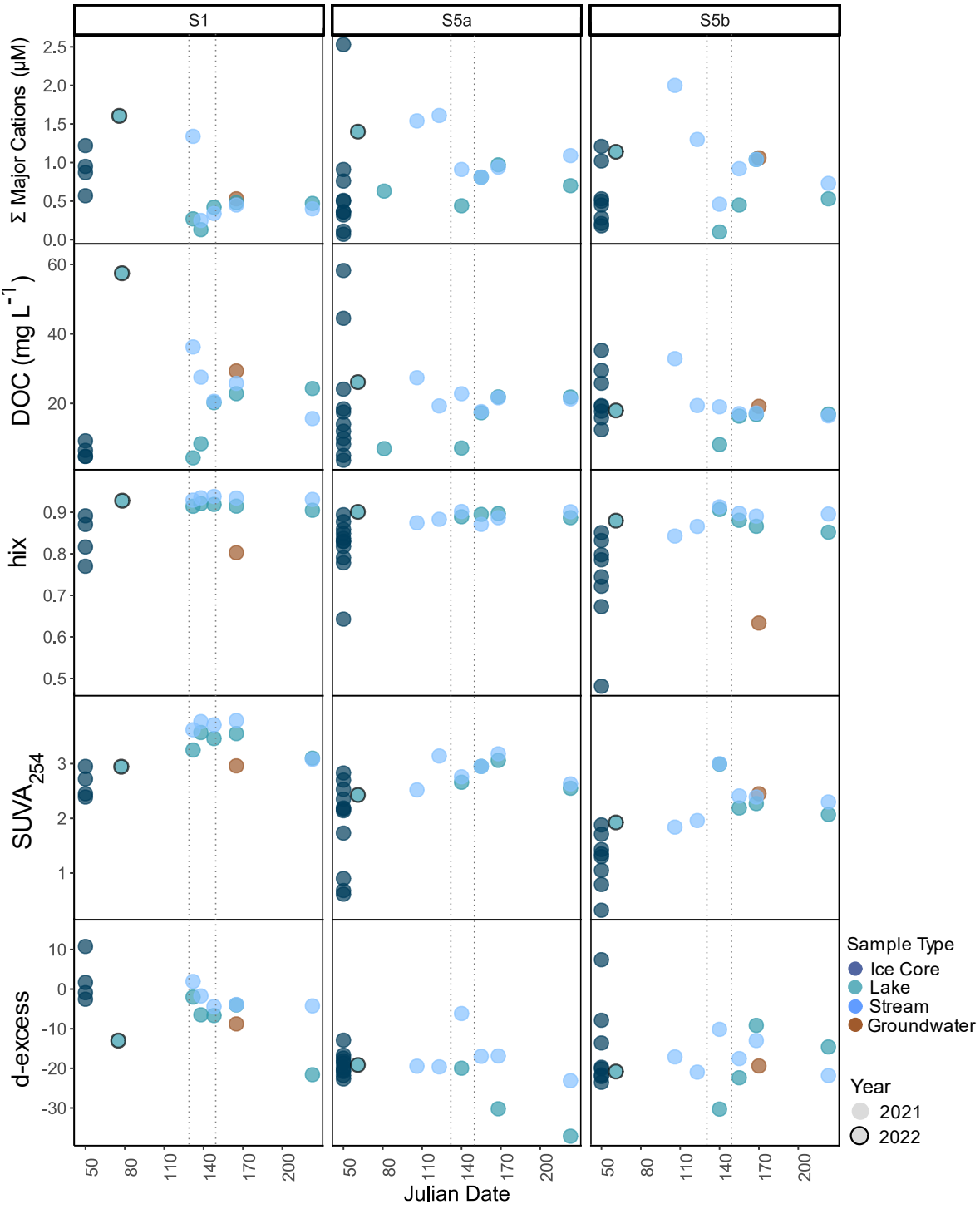

Figure 3-4. Concentrations of molar sum of major cations (Ca, Mg, K, Na), DOC, humification index (hix), absorbance metric $SUVA_{254}$ and d-excess of ice core, lake, stream, groundwater, and intra-icing water over time (2021-2022) at Sites 1, 5a and 5b. Sampling year denoted by black outline (for 2022) or no outline (for 2021). Winter, spring and summer demarcated by dotted grey black lines.

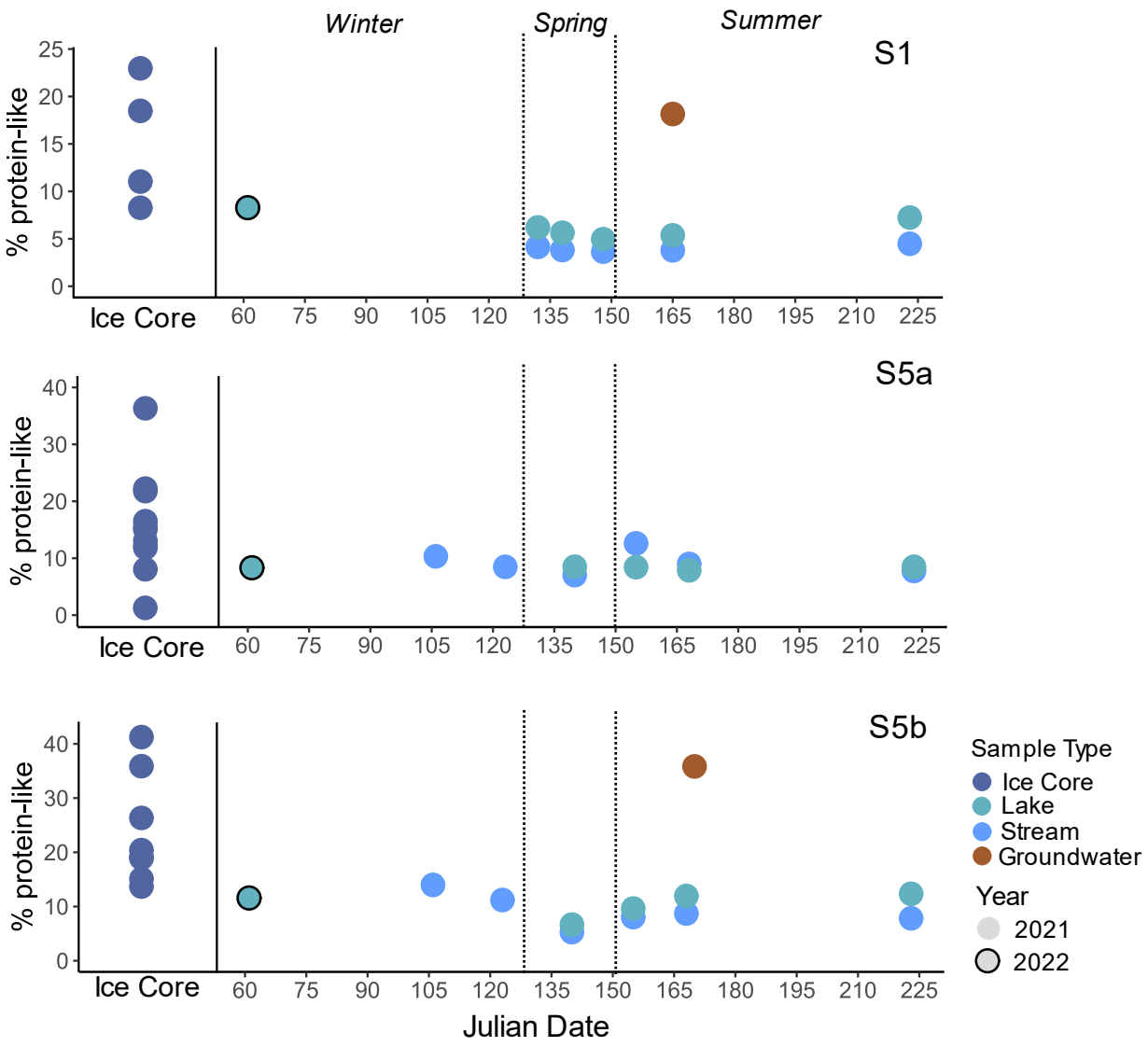

Figure 3-5. Percentage of protein-like (C3) dissolved organic matter (DOM) across three icings, paired source water (upstream lake and stream), and groundwater samples from 2021-2022. Sampling year denoted by black outline (for 2022) or no outline (for 2021).

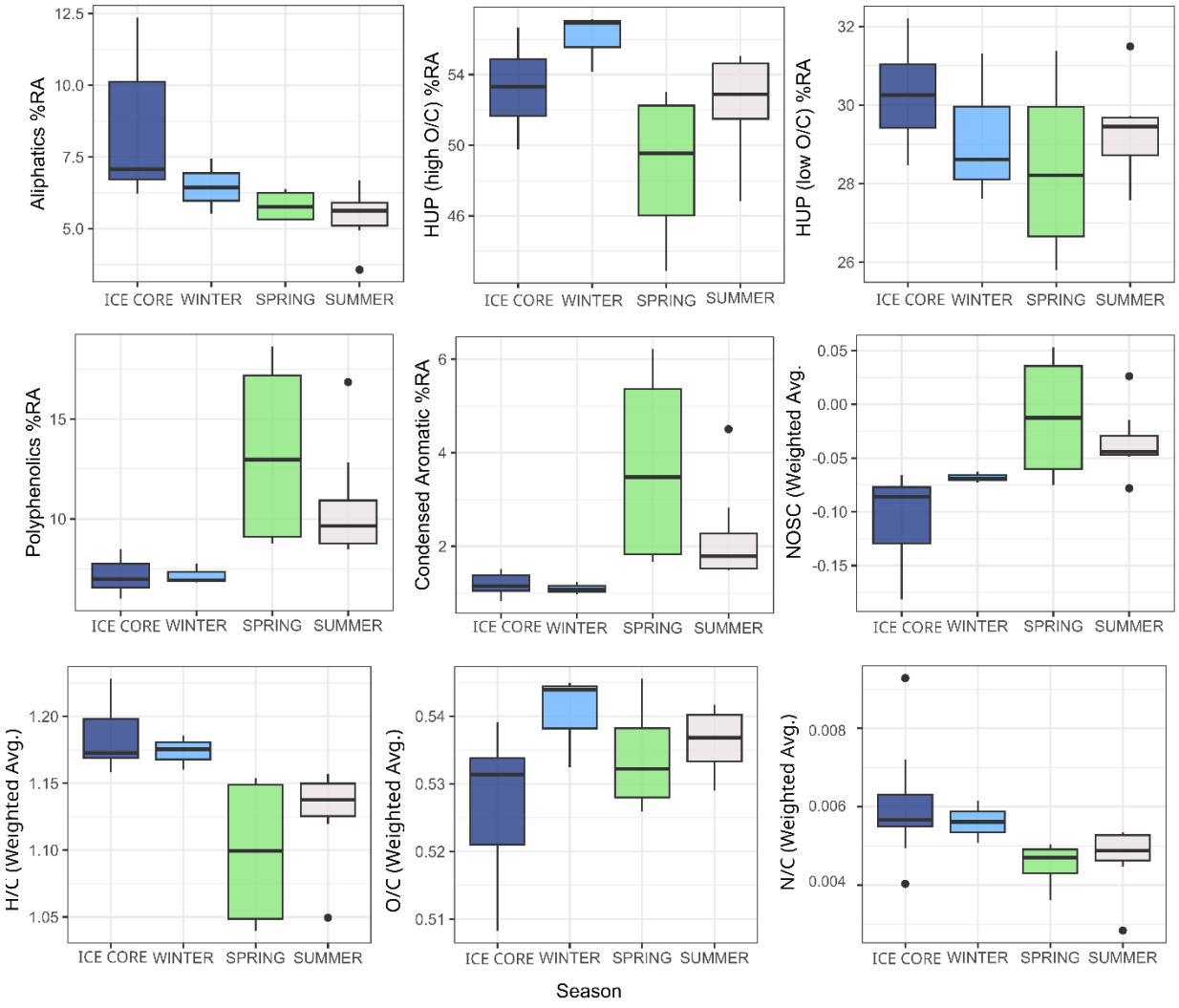

Figure 3-6. FT-ICR-MS: Percent relative abundance of each compound class sorted from least to most aromatic (aliphatics, $HUP_{High\ O/C}$, $HUP_{Low\ O/C}$, polyphenolics, and condensed aromatics), and weighted average of H/C, O/C, N/C and nominal oxidation state of carbon (NOSC) across seasons and icing meltwater. Winter, spring, and summer include pooled lake and stream samples.

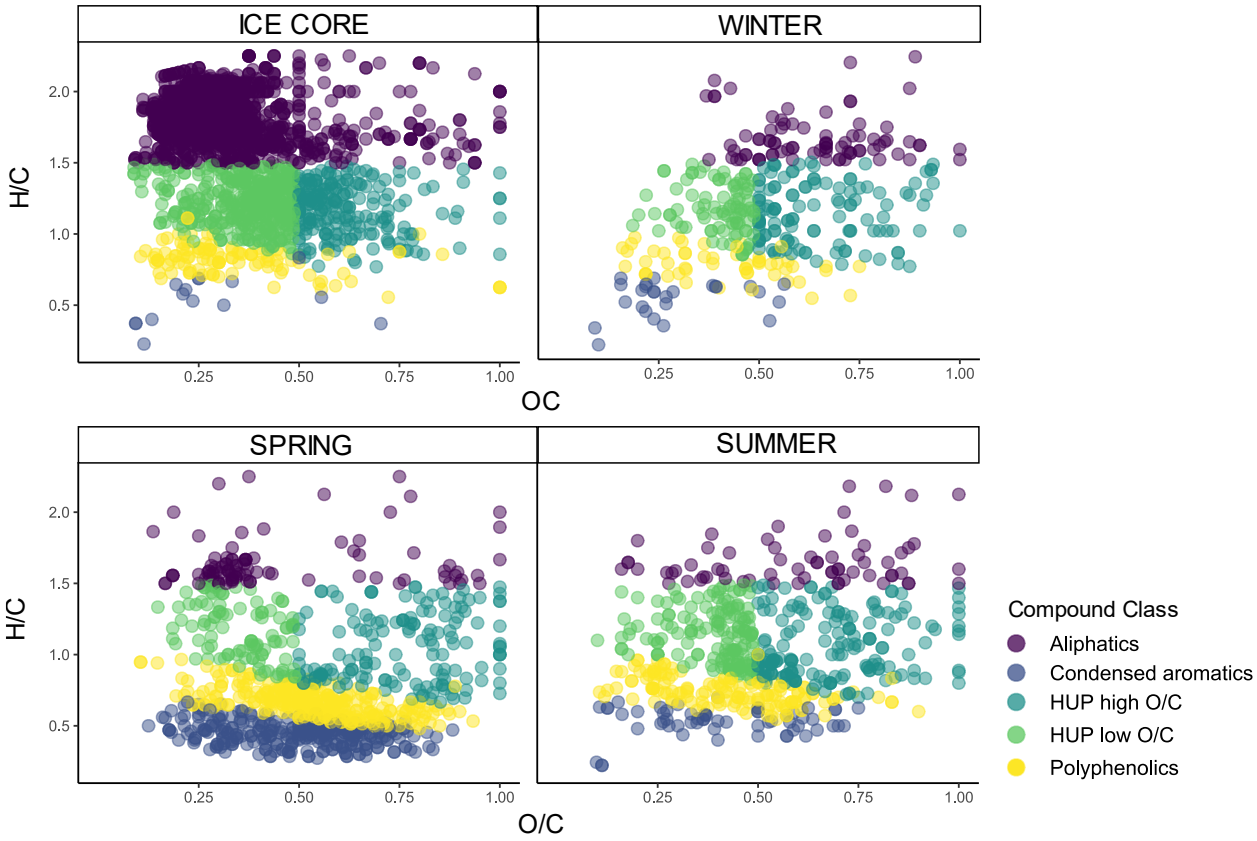

Figure 3-7. Unique molecular formulae within icing meltwater, winter, spring and summer samples as identified through FT-ICR-MS analysis. Winter, spring, and summer include pooled lake and stream samples.

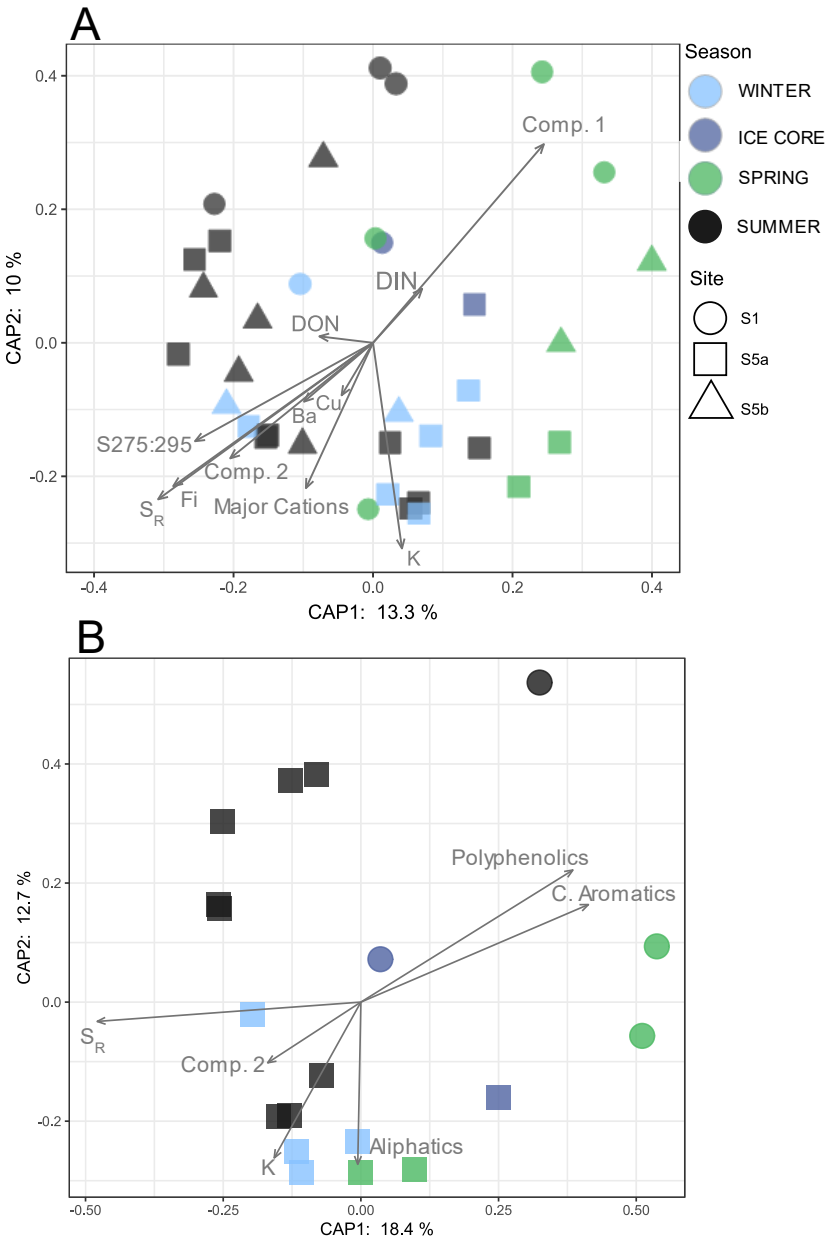

Figure 3-8. Panel A: Distance based redundancy analysis (dbRDA) of microbial community data as a function of significant water chemistry and DOM compositional drivers of winter, ice core, spring, and summer samples at S1, S5a and S5b. Panel B: dbRDA of microbial community data subset and significant FT-ICR-MS, water chemistry, and DOM compositional parameters of winter, ice core, spring and summer samples at S1 and S5a. dbRDA model summary and parameter significance shown in Table A2-4 for panel A and Table A2-5 for panel B. Winter, spring and summer include pooled lake and stream samples. Ice cores were pooled with winter surface waters for dbRDA analysis.

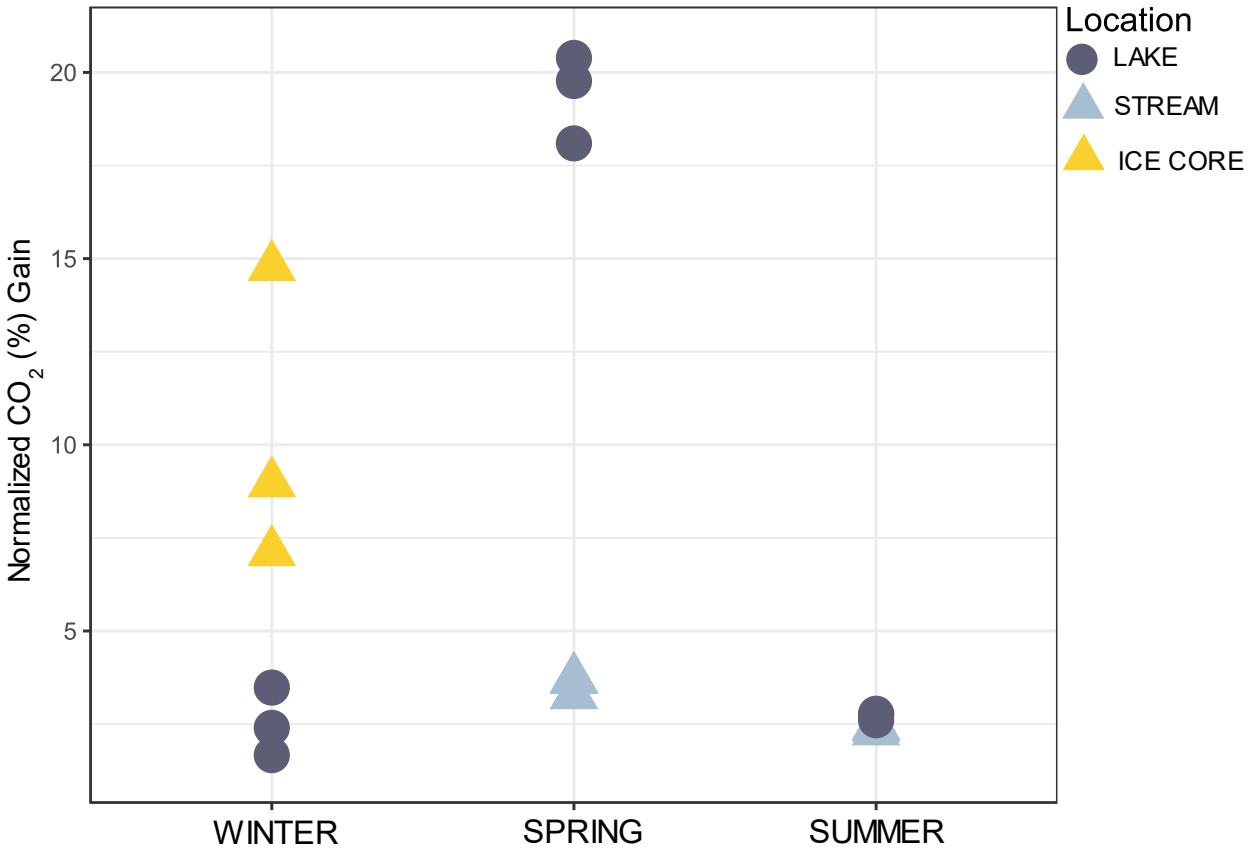

Figure 3-9. Normalized CO_2 percent gain over 28-day incubation period of lake, stream, and ice core samples from winter (April), spring (May) and summer (June). Incubation samples were collected from S1.

Chapter 4: General Conclusions

4.1 Summary of findings

In this thesis, I investigated the influence of fill-and-spill hydrological processes on icing dynamics, explored how icing chemistry was influenced by varying water sources, and evaluated the influence of icing chemistry on microbial communities and carbon mineralization in the lake-rich, fill and spill environment of the Taiga Shield. I found that icing formation was highly dynamic, and strongly influenced by wintertime fill and spill hydrology, which itself was governed by air temperatures and antecedent precipitation levels. Icing chemistry was impacted by physico-chemical processes occurring in lake basins and/or along flow paths, including anoxia, solute exclusion, and sediment-water interaction; these processes were strongly influenced by lake basin size. Furthermore, solute exclusion was important in modifying the chemical composition of water moving through fluvial networks in the winter, resulting in distinct chemistry between icings and surface waters. Compared to winter, spring and summer surface waters, icings were dilute in DOC, major cations and trace metals, but enriched in protein-like DOM. Solute exclusion trapped the highly bioavailable, aliphatic and protein-like fraction of DOM into icings, which was rapidly mineralized in an incubation experiment. Unique DOM composition was accompanied by variation in microbial community structure, with several distinct indicator taxa were found in winter and spring flow. Taken together, these results suggest that icings provide an energy-rich subsidy to flow as they thaw into the spring and summer, with the potential to modify carbon cycling and basal food webs as they persist on the landscape. As precipitation regimes shift, and wintertime air temperatures and baseflow continues to increase on the Taiga Shield, the dynamics of icing formation may also shift, with potential implications for stream chemistry, microbial communities and carbon cycling during the winter and the open water season.

4.2 Considerations and future research

While this study provides valuable insights into icing dynamics and chemistry, it is important to acknowledge its limitations. This study took place over two years, with water and icing sampling largely limited to the first year. While this allowed me to observe the effects of a lower precipitation year on icing formation in the second study year, fill and spill hydrology is highly dynamic in this region and warrants a longer study period than was possible for this thesis. Future work should consider monitoring icings over multiple years to fully understand the effects

of hydrological processes on icing chemistry, and to observe the influence of icing chemistry on microbial communities and basal food web processes. Additionally, this study was limited in spatial scale; the Taiga Shield covers an immense area, with a multitude of lakes which support icing formation. This project was based in the Taiga Shield High Boreal ecoregion located near Yellowknife, however the Taiga Shield features three other distinct ecoregions with regional differences in climate, vegetation and landscape features (Ecosystem Classification Group, 2008). Future work might expand the study of icings across these ecoregions and investigate spatial variation in icing chemistry at a broader spatial scale to fully understand the importance of this region in modifying wintertime chemistry via icing formation.

Microbial analysis within icings was limited in this thesis, given the high volume of ice required to collect microbial samples. Thus, future work could increase microbial sampling of icings to better understand spatial variation in microbial community structure across the extent and depth of icing features. It is unclear whether resident microbial communities in icings are influenced solely by the unique DOM composition of icings, or whether solute exclusion also plays a significant role in partitioning microbes between icings and open flow. Santibáñez et al., (2019) observed that microbes are preferentially included into the solid phase during lake ice formation, however we were unable to investigate this due to limited sample size. Future work may couple microbial sample collection from icings with more flowing water samples from within and beneath icings, to fully assess this phenomenon.

Finally, while beyond the scope of this work, it is important to understand how the effects of icing-specific alteration of in-stream chemistry propagate downstream in the winter, and in the spring and summer as icings thaw. Lakes on the Taiga Shield are connected in chains of varying length before reaching larger water bodies with longer residence times which tend to favour carbon burial (e.g., Great Slave Lake). Thus, it is important to quantify how much labile DOM released from icing thaw is mineralized into CO_2 before reaching larger water bodies to fully assess the potential of icings to modify carbon feedbacks in this region.

REFERENCES

Abbott, B. W., Larouche, J. R., Jones, J. B., Bowden, W. B., & Balser, A. W. (2014). Elevated dissolved organic carbon biodegradability from thawing and collapsing permafrost: Permafrost carbon biodegradability. *Journal of Geophysical Research: Biogeosciences*, *119*(10), 2049–2063. https://doi.org/10.1002/2014JG002678

Ackley, C., Tank, S. E., Haynes, K. M., Rezanezhad, F., McCarter, C., & Quinton, W. L. (2021). Coupled hydrological and geochemical impacts of wildfire in peatland-dominated regions of discontinuous permafrost. *Science of The Total Environment*, *782*, 146841. https://doi.org/10.1016/j.scitotenv.2021.146841

APHA, AWWA, & WEF. (2017a). 4110 Determination of anions by ion chromatography. In *Standard Methods For the Examination of Water and Wastewater* (Vols. 1–0). American Public Health Association. https://doi.org/10.2105/SMWW.2882.070

APHA, AWWA, & WEF. (2017b). 4500-NH3 Nitrogen (ammonia). In *Standard Methods For the Examination of Water and Wastewater* (Vols. 1–0). American Public Health Association. https://doi.org/10.2105/SMWW.2882.087

Aukes, Pieter Jan Karel. (2019). *Dissolved Organic Matter in the Canadian Arctic & Sub-Arctic: Importance of DOM Quality & Quantity in a Warming Climate* (PhD Thesis). UWSpace. Retrieved from http://hdl.handle.net/10012/14975

Balcarczyk, K. L., Jones, J. B., Jaffé, R., & Maie, N. (2009). Stream dissolved organic matter bioavailability and composition in watersheds underlain with discontinuous permafrost. *Biogeochemistry*, *94*(3), 255–270. https://doi.org/10.1007/s10533-009-9324-x

Ballantyne, C. K. (2017). *Periglacial geomorphology*. Hoboken, NJ: John Wiley & Sons.

Barbara, M. (2014). Uptake of Barium from Vermiculite by the Bacterium Pseudomonas fluorescens - New Indications for Barium as a Palaeoproxy. *The Open Geology Journal*, *8*(1), 118–123. https://doi.org/10.2174/1874262901408010118

Barnes, R. T., Butman, D. E., Wilson, H. F., & Raymond, P. A. (2018). Riverine Export of Aged Carbon Driven by Flow Path Depth and Residence Time. *Environmental Science & Technology*, *52*(3), 1028–1035. https://doi.org/10.1021/acs.est.7b04717

Barrett, P. M., Hull, E. A., Burkart, K., Hargrave, O., McLean, J., Taylor, V. F., et al. (2019). Contrasting arsenic cycling in strongly and weakly stratified contaminated lakes: Evidence for temperature control on sediment–water arsenic fluxes. *Limnology and Oceanography*, *64*(3), 1333–1346. https://doi.org/10.1002/lno.11119

Bartram, A. K., Lynch, M. D. J., Stearns, J. C., Moreno-Hagelsieb, G., & Neufeld, J. D. (2011). Generation of Multimillion-Sequence 16S rRNA Gene Libraries from Complex Microbial Communities by Assembling Paired-End Illumina Reads. *Applied and Environmental Microbiology*, *77*(11), 3846–3852. https://doi.org/10.1128/AEM.02772-10

Behnke, M. I., McClelland, J. W., Tank, S. E., Kellerman, A. M., Holmes, R. M., Haghipour, N., et al. (2021). Pan-Arctic Riverine Dissolved Organic Matter: Synchronous Molecular Stability, Shifting Sources and Subsidies. *Global Biogeochemical Cycles*, *35*(4). https://doi.org/10.1029/2020GB006871

Belzile, C., Gibson, J. A. E., & Vincent, W. F. (2002). Colored dissolved organic matter and dissolved organic carbon exclusion from lake ice: Implications for irradiance transmission and carbon cycling. *Limnology and Oceanography*, *47*(5), 1283–1293. https://doi.org/10.4319/lo.2002.47.5.1283

Bense, V. F., Kooi, H., Ferguson, G., & Read, T. (2012). Permafrost degradation as a control on hydrogeological regime shifts in a warming climate: GROUNDWATER AND DEGRADING PERMAFROST. *Journal of Geophysical Research: Earth Surface*, *117*(F3), n/a-n/a. https://doi.org/10.1029/2011JF002143

Berggren, M., Gudasz, C., Guillemette, F., Hensgens, G., Ye, L., & Karlsson, J. (2020). Systematic microbial production of optically active dissolved organic matter in subarctic lake water. *Limnology and Oceanography*, *65*(5), 951–961. https://doi.org/10.1002/lno.11362

Bernardet, J.-F., & Bowman, J. P. (2006). The Genus Flavobacterium. In M. Dworkin, S. Falkow, E. Rosenberg, K.-H. Schleifer, & E. Stackebrandt (Eds.), *The Prokaryotes* (pp. 481–531). New York, NY: Springer New York. https://doi.org/10.1007/0-387-30747-8_17

Blakney, G. T., Hendrickson, C. L., & Marshall, A. G. (2011). Predator data station: A fast data acquisition system for advanced FT-ICR MS experiments. *International Journal of Mass Spectrometry*, *306*(2–3), 246–252. https://doi.org/10.1016/j.ijms.2011.03.009

Bolyen, E., Rideout, J. R., Dillon, M. R., Bokulich, N. A., Abnet, C. C., Al-Ghalith, G. A., et al. (2019). Reproducible, interactive, scalable and extensible microbiome data science using QIIME 2. *Nature Biotechnology*, *37*(8), 852–857. https://doi.org/10.1038/s41587-019-0209-9

Brooks, J. R., Gibson, J. J., Birks, S. J., Weber, M. H., Rodecap, K. D., & Stoddard, J. L. (2014). Stable isotope estimates of evaporation : inflow and water residence time for lakes across the United States as a tool for national lake water quality assessments. *Limnology and Oceanography*, *59*(6), 2150–2165. https://doi.org/10.4319/lo.2014.59.6.2150

Bruhn, A. D., Stedmon, C. A., Comte, J., Matsuoka, A., Speetjens, N. J., Tanski, G., et al. (2021). Terrestrial Dissolved Organic Matter Mobilized From Eroding Permafrost Controls Microbial Community Composition and Growth in Arctic Coastal Zones. *Frontiers in Earth Science*, *9*, 640580. https://doi.org/10.3389/feart.2021.640580

Caceres, M. D., & Legendre, P. (2009). *Associations between species and groups of sites: indices and statistical inference*. *Ecology*. Retrieved from http://sites.google.com/site/miqueldecaceres/

Cáceres, M. D., Jansen, F., & Dell, N. (2022). *indicspecies: Relationship Between Species and Groups of Sites*. Retrieved from https://emf-creaf.github.io/indicspecies/

Callahan, B. J., Grinevich, D., Thakur, S., Balamotis, M. A., & Yehezkel, T. B. (2021). Ultra-accurate microbial amplicon sequencing with synthetic long reads. *Microbiome*, *9*(1), 130. https://doi.org/10.1186/s40168-021-01072-3

Campeau, A., Soerensen, A. L., Martma, T., Åkerblom, S., & Zdanowicz, C. (2020). Controls on the ^{14} C Content of Dissolved and Particulate Organic Carbon Mobilized Across the Mackenzie River Basin, Canada. *Global Biogeochemical Cycles*, *34*(12). https://doi.org/10.1029/2020GB006671

Carey, K. L. (1973). Icings developed from surface water and ground water.

Cavaco, M. A., St. Louis, V. L., Engel, K., St. Pierre, K. A., Schiff, S. L., Stibal, M., & Neufeld, J. D. (2019). Freshwater microbial community diversity in a rapidly changing High Arctic watershed. *FEMS Microbiology Ecology*, *95*(11), fiz161. https://doi.org/10.1093/femsec/fiz161

Coble, P. G. (1996). Characterization of marine and terrestrial DOM in seawater using excitation-emission matrix spectroscopy. *Marine Chemistry*, *51*(4), 325–346. https://doi.org/10.1016/0304-4203(95)00062-3

Connon, R., Devoie, É., Hayashi, M., Veness, T., & Quinton, W. (2018). The Influence of Shallow Taliks on Permafrost Thaw and Active Layer Dynamics in Subarctic Canada. *Journal of Geophysical Research: Earth Surface*, *123*(2), 281–297. https://doi.org/10.1002/2017JF004469

Corilo, Y. (2015). PetroOrg. Florida State University. Retrieved from http://software.petroorg.com

Crann, C. A., Murseli, S., St-Jean, G., Zhao, X., Clark, I. D., & Kieser, W. E. (2017). First Status Report on Radiocarbon Sample Preparation Techniques at the A.E. Lalonde AMS Laboratory (Ottawa, Canada). *Radiocarbon*, *59*(3), 695–704. https://doi.org/10.1017/RDC.2016.55

Crites, H., Kokelj, S. V., & Lacelle, D. (2020). Icings and groundwater conditions in permafrost catchments of northwestern Canada. *Scientific Reports*, *10*(1), 3283. https://doi.org/10.1038/s41598-020-60322-w

Cui, J., Tian, L., Biggs, T. W., & Wen, R. (2017). Deuterium-excess determination of evaporation to inflow ratios of an alpine lake: Implications for water balance and modeling. *Hydrological Processes*, *31*(5), 1034–1046. https://doi.org/10.1002/hyp.11085

Dahal, R. H., Chaudhary, D. K., Kim, D.-U., & Kim, J. (2020). Nine novel psychrotolerant species of the genus Pedobacter isolated from Arctic soil with potential antioxidant activities. *International Journal of Systematic and Evolutionary Microbiology*, *70*(4), 2537–2553. https://doi.org/10.1099/ijsem.0.004071

Darcy, J. L., Lynch, R. C., King, A. J., Robeson, M. S., & Schmidt, S. K. (2011). Global Distribution of Polaromonas Phylotypes - Evidence for a Highly Successful Dispersal Capacity. *PLoS ONE*, *6*(8), e23742. https://doi.org/10.1371/journal.pone.0023742

DeGrandpre, E. L., DeGrandpre, M. D., Colman, B. P., & Valett, H. M. (2021). Observations of River Solute Concentrations during Ice Formation. *ACS ES&T Water*, *1*(8), 1695–1701. https://doi.org/10.1021/acsestwater.1c00064

Devoie, É. G., Craig, J. R., Connon, R. F., & Quinton, W. L. (2019). Taliks: A Tipping Point in Discontinuous Permafrost Degradation in Peatlands. *Water Resources Research*, *55*(11), 9838–9857. https://doi.org/10.1029/2018WR024488

Dittmar, T., Koch, B., Hertkorn, N., & Kattner, G. (2008). A simple and efficient method for the solid-phase extraction of dissolved organic matter (SPE-DOM) from seawater: SPE-DOM from seawater. *Limnology and Oceanography: Methods*, *6*(6), 230–235. https://doi.org/10.4319/lom.2008.6.230

Douglas, T. A., Blum, J. D., Guo, L., Keller, K., & Gleason, J. D. (2013). Hydrogeochemistry of seasonal flow regimes in the Chena River, a subarctic watershed draining discontinuous permafrost in interior Alaska (USA). *Chemical Geology*, *335*, 48–62. https://doi.org/10.1016/j.chemgeo.2012.10.045

Drake, T. W., Wickland, K. P., Spencer, R. G. M., McKnight, D. M., & Striegl, R. G. (2015). Ancient low–molecular-weight organic acids in permafrost fuel rapid carbon dioxide production upon thaw. *Proceedings of the National Academy of Sciences*, *112*(45), 13946–13951. https://doi.org/10.1073/pnas.1511705112

Du, Y., Ramirez, C. E., & Jaffé, R. (2018). Fractionation of Dissolved Organic Matter by Co-Precipitation with Iron: Effects of Composition. *Environmental Processes*, *5*(1), 5–21. https://doi.org/10.1007/s40710-017-0281-4

Dufrêne, M., & Legendre, P. (1997). SPECIES ASSEMBLAGES AND INDICATOR SPECIES:THE NEED FOR A FLEXIBLE ASYMMETRICAL APPROACH. *Ecological Monographs*, *67*(3), 345–366. https://doi.org/10.1890/0012-9615(1997)067[0345:SAAIST]2.0.CO;2

ECCC. (2022a). Canadian Climate Normals 1981-2010 Station Data. Retrieved from https://climate.weather.gc.ca/climate_normals

ECCC. (2022b). Historical Data: Yellowknife A, Northwest Territories. Retrieved from https://climate.weather.gc.ca/historical_data/search_historic_data_e.html

Ecosystem Classification Group. (2008). *Ecological regions of the Northwest Territories, Taiga Shield*. Dept. of Environment and Natural Resources, Government. of the Northwest Territories.

Ensom, T., Makarieva, O., Morse, P., Kane, D., Alekseev, V., & Marsh, P. (2020). The distribution and dynamics of aufeis in permafrost regions. *Permafrost and Periglacial Processes*, *31*(3), 383–395. https://doi.org/10.1002/ppp.2051

Garcia-Robledo, E., Paulmier, A., Borisov, S. M., & Revsbech, N. P. (2021). Sampling in low oxygen aquatic environments: The deviation from anoxic conditions. *Limnology and Oceanography: Methods*, *19*(11), 733–740. https://doi.org/10.1002/lom3.10457

Gawor, J., Grzesiak, J., Sasin-Kurowska, J., Borsuk, P., Gromadka, R., Górniak, D., et al. (2016). Evidence of adaptation, niche separation and microevolution within the genus Polaromonas on Arctic and Antarctic glacial surfaces. *Extremophiles*, *20*(4), 403–413. https://doi.org/10.1007/s00792-016-0831-0

Gibson, J. J., Holmes, T., Stadnyk, T. A., Birks, S. J., Eby, P., & Pietroniro, A. (2020). 18O and 2H in streamflow across Canada. *Journal of Hydrology: Regional Studies*, *32*, 100754. https://doi.org/10.1016/j.ejrh.2020.100754

Giles, C. D., Isles, P. D. F., Manley, T., Xu, Y., Druschel, G. K., & Schroth, A. W. (2016). The mobility of phosphorus, iron, and manganese through the sediment–water continuum of a shallow eutrophic freshwater lake under stratified and mixed water-column conditions. *Biogeochemistry*, *127*(1), 15–34. https://doi.org/10.1007/s10533-015-0144-x

Glass, B. K., Rudolph, D. L., Duguay, C., & Wicke, A. (2021). Identifying groundwater discharge zones in the Central Mackenzie Valley using remotely sensed optical and thermal imagery. *Canadian Journal of Earth Sciences*, *58*(2), 105–121. https://doi.org/10.1139/cjes-2019-0169

Gonçalves-Araujo, R., Granskog, M. A., Bracher, A., Azetsu-Scott, K., Dodd, P. A., & Stedmon, C. A. (2016). Using fluorescent dissolved organic matter to trace and distinguish the origin of Arctic surface waters. *Scientific Reports*, *6*(1), 33978. https://doi.org/10.1038/srep33978

Guéguen, C., Cuss, C. W., Cassels, C. J., & Carmack, E. C. (2014). Absorption and fluorescence of dissolved organic matter in the waters of the Canadian Arctic Archipelago, Baffin Bay, and the Labrador Sea. *Journal of Geophysical Research: Oceans*, *119*(3), 2034–2047. https://doi.org/10.1002/2013JC009173

Guo, L., Cai, Y., Belzile, C., & Macdonald, R. W. (2012). Sources and export fluxes of inorganic and organic carbon and nutrient species from the seasonally ice-covered Yukon River. *Biogeochemistry*, *107*(1–3), 187–206. https://doi.org/10.1007/s10533-010-9545-z

Hall, D. K. (1980). Mineral Precipitation in North Slope River Icings. *ARCTIC*, *33*(2), 343–348. https://doi.org/10.14430/arctic2567

Hamilton-Taylor, J., & Davison, W. (1995). Redox-Driven Cycling of Trace Elements in Lakes. In A. Lerman, D. M. Imboden, & J. R. Gat (Eds.), *Physics and Chemistry of Lakes* (pp. 217–263). Berlin, Heidelberg: Springer Berlin Heidelberg. https://doi.org/10.1007/978-3-642-85132-2_8

Hamilton-Taylor, J., Smith, E. J., Davison, W., & Sugiyama, M. (2005). Resolving and modeling the effects of Fe and Mn redox cycling on trace metal behavior in a seasonally anoxic lake. *Geochimica et Cosmochimica Acta*, *69*(8), 1947–1960. https://doi.org/10.1016/j.gca.2004.11.006

Hansen, A. M., Fleck, J. A., Kraus, T. E. C., Downing, Von Dessonneck, T., & Bergamaschi, B. A. (2018). *Procedures for using the Horiba Scientific Aqualog® fluorometer to measure absorbance and fluorescence from dissolved organic matter*. U.S. Geological Survey.

Helms, J. R., Stubbins, A., Ritchie, J. D., Minor, E. C., Kieber, D. J., & Mopper, K. (2008). Absorption spectral slopes and slope ratios as indicators of molecular weight, source, and photobleaching of chromophoric dissolved organic matter. *Limnology and Oceanography*, *53*(3), 955–969. https://doi.org/10.4319/lo.2008.53.3.0955

Hendrickson, C. L., Quinn, J. P., Kaiser, N. K., Smith, D. F., Blakney, G. T., Chen, T., et al. (2015). 21 Tesla Fourier Transform Ion Cyclotron Resonance Mass Spectrometer: A National Resource for Ultrahigh Resolution Mass Analysis. *Journal of the American Society for Mass Spectrometry*, *26*(9), 1626–1632. https://doi.org/10.1007/s13361-015-1182-2

Hodgkins, R., Tranter, M., & Dowdeswell, J. A. (2004). The characteristics and formation of a high-arctic proglacial icing. *Geografiska Annaler: Series A, Physical Geography*, *86*(3), 265–275. https://doi.org/10.1111/j.0435-3676.2004.00230.x

Holmes, R. M., McClelland, J. W., Peterson, B. J., Tank, S. E., Bulygina, E., Eglinton, T. I., et al. (2012). Seasonal and Annual Fluxes of Nutrients and Organic Matter from Large Rivers to the Arctic Ocean and Surrounding Seas. *Estuaries and Coasts*, *35*(2), 369–382. https://doi.org/10.1007/s12237-011-9386-6

Hu, X., & Pollard, W. H. (1997a). Ground Icing Formation: Experimental and Statistical Analyses of the Overflow Process. *Permafrost and Periglacial Processes*, *8*(2), 217–235. https://doi.org/10.1002/(SICI)1099-1530(199732)8:2<217::AID-PPP251>3.0.CO;2-1

Hu, X., & Pollard, W. H. (1997b). The Hydrologic Analysis and Modelling of River Icing Growth, North Fork Pass, Yukon Territory, Canada. *Permafrost and Periglacial Processes*, *8*(3), 279–294. https://doi.org/10.1002/(SICI)1099-1530(199709)8:3<279::AID-PPP260>3.0.CO;2-7

Hughes, J. B., & Hellmann, J. J. (2005). The Application of Rarefaction Techniques to Molecular Inventories of Microbial Diversity. In *Methods in Enzymology* (Vol. 397, pp. 292–308). Elsevier. https://doi.org/10.1016/S0076-6879(05)97017-1

Imbeau, E., Vincent, W. F., Wauthy, M., Cusson, M., & Rautio, M. (2021). Hidden Stores of Organic Matter in Northern Lake Ice: Selective Retention of Terrestrial Particles, Phytoplankton and Labile Carbon. *Journal of Geophysical Research: Biogeosciences*, *126*(8). https://doi.org/10.1029/2020JG006233

IPCC, I. P. of C. C. (2021). *Climate Change 2021: The Physical Science Basis*. Cambridge, UK; New York, NY, USA.

ISO. (2019). Water quality — Determination of nitrogen — Part 1: Method using oxidative digestion with peroxodisulfate.

Jansen, J., MacIntyre, S., Barrett, D. C., Chin, Y., Cortés, A., Forrest, A. L., et al. (2021). Winter Limnology: How do Hydrodynamics and Biogeochemistry Shape Ecosystems Under Ice? *Journal of Geophysical Research: Biogeosciences*, *126*(6). https://doi.org/10.1029/2020JG006237

Kaiser, K., Canedo-Oropeza, M., McMahon, R., & Amon, R. M. W. (2017). Origins and transformations of dissolved organic matter in large Arctic rivers. *Scientific Reports*, *7*(1), 13064. https://doi.org/10.1038/s41598-017-12729-1

Kalff, J. (2002). *Limnology: inland water ecosystems*. Upper Saddle River, NJ: Prentice Hall.

Kane, D. L. (1981). Physical mechanics of aufeis growth. *Canadian Journal of Civil Engineering*, *8*(2), 186–195. https://doi.org/10.1139/l81-026

Koch, B. P., & Dittmar, T. (2006). From mass to structure: an aromaticity index for high-resolution mass data of natural organic matter. *Rapid Communications in Mass Spectrometry*, *20*(5), 926–932. https://doi.org/10.1002/rcm.2386

Kurek, M. R., Garcia-Tigreros, F., Wickland, K. P., Frey, K. E., Dornblaser, M. M., Striegl, R. G., et al. (2023). Hydrologic and Landscape Controls on Dissolved Organic Matter Composition Across Western North American Arctic Lakes. *Global Biogeochemical Cycles*, *37*(1). https://doi.org/10.1029/2022GB007495

Lalonde, K., Middlestead, P., & Gélinas, Y. (2014). Automation of ^{13} C/ ^{12} C ratio measurement for freshwater and seawater DOC using high temperature combustion. *Limnology and Oceanography: Methods*, *12*(12), 816–829. https://doi.org/10.4319/lom.2014.12.816

Lamontagne-Hallé, P., McKenzie, J. M., Kurylyk, B. L., & Zipper, S. C. (2018). Changing groundwater discharge dynamics in permafrost regions. *Environmental Research Letters*, *13*(8), 084017. https://doi.org/10.1088/1748-9326/aad404

Larouche, J. R., Bowden, W. B., Giordano, R., Flinn, M. B., & Crump, B. C. (2012). Microbial Biogeography of Arctic Streams: Exploring Influences of Lithology and Habitat. *Frontiers in Microbiology*, *3*. https://doi.org/10.3389/fmicb.2012.00309

LaRowe, D. E., & Van Cappellen, P. (2011). Degradation of natural organic matter: A thermodynamic analysis. *Geochimica et Cosmochimica Acta*, *75*(8), 2030–2042. https://doi.org/10.1016/j.gca.2011.01.020

Lawson, E. C., Bhatia, M. P., Wadham, J. L., & Kujawinski, E. B. (2014). Continuous Summer Export of Nitrogen-Rich Organic Matter from the Greenland Ice Sheet Inferred by Ultrahigh Resolution Mass Spectrometry. *Environmental Science & Technology*, *48*(24), 14248–14257. https://doi.org/10.1021/es501732h

Leppi, J. C., Arp, C. D., & Whitman, M. S. (2016). Predicting Late Winter Dissolved Oxygen Levels in Arctic Lakes Using Morphology and Landscape Metrics. *Environmental Management*, *57*(2), 463–473. https://doi.org/10.1007/s00267-015-0622-x

Littlefair, C. A., & Tank, S. E. (2018). Biodegradability of Thermokarst Carbon in a Till-Associated, Glacial Margin Landscape: The Case of the Peel Plateau, NWT, Canada. *Journal of Geophysical Research: Biogeosciences*, *123*(10), 3293–3307. https://doi.org/10.1029/2018JG004461

Liu, W., Fortier, R., Molson, J., & Lemieux, J. (2021). A conceptual model for talik dynamics and icing formation in a river floodplain in the continuous permafrost zone at Salluit, Nunavik (Quebec), Canada. *Permafrost and Periglacial Processes*, *32*(3), 468–483. https://doi.org/10.1002/ppp.2111

Lyon, S. W., Mörth, M., Humborg, C., Giesler, R., & Destouni, G. (2010). The relationship between subsurface hydrology and dissolved carbon fluxes for a sub-arctic catchment. *Hydrology and Earth System Sciences*, *14*(6), 941–950. https://doi.org/10.5194/hess-14-941-2010

Marsh, P., & Hey, M. (1989). The Flooding Hydrology of Mackenzie Delta Lakes near Inuvik, N.W.T., Canada. *Arctic*, *42*(1), 41–49.

Mathias, J. A., & Barica, J. (1980). Factors Controlling Oxygen Depletion in Ice-Covered Lakes. *Canadian Journal of Fisheries and Aquatic Sciences*, *37*(2), 185–194. https://doi.org/10.1139/f80-024

McKnight, D. T., Huerlimann, R., Bower, D. S., Schwarzkopf, L., Alford, R. A., & Zenger, K. R. (2019). Methods for normalizing microbiome data: An ecological perspective. *Methods in Ecology and Evolution*, *10*(3), 389–400. https://doi.org/10.1111/2041-210X.13115

Merchant, S. S., & Helmann, J. D. (2012). Elemental Economy. In *Advances in Microbial Physiology* (Vol. 60, pp. 91–210). Elsevier. https://doi.org/10.1016/B978-0-12-398264-3.00002-4

Michel, F. A. (2011). Isotope characterisation of ground ice in northern Canada: Isotope Characterisation of Ground Ice. *Permafrost and Periglacial Processes*, *22*(1), 3–12. https://doi.org/10.1002/ppp.721

Mielko, C., & Woo, M. (2006). Snowmelt runoff processes in a headwater lake and its catchment, subarctic Canadian Shield. *Hydrological Processes*, *20*(4), 987–1000. https://doi.org/10.1002/hyp.6117

Morse, P. D., & Wolfe, S. A. (2014). *Icings in the Great Slave region (1985-2014), Northwest Territories, mapped from Landsat Imagery* (No. 7720) (p. 7720). https://doi.org/10.4095/295540

Morse, P. D., & Wolfe, S. A. (2015). Geological and meteorological controls on icing (aufeis) dynamics (1985 to 2014) in subarctic Canada: Icing Dynamics in Subarctic Canada. *Journal of Geophysical Research: Earth Surface*, *120*(9), 1670–1686. https://doi.org/10.1002/2015JF003534

Morse, P. D., & Wolfe, S. A. (2017). Long-Term River Icing Dynamics in Discontinuous Permafrost, Subarctic Canadian Shield: River Icing Dynamics in Discontinuous Permafrost, Subarctic Canada. *Permafrost and Periglacial Processes*, *28*(3), 580–586. https://doi.org/10.1002/ppp.1907

Morse, P. D., Wolfe, S. A., Kokelj, S. V., & Gaanderse, A. J. R. (2016). The Occurrence and Thermal Disequilibrium State of Permafrost in Forest Ecotopes of the Great Slave Region, Northwest Territories, Canada: Discontinuous permafrost conditions, Great Slave region, NWT, Canada. *Permafrost and Periglacial Processes*, *27*(2), 145–162. https://doi.org/10.1002/ppp.1858

Mostovaya, A., Hawkes, J. A., Dittmar, T., & Tranvik, L. J. (2017). Molecular Determinants of Dissolved Organic Matter Reactivity in Lake Water. *Frontiers in Earth Science*, *5*, 106. https://doi.org/10.3389/feart.2017.00106

Müller, O., Seuthe, L., Bratbak, G., & Paulsen, M. L. (2018). Bacterial Response to Permafrost Derived Organic Matter Input in an Arctic Fjord. *Frontiers in Marine Science*, *5*, 263. https://doi.org/10.3389/fmars.2018.00263

Murphy, K. R., Stedmon, C. A., Graeber, D., & Bro, R. (2013). Fluorescence spectroscopy and multi-way techniques. PARAFAC. *Analytical Methods*, *5*(23), 6557. https://doi.org/10.1039/c3ay41160e

Niemann, H., Steinle, L., Blees, J., Bussmann, I., Treude, T., Krause, S., et al. (2015). Toxic effects of lab-grade butyl rubber stoppers on aerobic methane oxidation: Toxic effects of aerobic methane oxidation. *Limnology and Oceanography: Methods*, *13*(1), 40–52. https://doi.org/10.1002/lom3.10005

O'Donnell, J. A., Aiken, G. R., Butler, K. D., Guillemette, F., Podgorski, D. C., & Spencer, R. G. M. (2016). DOM composition and transformation in boreal forest soils: The effects of temperature and organic-horizon decomposition state. *Journal of Geophysical Research: Biogeosciences*, *121*(10), 2727–2744. https://doi.org/10.1002/2016JG003431

Ogata, Y., Watanabe, K., Takemine, S., Shindo, C., Kurokawa, R., & Suda, W. (2022). Whole-Genome Sequence of *Sediminibacterium* sp. Strain TEGAF015, Isolated from a Shallow Eutrophic Freshwater Lake in Japan. *Microbiology Resource Announcements*, *11*(11), e00882-22. https://doi.org/10.1128/mra.00882-22

Oksanen, J., Simpson, G. L., Blanchet, F. G., Kindt, R., Legendre, P., Minchin, P. R., et al. (2022). *vegan: Community Ecology Package*. Retrieved from https://github.com/vegandevs/vegan

Oliver, S. K., Soranno, P. A., Fergus, C. E., Wagner, T., Winslow, L. A., Scott, C. E., et al. (2016). Prediction of lake depth across a 17-state region in the United States. *Inland Waters*, *6*(3), 314–324. https://doi.org/10.1080/IW-6.3.957

Oren, A., & Chefetz, B. (2012). Sorptive and Desorptive Fractionation of Dissolved Organic Matter by Mineral Soil Matrices. *Journal of Environmental Quality*, *41*(2), 526–533. https://doi.org/10.2134/jeq2011.0362

Palmer, M. J., Chételat, J., Richardson, M., Jamieson, H. E., & Galloway, J. M. (2019). Seasonal variation of arsenic and antimony in surface waters of small subarctic lakes impacted by legacy mining pollution near Yellowknife, NT, Canada. *Science of The Total Environment*, *684*, 326–339. https://doi.org/10.1016/j.scitotenv.2019.05.258

Palmer, M. J., Chételat, J., Jamieson, H. E., Richardson, M., & Amyot, M. (2021). Hydrologic control on winter dissolved oxygen mediates arsenic cycling in a small subarctic lake. *Limnology and Oceanography*, *66*(S1). https://doi.org/10.1002/lno.11556

Parada, A. E., Needham, D. M., & Fuhrman, J. A. (2016). Every base matters: assessing small subunit rRNA primers for marine microbiomes with mock communities, time series and global field samples: Primers for marine microbiome studies. *Environmental Microbiology*, *18*(5), 1403–1414. https://doi.org/10.1111/1462-2920.13023

Parazoo, N. C., Koven, C. D., Lawrence, D. M., Romanovsky, V., & Miller, C. E. (2018). Detecting the permafrost carbon feedback: talik formation and increased cold-season respiration as precursors to sink-to-source transitions. *The Cryosphere*, *12*(1), 123–144. https://doi.org/10.5194/tc-12-123-2018

Paul, J. R., Kokelj, S. V., & Baltzer, J. L. (2021). Spatial and stratigraphic variation of near-surface ground ice in discontinuous permafrost of the taiga shield. *Permafrost and Periglacial Processes*, *32*(1), 3–18. https://doi.org/10.1002/ppp.2085

Pfahl, S., & Sodemann, H. (2014). What controls deuterium excess in global precipitation? *Climate of the Past*, *10*(2), 771–781. https://doi.org/10.5194/cp-10-771-2014

Phillips, R. W., Spence, C., & Pomeroy, J. W. (2011). Connectivity and runoff dynamics in heterogeneous basins. *Hydrological Processes*, n/a-n/a. https://doi.org/10.1002/hyp.8123

Pollard, W. H. (2005). Icing processes associated with high Arctic perennial springs, Axel Heiberg Island, Nunavut, Canada. *Permafrost and Periglacial Processes*, *16*(1), 51–68. https://doi.org/10.1002/ppp.515

Prowse, T. D., Wrona, F. J., Reist, J. D., Gibson, J. J., Hobbie, J. E., Lévesque, L. M. J., & Vincent, W. F. (2006). Climate Change Effects on Hydroecology of Arctic Freshwater Ecosystems. *AMBIO: A Journal of the Human Environment*, *35*(7), 347–358. https://doi.org/10.1579/0044-7447(2006)35[347:CCEOHO]2.0.CO;2

Quast, C., Pruesse, E., Yilmaz, P., Gerken, J., Schweer, T., Yarza, P., et al. (2012). The SILVA ribosomal RNA gene database project: improved data processing and web-based tools. *Nucleic Acids Research*, *41*(D1), D590–D596. https://doi.org/10.1093/nar/gks1219

Quince, C., Lanzen, A., Davenport, R. J., & Turnbaugh, P. J. (2011). Removing Noise From Pyrosequenced Amplicons. *BMC Bioinformatics*, *12*(1), 38. https://doi.org/10.1186/1471-2105-12-38

R Core Team. (2022). R: A language and environment for statistical computing. R Foundation for Statistical Computing, Vienna, Austria. Retrieved from http://www.R-project.org/

Rogers, J. A., Galy, V., Kellerman, A. M., Chanton, J. P., Zimov, N., & Spencer, R. G. M. (2021). Limited Presence of Permafrost Dissolved Organic Matter in the Kolyma River, Siberia Revealed by Ramped Oxidation. *Journal of Geophysical Research: Biogeosciences*, *126*(7). https://doi.org/10.1029/2020JG005977

Rouse, W. R., Blanken, P. D., Bussières, N., Walker, A. E., Oswald, C. J., Schertzer, W. M., & Spence, C. (2008). An Investigation of the Thermal and Energy Balance Regimes of Great Slave and Great Bear Lakes. *Journal of Hydrometeorology*, *9*(6), 1318–1333. https://doi.org/10.1175/2008JHM977.1

Santibáñez, P. A., Michaud, A. B., Vick-Majors, T. J., D'Andrilli, J., Chiuchiolo, A., Hand, K. P., & Priscu, J. C. (2019). Differential Incorporation of Bacteria, Organic Matter, and Inorganic Ions Into Lake Ice During Ice Formation. *Journal of Geophysical Research: Biogeosciences*, *124*(3), 585–600. https://doi.org/10.1029/2018JG004825

Šantl-Temkiv, T., Finster, K., Dittmar, T., Hansen, B. M., Thyrhaug, R., Nielsen, N. W., & Karlson, U. G. (2013). Hailstones: A Window into the Microbial and Chemical Inventory of a Storm Cloud. *PLoS ONE*, *8*(1), e53550. https://doi.org/10.1371/journal.pone.0053550

Sethuraman, A., Stancheva, R., Sanders, C., Caceres, L., Castro, D., Hausknecht-Buss, H., et al. (2022). Genome of a novel *Sediminibacterium* discovered in association with two species of freshwater cyanobacteria from streams in Southern California. *G3 Genes|Genomes|Genetics*, *12*(7), jkac123. https://doi.org/10.1093/g3journal/jkac123

Sinergise Ltd. (2021). Sentinel Hub. Retrieved from https://apps.sentinel-hub.com/eo-browser

Sipler, R. E., Kellogg, C. T. E., Connelly, T. L., Roberts, Q. N., Yager, P. L., & Bronk, D. A. (2017). Microbial Community Response to Terrestrially Derived Dissolved Organic Matter in the Coastal Arctic. *Frontiers in Microbiology*, *8*, 1018. https://doi.org/10.3389/fmicb.2017.01018

Sivarajah, B., Simmatis, B., Favot, E. J., Palmer, M. J., & Smol, J. P. (2021). Eutrophication and climatic changes lead to unprecedented cyanobacterial blooms in a Canadian sub-Arctic landscape. *Harmful Algae*, *105*, 102036. https://doi.org/10.1016/j.hal.2021.102036

Smith, A., Delavau, C., & Stadnyk, T. (2015). Identification of geographical influences and flow regime characteristics using regional water isotope surveys in the lower Nelson River,

Canada. *Canadian Water Resources Journal / Revue Canadienne Des Ressources Hydriques*, *40*(1), 23–35. https://doi.org/10.1080/07011784.2014.985512
Smith, D. F., Podgorski, D. C., Rodgers, R. P., Blakney, G. T., & Hendrickson, C. L. (2018). 21 Tesla FT-ICR Mass Spectrometer for Ultrahigh-Resolution Analysis of Complex Organic Mixtures. *Analytical Chemistry*, *90*(3), 2041–2047. https://doi.org/10.1021/acs.analchem.7b04159
Spence, C. (2006). Hydrological processes and streamflow in a lake dominated watercourse. *Hydrological Processes*, *20*(17), 3665–3681. https://doi.org/10.1002/hyp.6381
Spence, C., & Hedstrom, N. (2018). Hydrometeorological data from Baker Creek Research Watershed, Northwest Territories, Canada. *Earth System Science Data*, *10*(4), 1753–1767. https://doi.org/10.5194/essd-10-1753-2018
Spence, C., & Rouse, W. R. (2002). The Energy Budget of Canadian Shield Subarctic Terrain and Its Impact on Hillslope Hydrological Processes. *Journal of Hydrometeorology*, *3*(2), 208–218. https://doi.org/10.1175/1525-7541(2002)003<0208:TEBOCS>2.0.CO;2
Spence, C., & Woo, M. (2003). Hydrology of subarctic Canadian shield: soil-filled valleys. *Journal of Hydrology*, *279*(1–4), 151–166. https://doi.org/10.1016/S0022-1694(03)00175-6
Spence, C., Kokelj, S. V., & Ehsanzadeh, E. (2011). Precipitation Trends Contribute to Streamflow Regime Shifts in Northern Canada.
Spence, C., Kokelj, S. A., Kokelj, S. V., & Hedstrom, N. (2014). The process of winter streamflow generation in a subarctic Precambrian Shield catchment: SUBARCTIC WINTER STREAMFLOW GENERATION. *Hydrological Processes*, *28*(14), 4179–4190. https://doi.org/10.1002/hyp.10119
Spence, C., Kokelj, S. V., Kokelj, S. A., McCluskie, M., & Hedstrom, N. (2015). Evidence of a change in water chemistry in Canada's subarctic associated with enhanced winter streamflow. *Journal of Geophysical Research: Biogeosciences*, *120*(1), 113–127. https://doi.org/10.1002/2014JG002809
Spence, C., Hedstrom, N., Tank, S. E., Quinton, W. L., Olefeldt, D., Goodman, S., & Dion, N. (2020). Hydrological resilience to forest fire in the subarctic Canadian shield. *Hydrological Processes*, *34*(25), 4940–4958. https://doi.org/10.1002/hyp.13915
Spencer, R. G. M., Mann, P. J., Dittmar, T., Eglinton, T. I., McIntyre, C., Holmes, R. M., et al. (2015). Detecting the signature of permafrost thaw in Arctic rivers: SIGNATURE OF PERMAFROST THAW IN RIVERS. *Geophysical Research Letters*, *42*(8), 2830–2835. https://doi.org/10.1002/2015GL063498
Spencer, R. G. M., Kellerman, A. M., Podgorski, D. C., Macedo, M. N., Jankowski, K., Nunes, D., & Neill, C. (2019). Identifying the Molecular Signatures of Agricultural Expansion in Amazonian Headwater Streams. *Journal of Geophysical Research: Biogeosciences*, *124*(6), 1637–1650. https://doi.org/10.1029/2018JG004910
St. Jacques, J.-M., & Sauchyn, D. J. (2009). Increasing winter baseflow and mean annual streamflow from possible permafrost thawing in the Northwest Territories, Canada. *Geophysical Research Letters*, *36*(1), L01401. https://doi.org/10.1029/2008GL035822
Stevens, C. W., Kerr, D. E., Wolfe, S. A., & Eagles, S. (2017). *Predictive surficial geology, Yellowknife and Hearne Lake, Northwest Territories, NTS 85-J and NTS 85-I* (No. 200, 2nd, prelim. ed.) (p. 200). https://doi.org/10.4095/299516
St-Jean, G. (2003). Automated quantitative and isotopic (13C) analysis of dissolved inorganic carbon and dissolved organic carbon in continuous-flow using a total organic carbon

analyser. *Rapid Communications in Mass Spectrometry*, *17*(5), 419–428. https://doi.org/10.1002/rcm.926

St-Jean, G., Kieser, W. E., Crann, C. A., & Murseli, S. (2017). Semi-Automated Equipment for CO2 Purification and Graphitization at the A.E. Lalonde AMS Laboratory (Ottawa, Canada). *Radiocarbon*, *59*(3), 941–956. https://doi.org/10.1017/RDC.2016.57

Tarnocai, C., Canadell, J. G., Schuur, E. A. G., Kuhry, P., Mazhitova, G., & Zimov, S. (2009). Soil organic carbon pools in the northern circumpolar permafrost region: SOIL ORGANIC CARBON POOLS. *Global Biogeochemical Cycles*, *23*(2), n/a-n/a. https://doi.org/10.1029/2008GB003327

Tichý, L., & Chytrý, M. (2006). Statistical determination of diagnostic species for site groups of unequal size. *Journal of Vegetation Science*, *17*(6), 809. https://doi.org/10.1658/1100-9233(2006)17[809:SDODSF]2.0.CO;2

U.S. Environmental Protection Agency. (1996). Determination of Trace Elements in Waters and Wastes by Inductively Coupled Plasma-Mass Spectrometry. In *Methods for the Determination of Metals in Environmental Samples* (pp. 88–145). Elsevier. https://doi.org/10.1016/B978-0-8155-1398-8.50011-2

U.S. Environmental Protection Agency. (2000). Guidance for data quality assessment: practical methods for data analysis (No. EPA QA/G-9 QA00 Version). Retrieved from https://www.epa.gov/sites/default/files/2015-06/documents/g9-final.pdf

Viscek, J. A. (2020). The hydrology of northern boreal lakes in the Taiga Shield and Plains, Northwest Territories and the importance of catchment characteristics in mediating responses to climate. Brock University. Retrieved from http://hdl.handle.net/10464/14894

Vonk, J. E., Tank, S. E., Mann, P. J., Spencer, R. G. M., Treat, C. C., Striegl, R. G., et al. (2015). Biodegradability of dissolved organic carbon in permafrost soils and aquatic systems: a meta-analysis. *Biogeosciences*, *12*(23), 6915–6930. https://doi.org/10.5194/bg-12-6915-2015

Vonk, Jorien E., Mann, P. J., Davydov, S., Davydova, A., Spencer, R. G. M., Schade, J., et al. (2013). High biolability of ancient permafrost carbon upon thaw. *Geophysical Research Letters*, *40*(11), 2689–2693. https://doi.org/10.1002/grl.50348

Walvoord, M. A., & Kurylyk, B. L. (2016). Hydrologic Impacts of Thawing Permafrost-A Review. *Vadose Zone Journal*, *15*(6), vzj2016.01.0010. https://doi.org/10.2136/vzj2016.01.0010

Wang, C., Wang, Z., Kong, Y., Zhang, F., Yang, K., & Zhang, T. (2019). Most of the Northern Hemisphere Permafrost Remains under Climate Change. *Scientific Reports*, *9*(1), 3295. https://doi.org/10.1038/s41598-019-39942-4

Wankiewicz, A. (1984). Analysis of winter heat flow in an ice-covered Arctic stream. *Canadian Journal of Civil Engineering*, *11*(3), 430–443. https://doi.org/10.1139/l84-064

Watanabe, K., Komatsu, N., Ishii, Y., & Negishi, M. (2009). Effective isolation of bacterioplankton genus Polynucleobacter from freshwater environments grown on photochemically degraded dissolved organic matter: Isolation and ecological aspects of Polynucleobacter. *FEMS Microbiology Ecology*, *67*(1), 57–68. https://doi.org/10.1111/j.1574-6941.2008.00606.x

Wauthy, M., Rautio, M., Christoffersen, K. S., Forsström, L., Laurion, I., Mariash, H. L., et al. (2018). Increasing dominance of terrigenous organic matter in circumpolar freshwaters due to permafrost thaw. *Limnology and Oceanography Letters*, *3*(3), 186–198. https://doi.org/10.1002/lol2.10063

Wei, T., & Simko, V. (2021). *corrplot: Visualization of a Correlation Matrix*. Retrieved from https://github.com/taiyun/corrplot

Weishaar, J. L., Aiken, G. R., Bergamaschi, B. A., Fram, M. S., Fujii, R., & Mopper, K. (2003). Evaluation of Specific Ultraviolet Absorbance as an Indicator of the Chemical Composition and Reactivity of Dissolved Organic Carbon. *Environmental Science & Technology*, *37*(20), 4702–4708. https://doi.org/10.1021/es030360x

Weiss, S., Xu, Z. Z., Peddada, S., Amir, A., Bittinger, K., Gonzalez, A., et al. (2017). Normalization and microbial differential abundance strategies depend upon data characteristics. *Microbiome*, *5*(1), 27. https://doi.org/10.1186/s40168-017-0237-y

Welch, H. E., & Legault, J. A. (1986). Precipitation Chemistry and Chemical Limnology of Fertilized and Natural Lakes at Saqvaqjuac, N.W.T. *Canadian Journal of Fisheries and Aquatic Sciences*, *43*(6), 1104–1134. https://doi.org/10.1139/f86-140

Wickham, H. (2016). *ggplot2: Elegant Graphics for Data Analysis*. Springer-Verlag New York. Retrieved from https://ggplot2.tidyverse.org

Wickland, K. P., Aiken, G. R., Butler, K., Dornblaser, M. M., Spencer, R. G. M., & Striegl, R. G. (2012). Biodegradability of dissolved organic carbon in the Yukon River and its tributaries: Seasonality and importance of inorganic nitrogen. *Global Biogeochemical Cycles*, *26*(4), 2012GB004342. https://doi.org/10.1029/2012GB004342

Wolfe, S. A., & Kerr, D. E. (2014). *Surficial geology, Yellowknife area, Northwest Territories, parts of NTS 85-J/7, NTS 85-J/8, NTS 85-J/9 and NTS 85-J/10* (No. 183) (p. 183). https://doi.org/10.4095/293725

Wright, S. N., Thompson, L. M., Olefeldt, D., Connon, R. F., Carpino, O. A., Beel, C. R., & Quinton, W. L. (2022). Thaw-induced impacts on land and water in discontinuous permafrost: A review of the Taiga Plains and Taiga Shield, northwestern Canada. *Earth-Science Reviews*, *232*, 104104. https://doi.org/10.1016/j.earscirev.2022.104104

Wu, X., Wu, L., Liu, Y., Zhang, P., Li, Q., Zhou, J., et al. (2018). Microbial Interactions With Dissolved Organic Matter Drive Carbon Dynamics and Community Succession. *Frontiers in Microbiology*, *9*, 1234. https://doi.org/10.3389/fmicb.2018.01234

Yoshikawa, K., Hinzman, L. D., & Kane, D. L. (2007). Spring and aufeis (icing) hydrology in Brooks Range, Alaska: AUFEIS HYDROLOGY IN BROOKS RANGE. *Journal of Geophysical Research: Biogeosciences*, *112*(G4), n/a-n/a. https://doi.org/10.1029/2006JG000294

Zhang, Y., Olthof, I., Fraser, R., & Wolfe, S. A. (2014). A new approach to mapping permafrost and change incorporating uncertainties in ground conditions and climate projections. *The Cryosphere*, *8*(6), 2177–2194. https://doi.org/10.5194/tc-8-2177-2014

Zhou, C., Liu, Y., Liu, C., Liu, Y., & Tfaily, M. M. (2019). Compositional changes of dissolved organic carbon during its dynamic desorption from hyporheic zone sediments. *Science of The Total Environment*, *658*, 16–23. https://doi.org/10.1016/j.scitotenv.2018.12.189

Zhou, Y., Hiller, C., Andersson, S., Jakobsson, E., Zhou, L., Hawkes, J. A., et al. (2023). Selective Exclusion of Aromatic Organic Carbon During Lake Ice Formation. *Geophysical Research Letters*, *50*(4). https://doi.org/10.1029/2022GL101414

APPENDICES

Appendix 1: Supporting Information for Chapter 2

Table A1-1. Sampling frequency for source water, stream, and ice samples at focal and secondary sites.

Site	Dates	Source Water	Stream	Ice
S5a	2021-03-17	X	X	X
	2021-03-22		X	
	2021-03-26		X	
	2021-04-16	X	X	
	2021-05-03	X	X	
S5b	2021-03-19			X
	2021-04-28		X	
	2021-05-03	X	X	
S8	2021-03-18	X		X
	2021-03-22	X		
S3	2021-03-18			X
S1	2021-03-22	X		
	2021-04-14	X		X
	2021-04-17	X		
	2021-04-28	X		
S6	2021-03-18			X
	2021-03-22	X		
BC	2021-03-23	X		X
JL	2022-02-15	X		
	2022-03-04			X

Table A1-2. Supplementary description of site physical features and field observations.

Site	Local Catchment Characteristics	Topography / Channel Features	Field Notes
S1	Thin patch of spruce forest around lake edge and expansive bedrock outcrops beyond shoreline	Small hillslope on southern end of icing	2021-04-17: Noted slight sulfur smell in lake. Negative ORP (< -20 mV) throughout water column. Measured [S^{2-}] 321 mg/L, [Fe^{2+}] 2.7 mg/L.
			2021-04-21 – water column oxygenated, high ORP (surface 198 mV, bottom 55 mV), high DO% (surface 123 %/L, bottom 21 %/L)
S3	Forested, bedrock to southwest of icing	Gently sloping	
S5a	Forested	Small hillslope on eastern side of channel	2021-03-17: Noted sulphur smell emitting from bottom of core taken at outlet end of icing. Observed dilation crack at pond outlet, and pond ice is domed upwards.
		Beaver dam near pond outflow	2021-04-12: Pond ice has levelled, observed large crack in ice at pond outlet.
			2021-04-16: Ice is hollowed out beneath primary ice layer of icing. Circular shapes observed on ice surface where ice had previously domed upwards. Pond is oxygenated throughout water column (> 100 DO %/L).
BC	Mostly bedrock.	Hillslopes on both sides of stream channel	
S6	Forested on eastern side of lake, bedrock on western side		
S5b	Forested, thin layer of bedrock around lake.	Lake outflow bay very shallow, interaction with bottom substrate prior to outflow	Inflow creek to S5b lake is tea-coloured.
S8	Forested along southern end of lake and along channel, bedrock to north/northeast.	Series of beaver dams before channelized section of flow	

Table A1-3. Properties of the three fluorescence components identified using PARAFAC analyses, including excitation (Ex.) and emission (Em.) peak values, similarity scores, related references for similar components from the OpenFluor database, and potential compositional characteristics (Coble, 1996; Murphy et al., 2013)

Component	**Ex. (nm)**	**Em. (nm)**	**Similarity Score**	**References**	**Potential characteristics**
C1	240 (335)	467	0.99	Gonçalves-Araujo et al. 2016 (C1)	Terrestrial humic-like. aromatic, high molecular weight,
			0.99	Imbeau et al. 2021 (C1)	
C2	240 (305)	407	0.98	Gonçalves-Araujo et al. 2016 (C2)	Terrestrial humic-like, aromatic, high molecular weight
			0.99	Imbeau et al. 2021 (C2)	
			0.95	Wauthy et al. 2018 (C4)	
C3	280 (240)	334	0.97	Gonçalves-Araujo et al. 2016 (C3)	Amino acid or protein-like, tryptophan-like, linked to aquatic productivity, microbial origin
			0.95	Imbeau et al. 2021 (C3)	
			0.98	Gao and Guéguen 2018 (C4)	
			0.97	Wauthy et al. 2018 (C5	

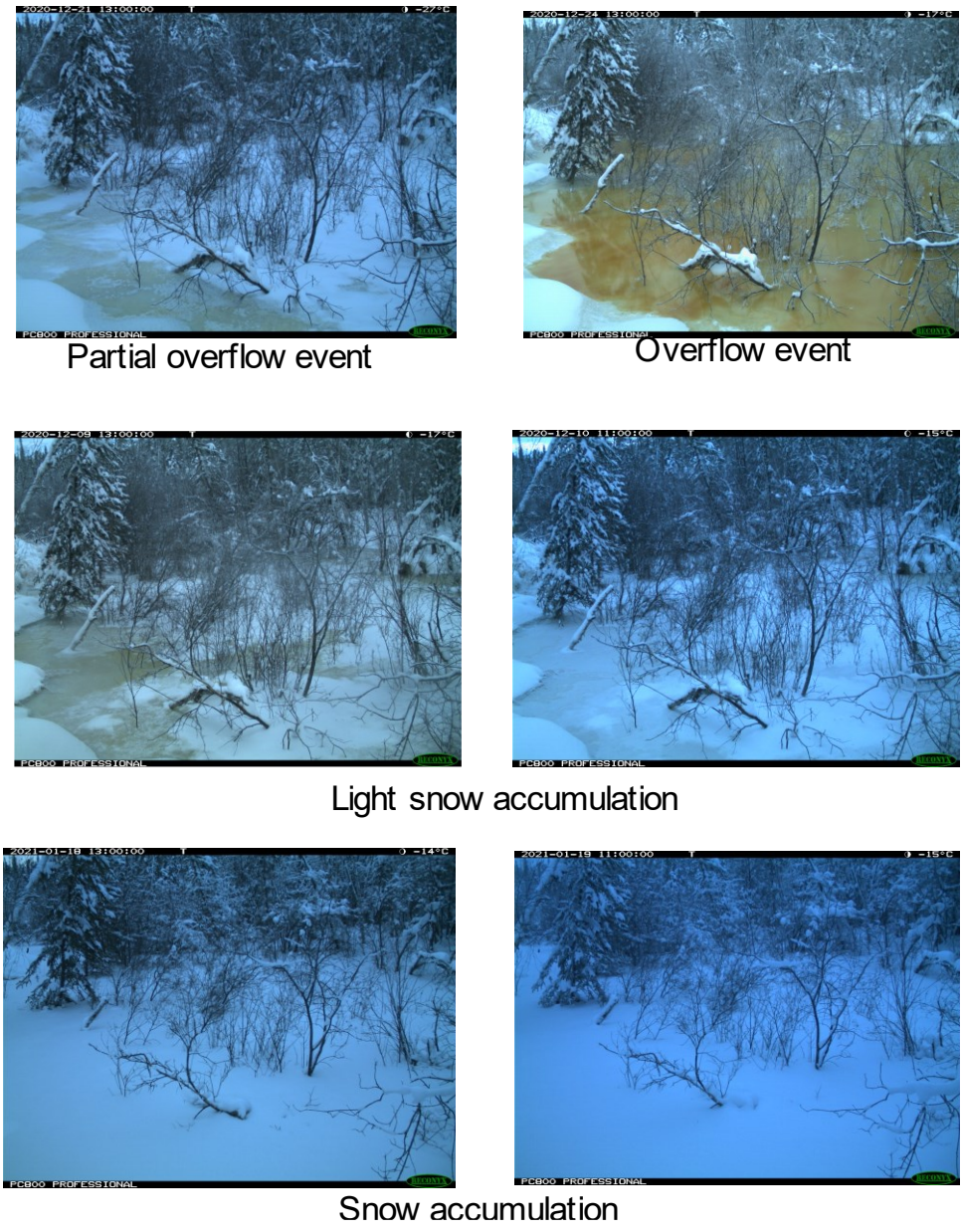

Figure A1-1. Example of classification of partial overflow events, overflow events, light snow accumulation and snow accumulation for trail camera data at S5b shown in Figure 3.

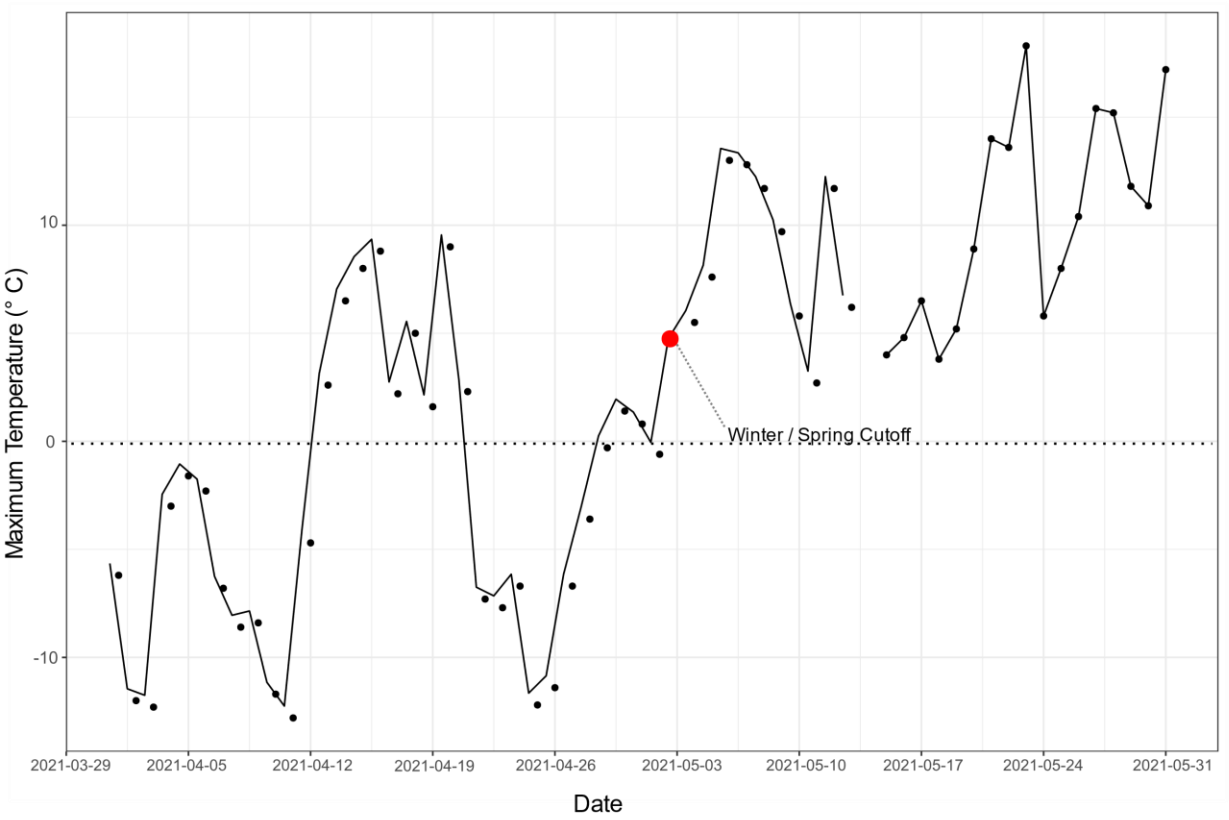

Figure A1-2. Record of daily maximum temperatures from April – May 2021 and the cutoff date determined between the winter and spring season (in red). Data obtained from Environment and Climate Change Canada, from the Yellowknife A station (ECCC, 2022b).

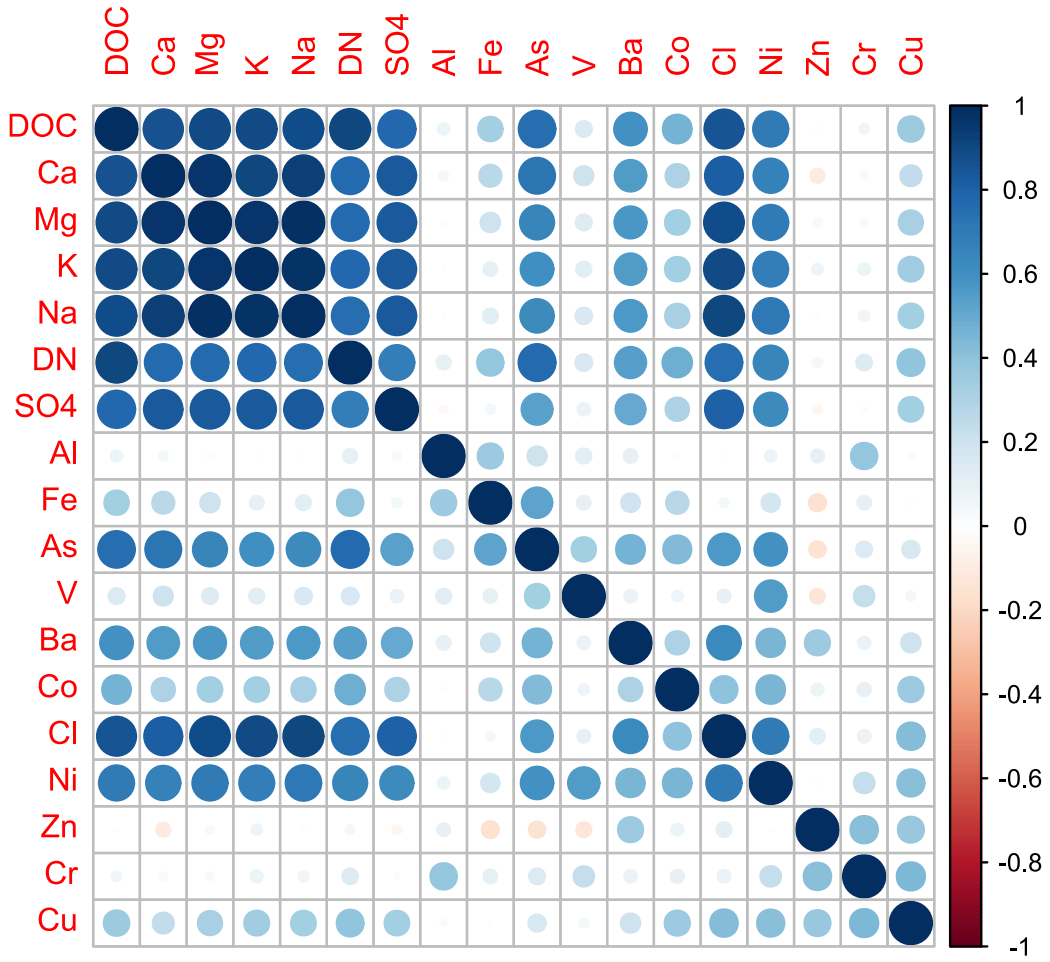

Figure A1-3. Correlation plot showing Pearson's R for all water quality variables at S1, S5a, S5b, S6, S8, S1, and BC.

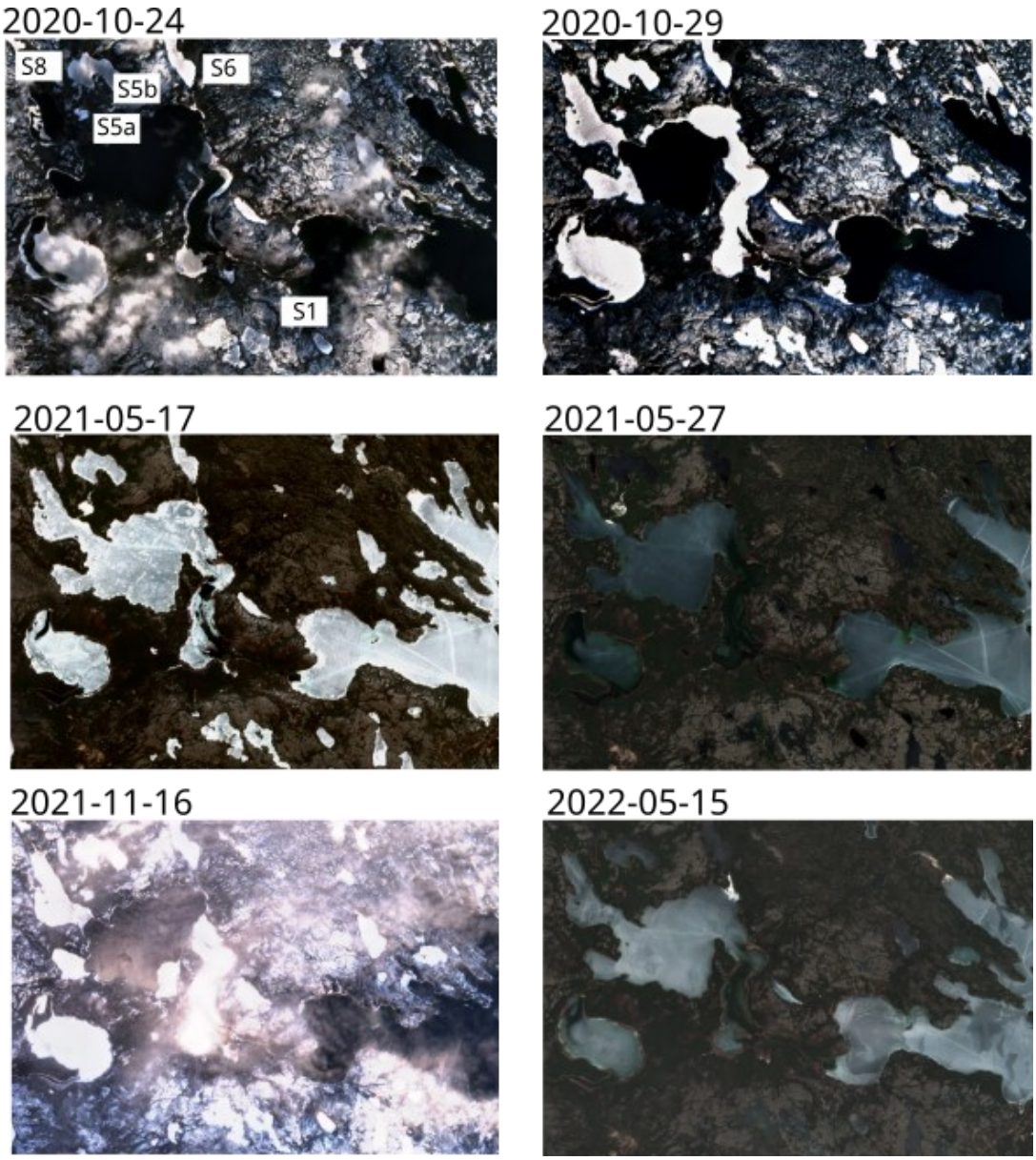

Figure A1-4. Sentinel 2-L2A satellite imagery (true colour band) showing the ice covered period in 2020-2021 during the sampling campaign at S1, S5a, S5b, S6, and S8, and the ice covered period in the following winter (2021-2022).

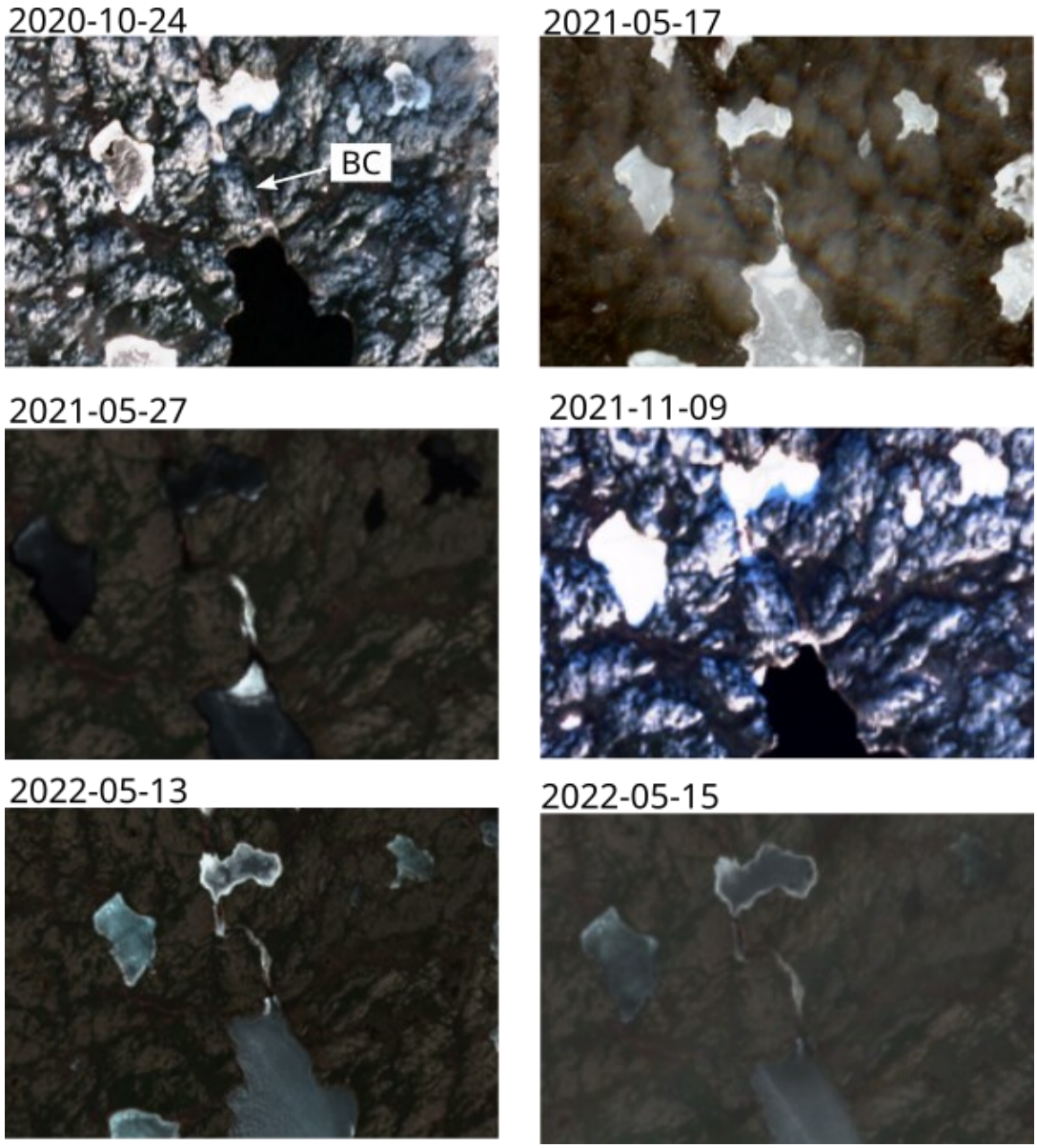

Figure A1-5. Sentinel 2-L2A satellite imagery (true colour band) showing the ice covered period in 2020-2021 during the sampling campaign at BC and the ice covered period in the following winter (2021-2022).

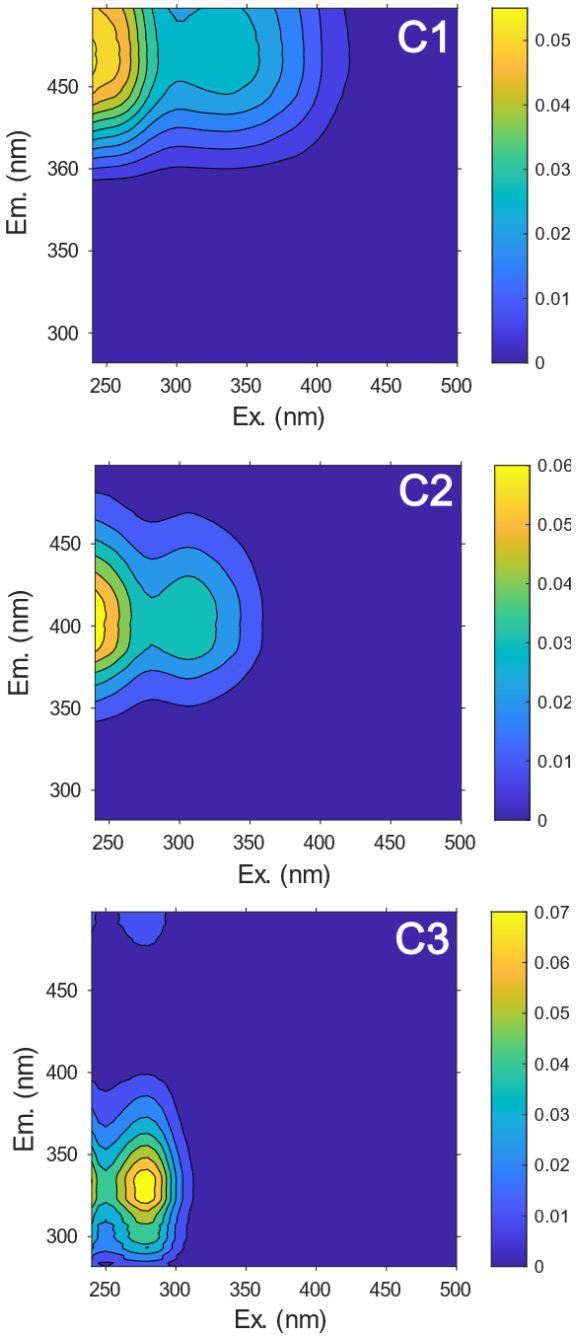

Figure A1-6. PARAFAC components of excitation-emission matrices measured in icing samples from seven icings, plus source water and stream samples from three focal sites (S1, S5a, S5b). Three fluorescence components (C1-C3) were identified. Colour bar represents fluorescence intensity in Raman units.

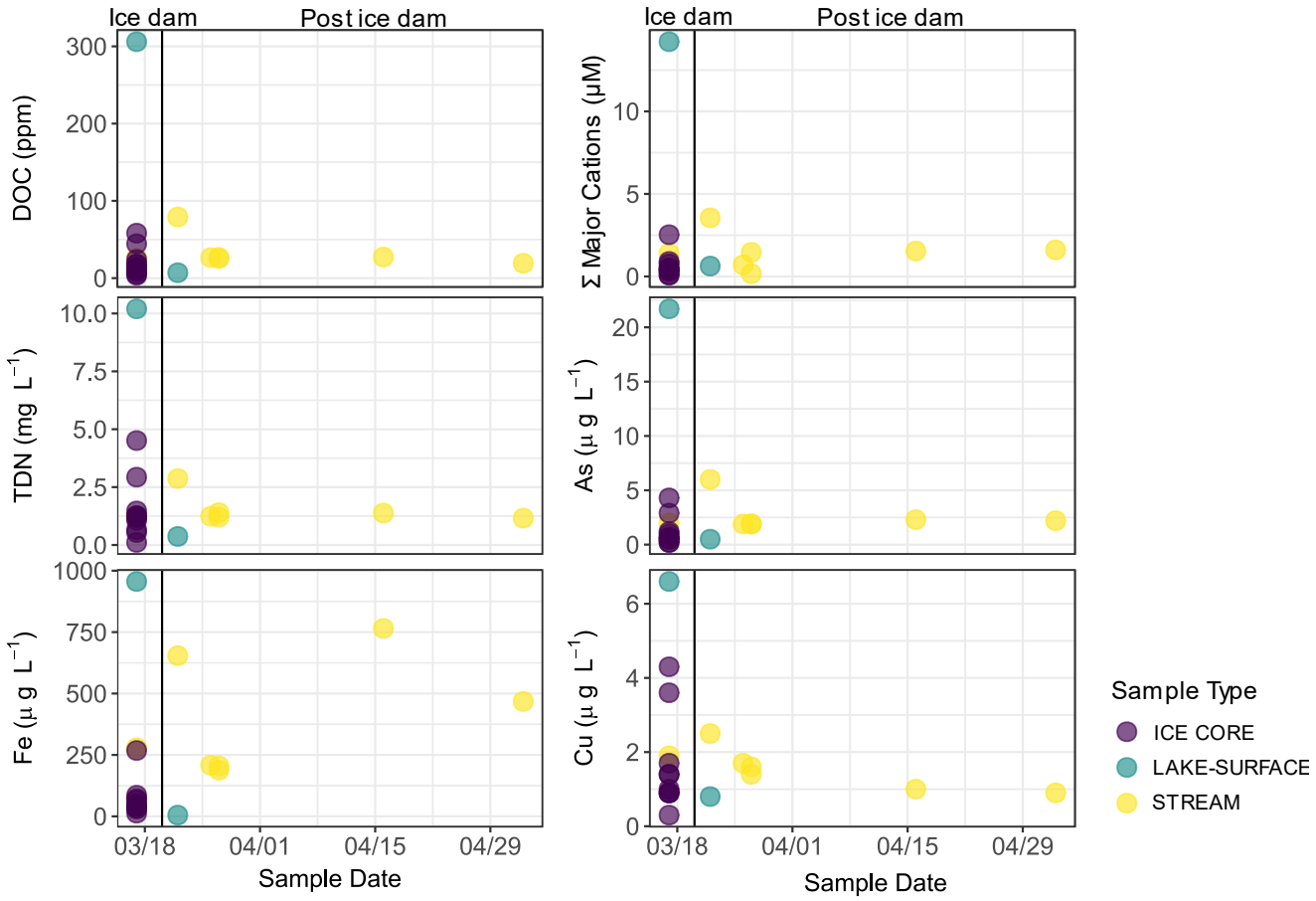

Figure A1-7. Concentrations of DOC, molar sum of cations, TDN, and trace metals (dAs, dFe, dCu) of ice core, lake surface and stream water at S5a over time (Month-Day, during 2021). Vertical line denotes the period when an ice dam was present at the S5a lake, and the period after the breakup of the dam, demarcated by lake level records in Figure 2-4.

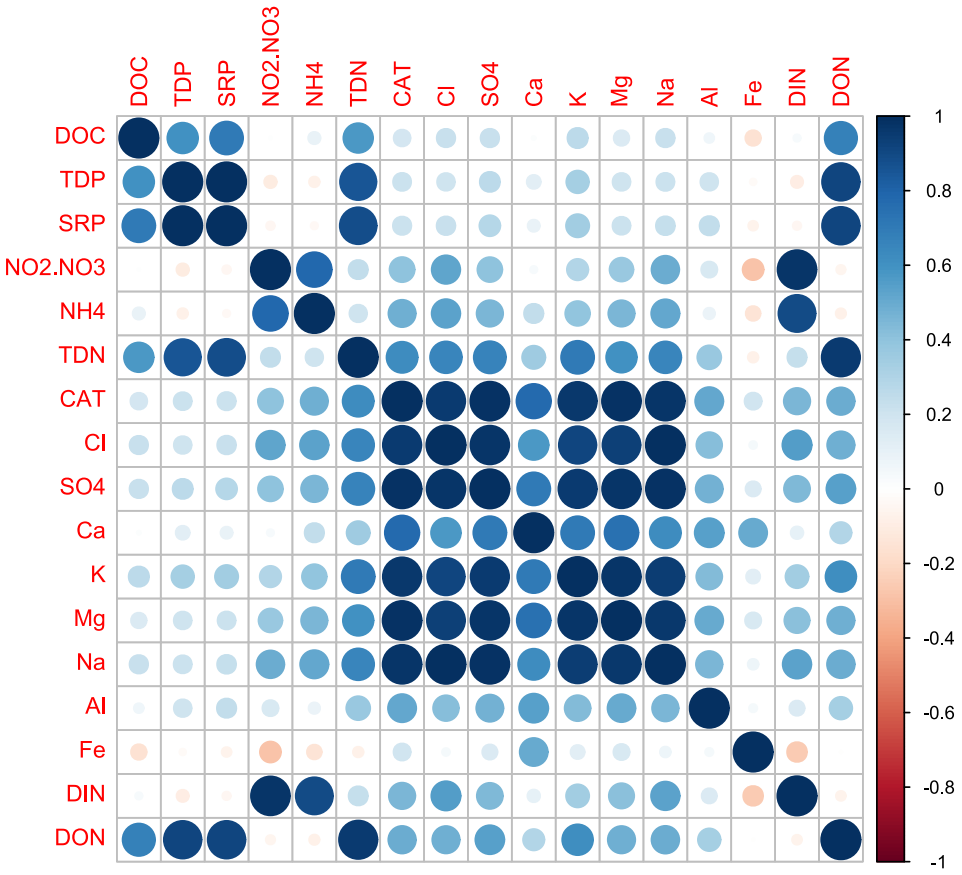

Figure A1-8. Correlation plot showing Pearson's R for water quality variables at JL.

Appendix 2: Supporting Information for Chapter 3

Table A2-1. Sampling frequency for source water, stream, and ice core samples at S1, S5a, S5b in 2021.

Julian Date	S1	S5a	S5b
Ice cores			
76 to 102		Ice core sampling[a,b,c]	
Winter open water			
61	X	X[a,c]	X
106		X[a,b,c]	
107	X		
111	X[c]		
118	X		
123		X[a,c]	X
Spring			
125	X		
132	X[c]		
138	X		
140		X[a,b,c]	X
148	X		
Summer			
155		X[a,c]	X
165	X[c]		
168		X[a,b,c]	X
223	X	X[a,b,c]	X

[a] Sample subset for ^{13}C-DOC analysis. [b] Sample subset for ^{14}C-DOC analysis. [c] Sample subset for FT-ICR-MS analyses.

Table A2-2. Total number and percentage (%) of unique (in brackets) FT-ICR-MS formulae across icing, winter, spring and summer samples within each compound class.

	Aliphatics	**$HUP_{High\ O/C}$**	**$HUP_{Low\ O/C}$**	**Polyphenolics**	**Condensed Aromatics**
			Total (Unique)		
Icing	10805 (14.38)	34165 (0.57)	23656 (1.40)	10837 (0.88)	2944 (0.44)
Winter	2614 (2.56)	11980 (0.81)	7643 (1.06)	3960 (1.19)	1124 (2.40)
Spring	3681 (2.12)	15960 (0.86)	10669 (0.84)	6788 (3.70)	2743 (8.06)
Summer	6340 (0.96)	32089 (0.44)	20894 (0.64)	12424 (1.00)	4114 (1.34)

Table A2-3. Permutational analysis of variance (perMANOVA) of microbial community data (ASV counts) as a function of season (winter, spring, summer) and site (S1, S5a, S5b), using bray-curtis distance, and pairwise perMANOVA results of season and site, using bray-curtis distance and Bonferroni p-value adjustment. Winter group includes icing samples.

perMANOVA ASV ~ Season * Site					
Variable	Df	Sum Sq	R^2	F	p
Season	2	1.34	0.13	2.58	0.001
Site	2	1.32	0.13	2.54	0.001
Season:Site	4	1.14	0.11	1.01	0.254
Residual	26	6.77	0.64		
Pairwise Testing					
Season	F	R^2	p	Adjusted p	
Winter vs. Summer	1.94	0.072	0.008	0.024	
Winter vs. Spring	2.14	0.12	0.014	0.042	
Summer vs. Spring	2.87	0.11	0.002	0.006	
Site					
S1 vs. S5a	2.63	0.099	0.002	0.006	
S1 vs. S5b	1.84	0.10	0.020	0.060	
S5a vs. S5b	2.02	0.078	0.010	0.030	

Table A2-4. Distance based redundancy analysis (dbRDA) of microbial community data (ASV counts) and chemistry parameters chosen via forward/reverse selection, using bray-curtis distance and adjusted R^2, and analysis of variance (ANOVA) results showing significance of chemistry parameters in model output.

Formula			
asv ~ S_R + K + CAT + $S_{275\text{-}295}$ + Fi + Comp. 1 % + Comp 2 % + DON + DIN + Ba + Cu			
Model Summary			
	Inertia	**Proportion**	**Rank**
Total	10.5756	1.0000	
Constrained	5.4742	0.2869	11
Unconstrained	5.1014	0.7131	23
ANOVA Results			
Variable	**df**	**F**	**p**
S_R	1	3.2423	0.005
K	1	2.2916	0.005
CAT	1	2.3135	0.005
$S_{275\text{-}295}$	1	2.2615	0.005
Fi	1	1.9029	0.010
Comp. 1 %	1	2.0016	0.005
Comp. 2 %	1	1.9506	0.015
DON	1	1.8509	0.010
DIN	1	1.6362	0.035
Ba	1	1.6501	0.040
Cu	1	1.5354	0.020

Table A2-5. Distance based redundancy analysis (dbRDA) of microbial community data subset (ASV counts) and FT-ICR-MS data plus chemistry parameters chosen via forward/reverse selection, using bray-curtis distance and adjusted R^2, and analysis of variance (ANOVA) results showing significance of chemistry parameters in model output.

Formula			
asv ~ S_R + Aliphatics + Polyphenolics + Condensed Aromatics + K + Comp. 2			
Model Summary			
	Inertia	**Proportion**	**Rank**
Total	5.4611	1.0000	
Constrained	3.1153	0.3557	6
Unconstrained	2.3458	.6443	12
ANOVA Results			
Variable	**df**	**F**	**p**
S_R	1	4.8566	0.001
Aliphatics (%RA)	1	2.4037	0.001
Polyphenolics (%RA)	1	1.7582	0.040
Condensed Aromatics (%RA)	1	2.8202	0.001
K	1	1.7181	0.047
Comp. 2 %	1	2.3798	0.0004

Table A2-6. Mixed effect model output of incubation experiment variables (%O_2 loss, rate of O_2 loss, % CO_2 gain), as a function of initial chemistry parameters, chosen via forward/reverse selection, and analysis of variance (ANOVA) results showing significance of initial chemistry parameters in model output.

Model 1: % O_2 loss ~ TDP + bix						
	Coefficient	Df	Sum Sq	Mean Sq	F value	p
Intercept	-0.653					
TDP	0.00786	1	0.0417	0.0417	96.203	0.0022
bix	0.831	1	0.0115	0.0115	26.570	0.014
Residuals		3	0.00130	0.000434		
Model 2: Rate O_2 loss ~ SRP + bix						
	Coefficient	Df	Sum Sq	Mean Sq	F value	p
Intercept	-0.0242					
SRP	-0.00278	1	3.574e-05	3.574e-05	19.642	0.0214
bix	0.0504	1	2.204e-05	2.208e-05	12.119	0.0400
Residuals		3	5.455e-06	1.818e-06		
Model 3: %CO_2 gain ~ C + bix						
	Coefficient	Df	Sum Sq	Mean Sq	F value	p
Intercept	0.505					
Peak C	-0.311	1	0.0141	0.0141	21.447	0.0189
bix	-0.686	1	0.00759	0.00759	11.550	0.0425
Residuals		3	0.00197	0.000657		

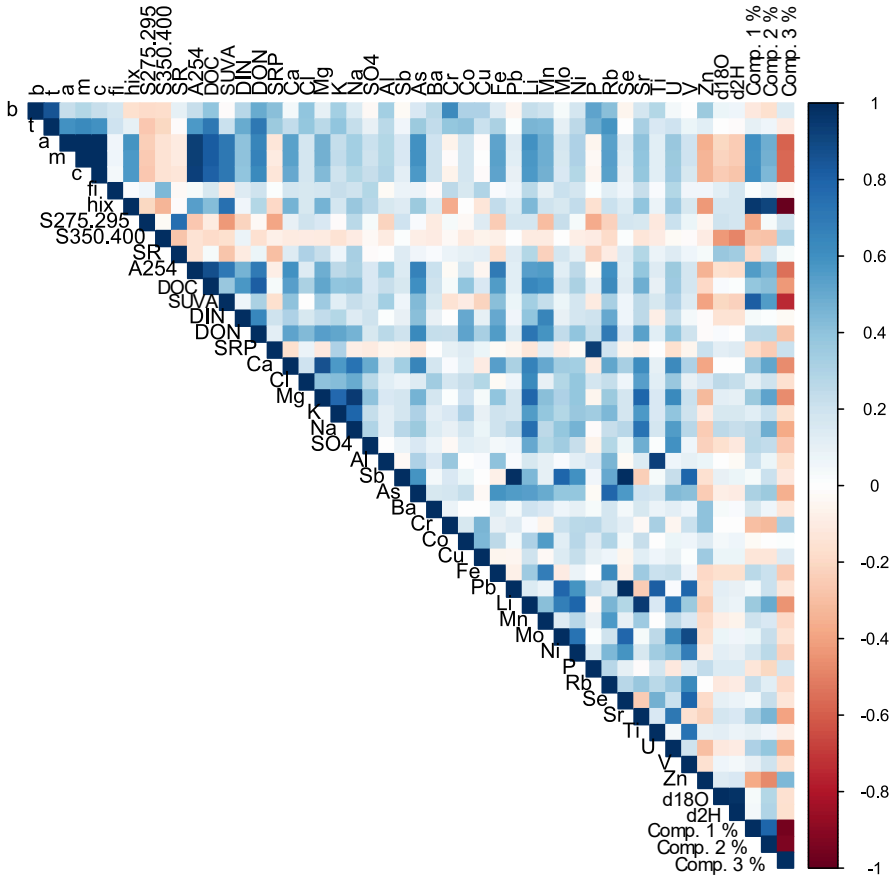

Figure A2-1. Correlation plot showing Pearson's R for all water chemistry variables.

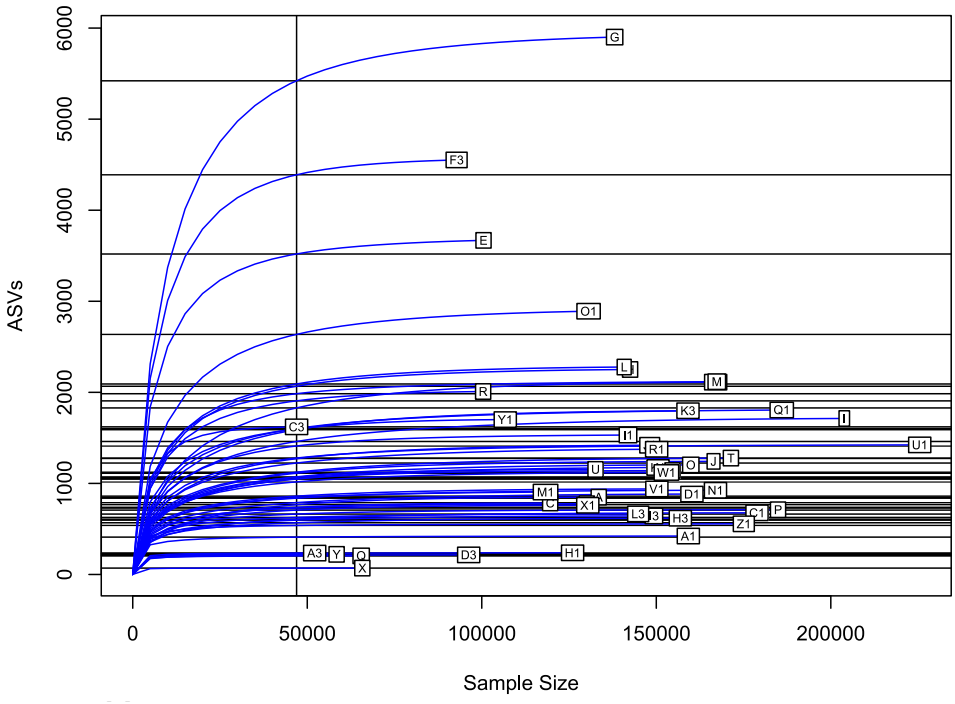

Figure A2-2. Rarefaction curve of microbial community data, with rarefaction depth (46, 492) illustrated with vertical black line.

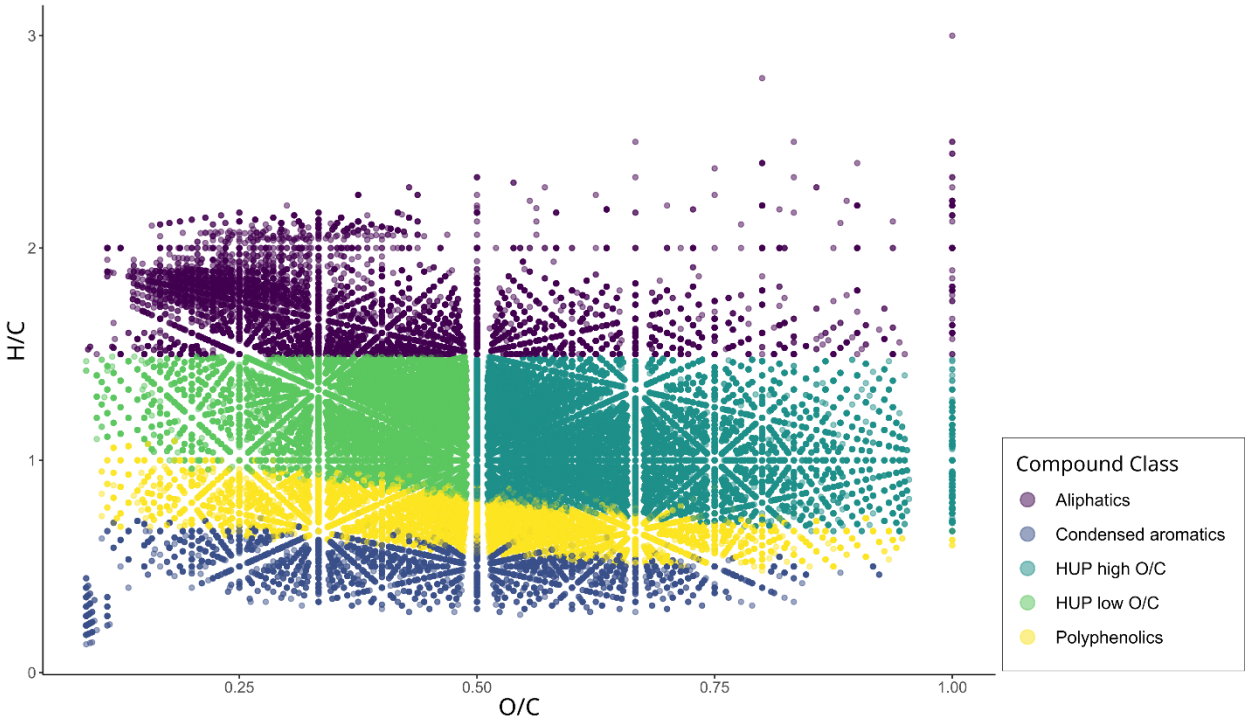

Figure A2-3. All molecular formulae identified through FT-ICR-MS analysis.

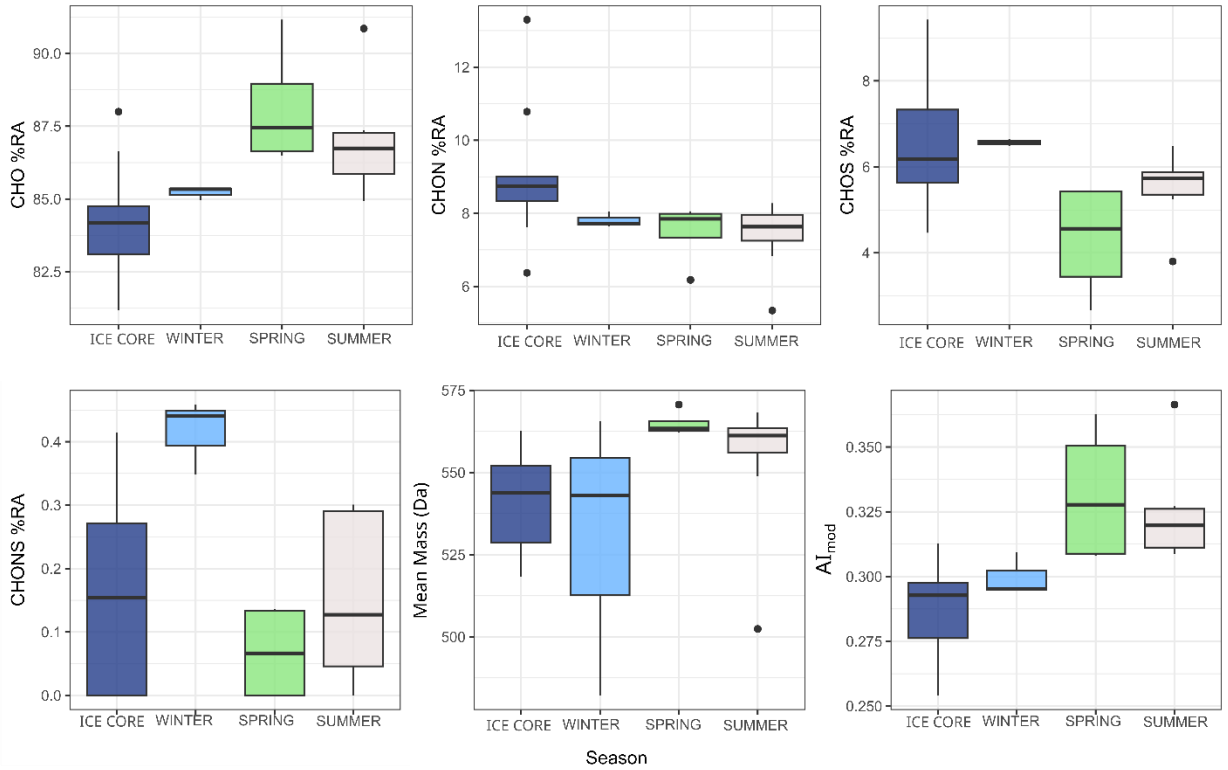

Figure A2-4. FT-ICR-MS. Percent relative abundance of CHO, CHON, CHOS, and CHONS containing formulae, mean mass, and modified aromaticity index (AI_{mod}) across seasons and icing meltwater. Winter, spring and summer include pooled lake and stream samples.

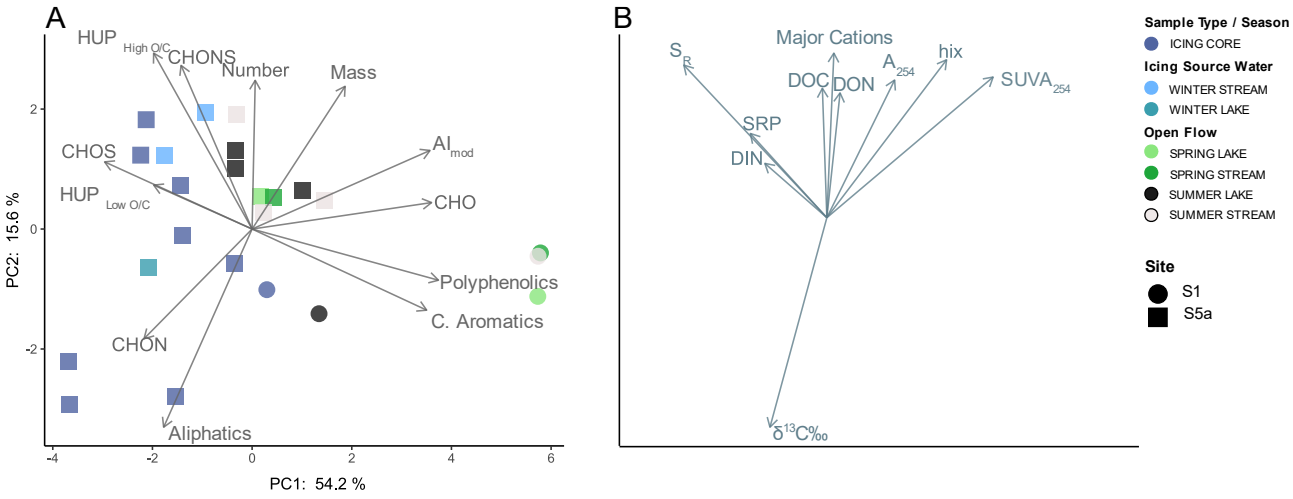

Figure A2-5. Panel A: Principal component analysis (PCA) of compositional metrics from FT-ICR-MS. C. Aromatics = Condensed Aromatics. Panel B: Overlay of select chemistry variables (sum of major cations, DOC, S_R, A_{254}, $SUVA_{254}$, hix, DIN, DON, SRP, $\delta^{13}C$ ‰). C. Aromatics = Condensed Aromatics.

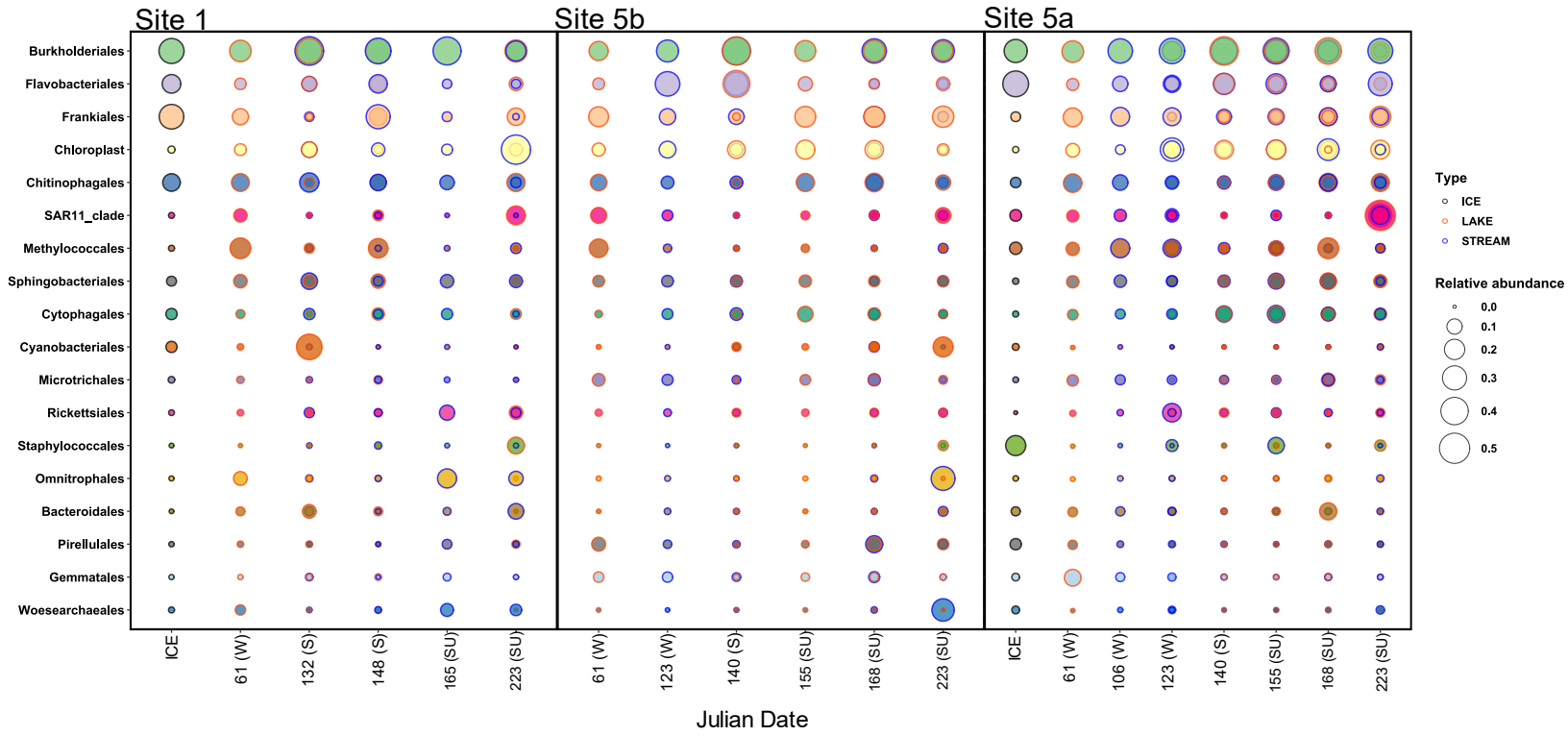

Figure A2-6. Relative abundance of top 18 orders identified across Sites (S1, S5b, S5a) and time, represented by Julian date and acronyms W (winter), S (spring) and SU (summer). Sample types shown by black (ice cores), red (lake) and blue (stream) circle outlines.

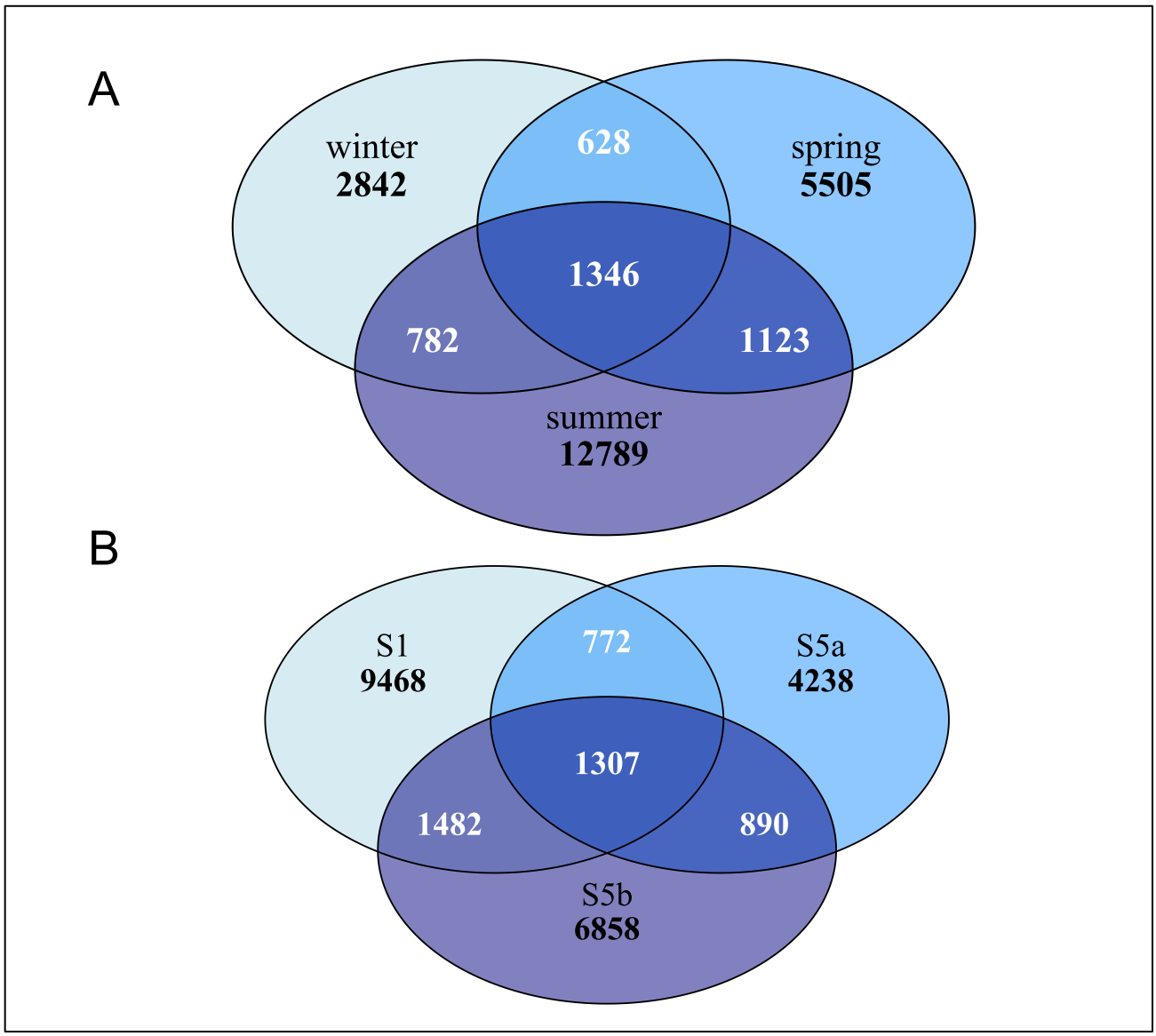

Figure A2-7. Venn diagrams of unique and shared ASVs identified across seasons (panel A) and sites (panel B). Winter includes pooled surface water and icings.

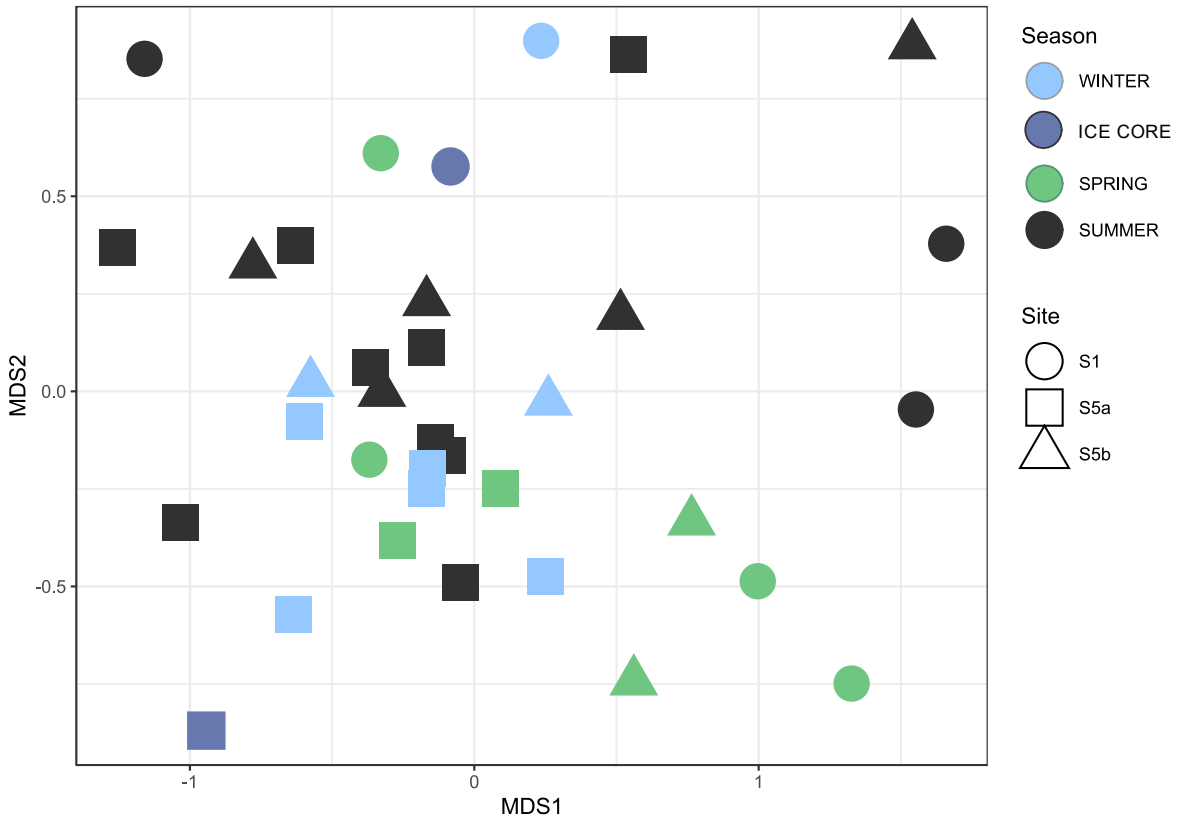

Figure A2-8. Non-metric multidimensional scaling (NMDS) of microbial community data for winter, ice core, spring and summer samples at S1, S5a and S5b. Stress is 0.14. Winter, spring and summer groups include lake and stream samples. perMANOVA show seasons (p=0.001) and sites (p=0.001) to be significantly different (Table A2-3); ice cores were pooled with winter surface waters for perMANOVA.

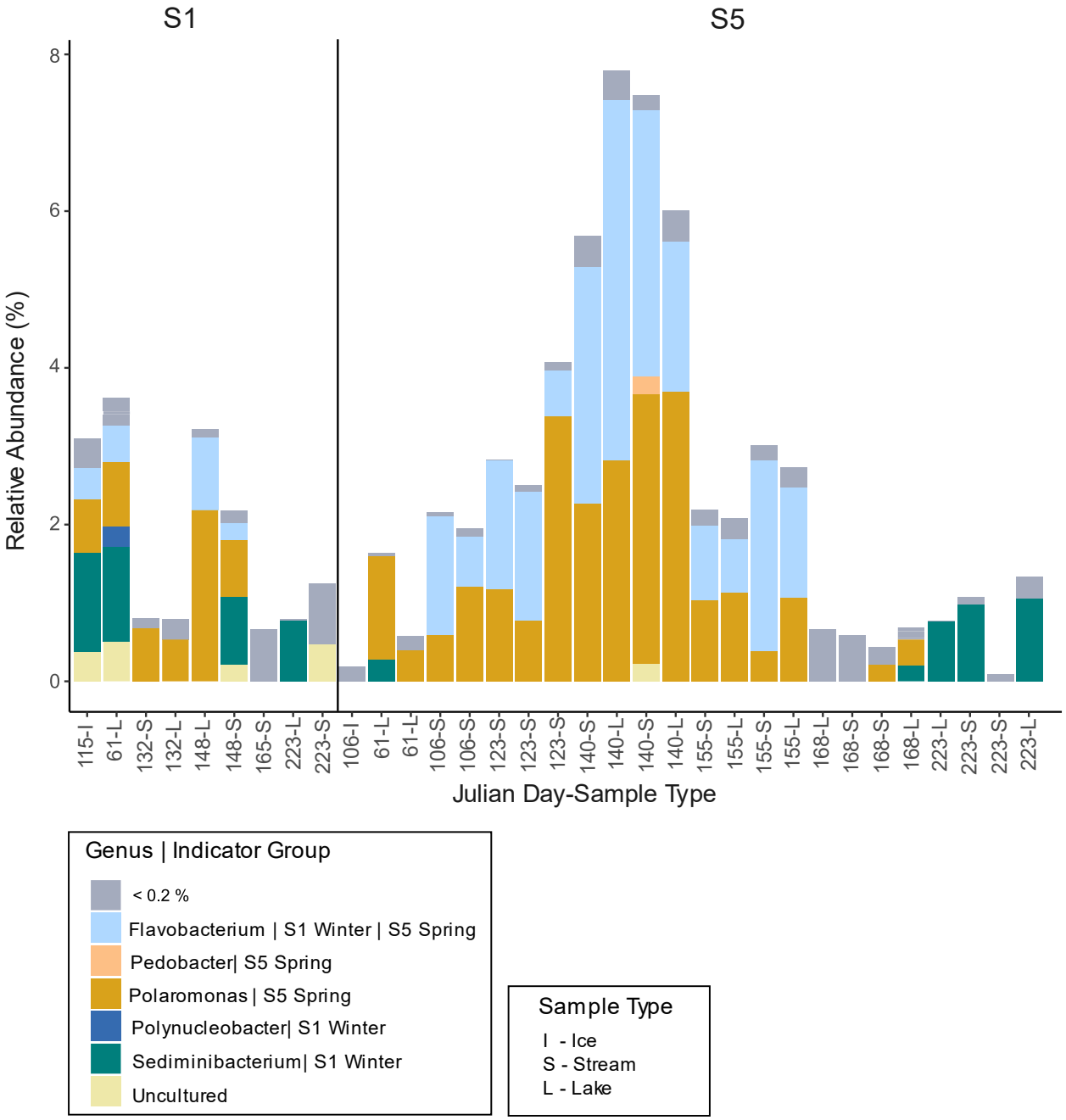

Figure A2-9. Relative abundance (%) of indicator genera at icing meltwater, stream and lake samples at S1 and S5 over time. S5 includes S5a and S5b. Ice cores were pooled with winter surface waters for indicator species analysis.

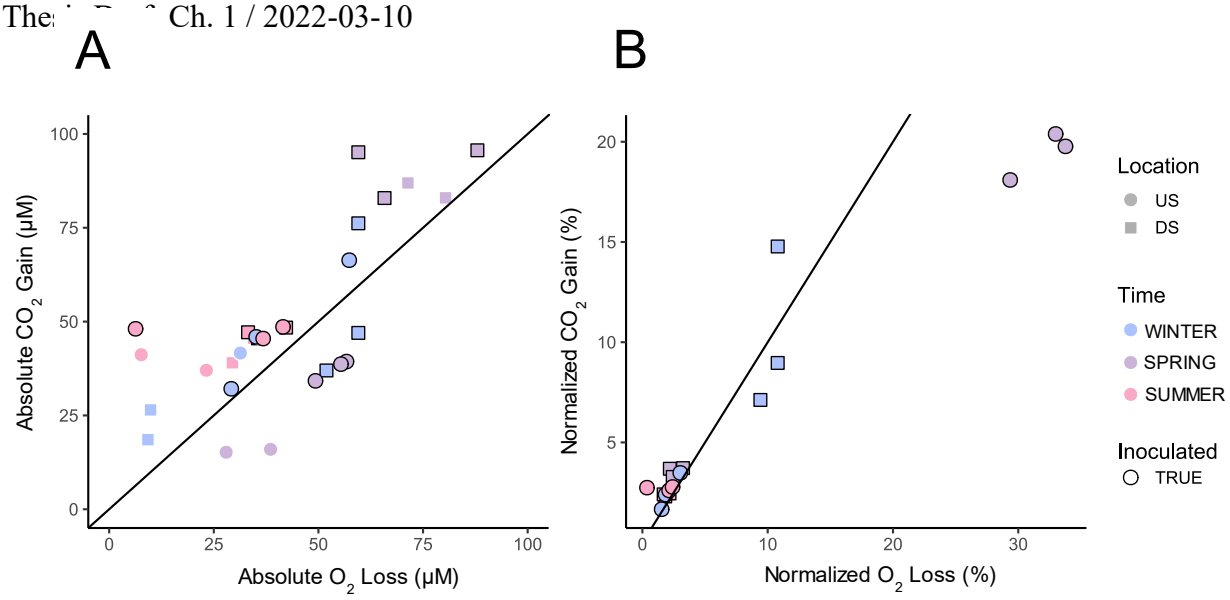

Figure A2-10. Biplots showing incubation experiment results (absolute O_2 loss vs. percent CO_2 gain) from T_0 to T_f, with a diagonal line representing a 1:1 molar ratio of CO_2:O_2. Panel A shows absolute CO_2 gain, with inoculated and non-inoculated samples. Panel B shows O_2 loss/CO_2 gain normalized by initial DOC concentrations of samples; non-inoculated samples are absent as they were not measured for initial DOC concentration.

Supplemental Information

3.2.5 Sample processing for chemical analyses

Samples for SRP were filtered into 50 mL plastic bottles and kept frozen until analysis. Samples for δ^{13}C-DOC were filtered into 40 mL pre-combusted glass EPA vials and acidified to pH 2 using trace-metal grade hydrochloric acid. Samples for Δ^{14}C-DOC were filtered into 500 mL PC bottles and kept frozen until analysis. Samples for FT-ICR-MS a were filtered into 50 mL PC bottles and kept frozen until analysis.

3.2.9 Incubation setup, chemical analyses and statistical analyses

Approximately 2.5 L of water was collected at each sampling location; the winter icing sample consisted of a composite core sample which was thawed in the dark at 4 °C before filtration. To remove existing microbes from samples, water was filtered within 6 h of collection using 0.2-µm Sterlitech PES filters and then frozen in the dark at -20 °C. The fate of water transiting from S1 is River Lake, which was chosen as the inoculant source. Water from River Lake was collected on October 7th and transported to the University of Alberta where the incubation began on October 8th.

A day before the incubation, frozen water samples were thawed at room temperature in the dark. Sample waters were re-filtered using 0.45-µm Sterlitech PES filters, and inoculant water was filtered using muffled (450°C for 4h) glass fibre (Whatman GF/C 1.2-µm nominal pore size) filters to introduce indigenous microbial communities (J. E. Vonk et al., 2015). Sample water was inoculated (6% final inoculant volume) and 120 mL poured into triplicate glass bottles with an oxygen SPOT sensor on the interior wall (PreSens, Germany); duplicate samples without inoculant were also prepared. A 5mL aliquot of water was extracted from each bottle for DIC analysis, and the volume replaced to fill each bottle without headspace. Bottles were capped with chlorobutyl isoprene stoppers (Niemann et al., 2015) and sealed with an aluminum crimp top to ensure no O_2 exchange occurred. Bottles were placed in a dark incubator. Two extra samples were prepared for each treatment (inoculant and no inoculant) to perform initial chemistry analyses and these samples were kept at 4 °C until analysis.

Oxygen concentration was measured using spot sensors (PreSens) immediately after placing bottles in the incubator (T_0), within 12 h, and every 24 h until the end of the 28-day incubation

(T_f). Oxygen concentration was also recorded in four bottles containing Milli-Q water to verify sensor function. DIC concentration was measured at T_0 to T_f with a DIC Analyzer (Apollo SciTech) at the University of Alberta (Wickland et al., 2012). DIC measurements were calibrated using certified reference material for oceanic CO_2 measurements from Scripps Institute of Oceanography (San Diego, California).

Samples for water chemistry analyses were filtered on T_0 to T_f, using a glass filter assembly and 0.45-µm Sterlitech PES filters. Nutrients (TDN, NO_2^-+NO_3^-, NH_4^+, TDP, SRP) were measured at the Biogeochemical Analytical Service Laboratory (BASL) at the University of Alberta via flow injection analysis. DOC concentration and composition (via fluorescence spectroscopy) was measured at the University of Alberta following the methods in Section 3.2.7.2 and absorbance/fluorescence metrics identified include: A_{254}, $SUVA_{25}$, $S_{275\text{-}295}$, $S_{350\text{-}400}$, S_R, fluorescence peaks A, T, B, C, hix and Fi. During DOC analysis, flocculation was observed in several sample bottles, and using remaining sample water, particulate organic carbon (POC) was analyzed to quantify total organic carbon and determine an accurate estimate of C mineralization. POC samples were prepared by filtering water with 25 mm, pre-muffled (450°C for 4h) glass fibre (Whatman GF/F 0.7-µm nominal pore size) filters in a glass filter assembly and recording the volume passed through each filter. Filters were stored in sterile petri dishes at -20 °C until sample processing for POC analysis. Sample processing involved fumigation of filters with HCl at room temperature to convert carbonate to CO_2, leaving only organic carbon on filters. Filters were first dried for 24 h at 60 °C, then weighed and transferred to pre-combusted glass petri-dishes, which were also weighed to calculate filter weight at the end of the fumigation. Filters were wetted with Milli-Q water and placed in a desiccator with a beaker of concentrated (12M) HCl for 24 h. Filters were then placed in a new desiccator containing NaOH pellets and drierite at the bottom and desiccated for 24 h. Samples were re-dried at 60 °C and weighed, then encapsulated into tin capsules for POC analysis. POC analyses were conducted at the Biogeochemical Analytical Service Laboratory at the University of Alberta via combustion in an elemental analyzer.

Initial and final measurements of O_2 and CO_2 were used to calculate the absolute change of O_2/CO_2 in mg/L, these values were then converted to molar equivalents in uM. Each sample was then normalized by its T_0 TOC concentration (in uM), and then triplicate (inoculated treatments)

were averaged to obtain one value of normalized percent O_2 loss/CO_2 gain per sampling date and location, for use in mixed effects models. As T_0 DOC data was not collected for non-inoculated samples, this data was not normalized. Rates of O_2 loss in mg/l d^{-1} were calculated by doing a ln transformation on each O_2 measurement, and then fitting a linear model to the 28-day record, where slope equaled the rate of O_2 loss. Biplots were used to visualize absolute versus normalized O_2 loss versus CO_2 gain across treatments, sampling locations and dates (Figure A2-10) (Wickham, 2016). Normalized CO_2 gain across inoculated samples was displayed using point plots (Wickham, 2016).